The Pennsylvania State University

The Graduate School

Integrative Biosciences Graduate Program

HEAVY CHAIN FERRITIN SIRNA DELIVERED BY CATIONIC LIPOSOMES ENHANCES RADIATION AND CHEMOTHERAPEUTIC EFFICACY FOR TREATMENT OF GLIOMA

A Dissertation in

Integrative Biosciences

by

Xiaoli Liu

© 2010 Xiaoli Liu

Submitted in Partial Fulfillment
of the Requirements
for the Degree of

Doctor of Philosophy

December 2010

The dissertation of Xiaoli Liu was reviewed and approved* by the following:

James R. Connor
Distinguished Professor of Department of Neurosurgery
Dissertation Advisor
Chair of Committee

Ira Ropson
Associate Professor of Department of Biochemistry and Molecular Biology

Kathryn LaNoue
Distinguished Professor of Department of Cellular and Molecular Physiology

A.B.Madhankumar
Assistant Professor of Department of Neurosurgery
Special Member

Alistair Barber
Associate Professor of Department of Ophthalmology and Cellular & Molecular Physiology

Peter Hudson
Willaman Professor of Biology
Director of Huck Institutes of Life Sciences

*Signatures are on file in the Graduate School

ABSTRACT

Approximately fifty percent of gliomas, especially glioblastoma multiforme (GBMs), are resistant to radiation and chemotherapy. Therefore, efforts to develop new mechanisms to enhance the efficacy of current treatment strategies are clearly warranted. Glioma cells, similar to many other malignant cells, have a robust appetite for iron to support their rapid growth and high metabolic rate. With elevated levels of iron uptake, a mechanism to protect cells from augmented iron induced oxidative damage is needed. This protection is likely provided by the intracellular iron storage protein ferritin. Ferritin has been detected in the cytosol, mitochondria and nucleus of almost all malignant tumor cells. Overexpression of H-ferritin in nuclei of glioma cells appear to protect DNA from iron induced oxidative damage and promote transcription. Overexpression of H-ferritin in nuclei of breast cancer cells and cervical cancer cells was also found to be associated with drug resistance. These findings lead to the **central hypothesis** of my thesis, silencing of H-ferritin by siRNA enhances the radiation and chemotherapeutic efficacy for treatment of glioma. It is anticipated that silencing of H-ferritin using gene therapy will decrease resistance to chemo/radiation therapy. To deliver a therapeutic dose of siRNA, I had to first develop a delivery system and chose cationic liposomes. Thus, there were three specific aims for my thesis: **Aim1**: development and characterization of cationic liposomes described in chapter 2. **Aim2**: investigation of whether silencing of heavy chain ferritin using gene therapy enhances radiation and chemotherapeutic efficacy for the treatment of glioma (illustrated in **chapter 3.I**). Aim 2 was further expanded to investigate the treatment of breast cancer, as well as malignant peripheral nerve sheath tumors. **Aim3**: examination of the potential roles of H-ferritin in the progression of malignant cancers (illustrated in **chapter 3.II**). A number of cell lines; human glioma U251 and U87 cells, neurofibrama #215 sNF96.2 cells, and breast cancer MCF-7 cells were selected for our

in vitro models, and athymic nude mice were selected as our *in vivo* model. Cationic liposomes (C-liposomes) were prepared and characterized for use as a gene delivery vehicle. The cytotoxicity of C-liposomes was tested *in vitro* and *in vivo*. SiRNA was incorporated into C-liposomes to form C-liposomes:siRNA complexes. The uptake of C-liposomes:siRNA into glioma cells was confirmed, and the mechanism of uptake was identified. Radiation and chemotherapeutic efficacy were assessed after H-ferritin was down regulated. The potential role of H-ferritin in biological pathways was investigated by evaluating the effects on DNA conformation, the DNA repair related protein MGMT, DNA synthesis (by evaluating incorporation of BrdU and ^{3}H-thymidine) and apoptotic activities.

The C-liposomes exhibited safe, applicable, and stable traits, and its uptake into glioma cells depended on the endosomal pathway. Immunoblotting analysis demonstrated that siRNA delivered in this manner, decreased H-ferritin protein expression by 90% in U251 cells, and 70% in MCF-7 cells within 48 hours. This decrease in H-ferritin expression was associated with a decrease in the LD50 for, nitrosoureas carmustine (BCNU), from concentrations greater than 100 μM to 40 μM in the U251 cells, 30 μM in MCF-7 cells, and 18 μM in MPNST cells. In addition, knockdown of H-ferritin was associated with a 50% increase in cell death of U251 cells using 20 Gy of radiation *in vitro*. The *in vivo* efficacy of siRNA delivered by C-liposomes was tested in an athymic nude mouse subcutaneous glioma tumor model. Intratumoral injections of C-liposomes containing H-ferritin siRNA reduced the required effective dose of BCNU for tumor suppression by more than 50%. Moreover, intratumoral injections of C-liposomes containing H-ferritin siRNA with 4Gy radiation suppressed tumor progression by more than 90% compared with C-liposomes containing non-specific siRNA.

The interaction of H-ferritin with DNA in the presence of BCNU was investigated *in vitro* by supercoil relaxation assays. These assays demonstrated that H-ferritin maintained DNA

in a relaxed form, which would promote DNA transcription even in the presence of radiation and chemotoxins. In addition to the protective function on H-ferritin on DNA, the anti tumor effect of H-ferritin siRNA was associated with activation of the apoptotic caspase-3 pathway. However, H-ferritin did not appear to facilitate DNA repair through the MGMT pathway.

In conclusion, our study demonstrated that the vulnerability of cancer cells to radiation and chemotherapy can be increased by reducing H-ferritin expression. The importance of ferritin in cancer cell biology suggests that efficient delivery of siRNA could be a viable therapeutic option. As importantly, we have demonstrated that siRNA can be delivered effectively by C-liposomes in an *in vivo* tumor model.

TABLE OF CONTENTS

LIST OF FIGURES ix

LIST OF ABREVIATIONS xii

ACKNOWLEDGEMENTS.....xiv

Chapter 1 Literature review 1

1.1 Introduction.....1

1.2 Glioma 2

1.3 Carmustine BCNU 5

1.4 Small interferon RNA 8

1.5 Small hairpin RNA.....11

1.6 Iron.....12

1.7 Ferritin.....16

1.8 Cationic liposomes.....20

1.9 Figures and legends of chapter of chapter 1.....26

Chapter 2 Development and characterization of cationic liposomes 37

2.1 Introduction.....37

2.2 Materials and methods 39

2.3 Characterization of the complex of C-liposomes:siRNAs 43

2.4 Development of Interleukin-13 conjugated C-liposomes:siRNAs.....44

2.5 Results.....48

2.6 Summary.....53

2.7 Figures and legends of chapter 2.....54

Chapter 3 The Functional Role of H-ferritin in Cancer development and impact of decreasing H-Ferritin expression on Radiation and Chemotherapeutic Efficacy in the Treatment of Glioma.....67

Chapter 3 Part I H-ferritin siRNA enhances radiation and chemotherapeutic efficacy for treatment of glioma.....67

3.I.1 Introduction.....68

3.I.2 Materials and methods.....68

3.I.3 Results.....73

3.I.4 Summary.....77

3.I.5 Figures and legends of chapter 3(part I).....79

Chapter 3 Part II Functional role of H-ferritin in cancer development.....92

3.II.1 Introduction.....92

3..II.2 Materials and methods.....92

3.II..3 Results.....96

3.II.4 Summary.....98

3.II.5 Figures and legends of chapter 3(part II).....99

Chapter 4 Discussion.....108

4.1 Introduction.....108

4.2 Advanteges and pitfalls of C-liposomes.....108

4.3 Scientific significance of a synergistic strategy of H-ferritin down-regulation by gene therapy with conventional treatments 111

4.4 Clinic significance of a synergistic strategy of H-ferritin down-regulation by gene therapy with conventional treatments 114

4.5 Summary 115

4.6 Future directions 116

References 121

LIST OF FIGURES

Figure **1.1**: Gliomas. 26

Figure **1.2**: Carmustine BCNU 27

Figure **1.3**: The decomposition of BCNU. 28

Figure **1.4**: The sequence of heavy chain ferritin siRNA. 29

Figure **1.5**: The mechanism of small inteferon RNA. 30

Figure **1.6**: The mechanism of C-liposomes:siRNA 31

Figure **1.7**: The properties of Iron and the Fenton reactions. 32

Figure **1.8**: Ferritin 33

Figure **1.9**: The structure of DC-cholesterol/DOPE. 34

Figure **1.10**: Structure of liposome 35

Figure **2.1**: Characterization of C-liposomes. 53

Figure **2.2**: The optimal ratio of C-liposomes:siRNA 54

Figure **2.3**: Lack of cytotoxicity of C-liposomes in U251 cells, as tested by an MTS assay. 55

Figure **2.4** Lack of Toxicity of C-liposomes *in vivo*, as evaluated by an automated chemistry analyzer and kits. 56

Figure **2.5**: Internalization of C-liposomes:siRNA through endosomal pathway in U251 cells. 57

Figure **2.6**: Encapsulation of siRNA by newly parpared C-liposomes tested by 1% agarose gel 58

Figure **2.7**: Stability of the C-liposomes:siRNAs complex in RNase A at 37^{o}C tested by 1% agarose gel. 59

Figure **2.8**: Stability of the C-liposomes:siRNAs complex in human serum tested by 1% agarose gel. 60

Figure **2.9**: Encapsulation of siRNA using maleilide cationic liposomes by No.1 formulation tested by 1% agarose gel. 61

Figure **2.10**: Encapsulation of siRNA using maleilide cationic liposomes by bNo.2 formulation tested by 1% agarose gel 62

Figure **2.11**: The size distribution of IL-13-M-C-liposomes determined by dynamic light scattering. 63

Figure **2.12**: The zeta potential of IL-13-M-C-liposomes, as measiured by PALS Zeta Potential Analyzer (Win36), Broohaven Instruments Corp. 64

Figure **1.1** Encapsulation of siRNA using IL-13-M-Cliposomes by No.2 formulation, as tested by 1% agarose gel. 65

Figure **3.1**: H-ferritin expression in malignant tumor cells detected by immunicytochemistry. 79

Figure **3.2**: H-ferritin in U25 cells ia associated with the glioma stem cell marker CD133, as tested by immunocytochemistry 80

Figure **3.3**: H-ferritin in U87 cells ia associated with the glioma stem cell marker CD133, as tested by immunocytochemistry. 81

Figure **3.4**: H-ferritin in NF#215 cells ia associated with the glioma stem cell marker CD133, as tested by immunocytochemistry 82

Figure **3.5**: Down regulation of H-ferrritin expression in U251 cells, as tested by Western blot. 83

Figure **3.6**: Down regulation of H-ferrritin expression in MCF-7 cells, as tested by Western blot 84

Figure **3.7**: H-ferritin siRNA increases the chemotherapeutic sensitivity of glioma U251 cells, as tested by an SRB assay 85

Figure **3.8**: H-ferritin siRNA increases the chemotherapeutic sensitivity of glioma MCF-7cells, as tested by an SRB assay 86

Figure **3.9**: H-ferritin siRNA increases the chemotherapeutic sensitivity of glioma sNF96.2 cells, as tested by an SRB assay. 87

Figure **3.10**: H-ferritin siRNA increases the sensitivity of glioma U251 cells to radiation, as tested by an MTS assay 88

Figure **3.11**: Down regulation of H-ferritin in a tumor xenograft model, as analyzed by Western blot. 89

Figure **3.12**: H-ferritin siRNA is an effective adjuvant for chemotherapy in a subcutaneous tumor mouse model. 90

Figure **3.13**: H-ferritin siRNA is an effective adjuvant for radiation therapy in a subcutaneous tumor mouse model. 91

Figure **3.14**: H-ferritin attenuated the effects of BCNU on DNA, as evidenced by a supercoil relaxation assay 99

Figure **3.15**: Influence of H-ferritin on DNA relaxation, as evidence by a supercoil relaxation assay 101

Figure **3.16**: Influence of H-ferritin on DNA relaxation under redation, as evidence by a supercoil relaxation assay 102

Figure **3.17**: MGMT expression in MCF-7 cells, as tested by Western blot 103

Figure **3.18**: H-ferritin is associated with apoptosis in U251 cells 104

Figure **3.19**: H-ferritin is associated with apoptosis in MCF-7 cells 105

Figure **3.20**: BrdU incorporation, as tested by immunocytochemistry. 106

Figure **3.21**: ^{3}H-Thymidine incorporation in U251 cells. 107

Figure **3.22**: ^{3}H-Thymidine incorporation in U87 cells. 108

LIST OF ABBREVIATIONS

α	alpha
BCNU	1,3-Bis(2-chloroethyl)-1-nitrosourea, carmustine
ß	beta
^{o}C	degree celsius
C-liposome	cationic liposome
CSC	cancer stem cells
DC-Cholesterol:	3beta-[N-(N',N'-dimethylaminoethane) carbamoyl] cholesterol
DMEM	Dulbecco's Modified Eagle Medium
DOPE:	dioleoylphosphatidylethanolamine (1,2-dioleoyl-sn-glycero-phosphoethanolamine
DPPC	1,2-dipalmitoyl-sn-glycerol-3-phosphochlorine
DDAB	dimethyl-dioctadecyl-ammonium bromide.
DOTM	N-[1-(2,3-dioleyloxy)propyl]-N,N,N-trimethylammonium chloride.
DOTAP	1,2 Dioleoyl-3-trimethylammonium-propane. LIC100
EGFR	epidermal growth factor receptor
FITC	fluorescein isothiocyanate
GBM	glioblastoma multiforme
HF, H-ferritin	heavy chain ferritin
IL-13	interleukin 13
LF, L-ferritin	light chain ferritin

MTS	3-(4,5-dimethylthiazol-2-yl)-5-(3-carboxymethoxyphenyl)-2-(4-sulfophenyl)-2H-tetrazolium
NS	none specific
PDI	poly Index dispersity (describe the size distribution)
shRNA	short hairpin RNA
siRNA	small interferon RNA
SRB	sulforhodamine B
Zeta potential	the potential difference between the dispersion medium and the stationary layer of fluid attached to the dispersed particle

ACKNOWLEDGEMENTS

I really appreciated all the understanding, encouragement and support my family gave me during the most important time period of this graduate program. I am grateful particularly with my intelligent husband Dr. Qingxian Yang and gifted sister Dr. Lina Liu who helped me spiritually and physically to reach one of the goals of my life. I am also very thankful for my mother for her unconditional love. And I am also appreciated with the support from my sons Bei Yang and Gary W. Yang.

I would like to thank Chemical Biology option for giving me this great opportunity to pursue the beautiful dream of my childhood and made my dream become true. I want to thank my thesis committee (Dr. James R. Connor, Dr. Ira Ropson, Dr. Kathryn LaNoue, Dr. A. B. Madhankumar and Dr. Alistair Barber) for your intellect guidance, for your intention and precious time during so many years. My special thanks go to Dr. James R. Connor for your excellent leadership and perspective directions that assisted me healthily grow up to be able on the right track of becoming a fully developed scientist. I am very appreciated with that you allow me to accomplish my thesis project in your laboratory. My special thank also go to Dr. Madhankumar for your broad scientific knowledge and your skillful laboratory techniques.

I would also like to thank Dr. Vessel, Dr. Ann Marie, Dr. James Hopper, and Dr. Anita K. Hopper for all your support when I encounter the difficulty during the time period of the graduate program.

I am also very appreciative with the friendship of Dr. Fan Chen who accompanied me through my graduate program for so many years.

Finally, I want to express my great appreciation again for all the members who works in Dr. Connor's laboratory and all of you I mentioned here. Without your support I do not think that I am able to get this far.

Chapter 1

Literature Review

1.1 Introduction

The long-term **goal** of this project is to develop a **novel synergetic therapeutic strategy** that combines gene therapy with radiation or chemotherapy for the treatment of glioma. This novel synergetic therapeutic strategy may be useful for treating a malignant tumors, including breast cancer and malignant peripheral nerve sheath tumors (MPNST). In the present thesis project, heavy chain ferritin (H-ferritin) was down regulated by small interfering RNA (siRNA) delivered by cationic liposomes (C-liposomes). Down regulation of H-ferritin made malignant glioma cells vulnerable and, thus, they become more sensitive and less resistant to radiation and chemotoxins. The rationale for the study, that down regulation of H-ferritin sensitizes glioma cells to radiation and chemotherapy, is based on the following previous findings:

1. We observed that H-ferritin was present in nuclei of human astrocytoma cells [1, 2] and overexpressed in breast cancer cells [3, 4].

2. We found that H-ferritin interacts with DNA, specifically protecting DNA from oxidative damage [1, 2, 5] and promoting transcription [6].

3. We learned that H-ferritin prevents apoptosis in breast cancer and malignant mesothelioma cells [7-11].

4. We discovered that upregulation of H-ferritin negatively mediate immune responses in tumor cells [12-18].

5. We observed that H-ferritin overexpression has been associated with the development of drug resistance [19, 20].

Ferritin is an iron storage protein that plays a key role in maintaining the homeostasis of cellular iron, which is an essential trace element for life. The importance of ferritin in iron metabolism and the above findings, provide a firm basis for our **central hypothesis** that down regulation of H-ferritin will sensitize malignant tumor cells to radiation/chemotoxins, and thereby effectively increase the efficacy of radiation and chemotherapy for the treatment of glioma and other malignant tumors. Prior research and background information related to this project are reviewed in the subsequent sections. Glioma, its formation and treatment, methodology of radiation and chemotherapy, the characteristics of the anti-cancer drug BCNU, iron metabolism, the function of ferritin in cell biology, siRNA related gene therapy for treatment of glioma, and the characteristics of the gene delivery vehicle C-liposomes are all discussed as following.

1.2 Glioma

1.2.1 Glial origin

Normal brain tissue consists of two different materials: neurons and non-neuronal (supportive) tissues [21]. The non-neuronal tissues consist of astrocytes, oligodendrocytes, microglia, ependymal cells, radial glial, satellite, and Schwann cells, which all differentiated from original glial cells. Glial originating cells have two main functions: they physically surround and hold neurons, and chemically provide nutrients and oxygen to neurons. These supportive cells of glial origin settled in a special location of the brain where their functions were necessary. Astrocytes are involved in several functions, including the uptake of excess neurotransmitters and formation of the blood-brain barriers. Oligodendrocytes function to cover axons of neurons with myelin sheathes. Microglias are programmed macrophages that are able to perform phagocytosis, which protect neurons in central nervous system.

1.2.2 Formation of glioma

Brain tumors arise when neurons or the cells of supportive tissues divide abnormally or uncontrollably. Brain tumors can be primary (originating from the brain) or secondary (metastatically transferred to the brain from another part of the body). Glioma, as the images shown in **Figure 1.1**, especially glioblastoma multiforme (GBM) is a malignant brain tumor of the central nervous system (CNS) that arises from cells of glial origin. Glioma includes astrocytoma, ependymoma, ganglioglioma and oligodendroglioma, which are classified from grade I to IV (WHO) according to their malignancy. The cause of glioma is unknown, however, a number of macro environmental factors have been proposed, including exposure to an oil refinement factory, the rubber-industry, organic agents, and smoking [22]. The micro environmental cause of glioma is similarly unclear. In recent years, the ideas that cancer may be initiated by a rare fraction of multipotent cells called “cancer stem cells” (CSC), has grown [23]. However, the techniques for isolating this CSC and biological theory of CSC have yet to be completely established. Glioma accounts for 70% of all brain tumors [24] and has increased in

incidence from 1977 to 2000 especially amongst older patients. In western countries, astrocytoma affects caucasians with higher incidence than African/Asian populations [25]. Males are more often affected than females, and gender differences have been shown to be greater in older age groups [26].

1.2.3 Impact of glioma

Glioma growth in the brain is particularly threatening, because the brain is delicately designed in a narrow and closed system, and brain cells performs complicated functions. Tiny abnormal cellular growth can generate severe consequences, depending on the location of the lesion. Although the incidence of primary glioma accounts for only 1.35% of all cancers in the United States, it ranks second in the cause of death amongst all neurological diseases [27]. Gliomas comprise approximately 60% of all cases amongst pediatric brain tumors [28], and together with leukemia, are the leading cause of cancer related mortality in children [29]. GBM, the most common and deadly brain tumor with an average survival of 12 months, is characterized by abnormal cellular proliferation, aggressive angiogenesis, invasiveness, and potential drug resistance [30].

1.2.4 The challenge for the treatment of glioma

Treating glioma is challenging, because of the difficulties in delivering effective amounts of chemotoxic agents through the blood-brain-barrier, and completely resecting tumor tissue in the brain. Higher dosages of chemotherapeutic agents are generally not an option, because they are often accompanied by devastating adverse side effects offsetting the benefit [31]. Conventional treatment with surgical removal followed by chemo/radiation therapy is ineffective, due to genomic instability and invasiveness of glioma that escapes surgical removal and radiation. Recent novel approaches such as gene therapy [32, 33], immunotherapy [34, 35],

antiangiogenetic therapy [36], and antibody based approaches [37] have been promising. However, preliminary clinical results of these approaches have not translated into significantly improved survival [27, 38]. Therefore, efforts to develop new mechanisms to enhance efficacy of treatment are clearly warranted. To address this critical issue, the present research was designed using a synergetic approach of gene therapy silencing the H-ferritin gene followed by chemotherapy/radiation therapy for the treatment of malignant glioma. This thesis work demonstrated that H-ferritin downregulation by gene therapy is able to increase the efficacy of radiation and chemotherapy, while lowering the conventional dosage of these agents. This decrease in dosage is expected to reduce the side effects of anti cancer drugs such as BCNU, which was used in this study.

1.3 Carmustine BCNU

1.3.1 Treatment of glioma and the mechanism of BCNU

In this work, the anti cancer drug 1,3-Bis(2-chloroethyl)-1-nitrosourea, carmustine (BCNU) was utilized. BCNU (MW 214.049 g/mol, formula $C_5H_9CL_2N_3O_2$) as shown in **Figure 1.2**, was created by Southern Research Institute and **Cancer Chemotherapy National Service in 1962**, and was accepted for clinical development for the treatment of brain tumors in the same year it was discovered. The mechanism of BCNU as an anti-cancer drug is described in **Figure 1.3** as follows: 1) BCNU is decomposed to generate chloroethyl carbonium irons. 2) Chloroethyl carbonium irons react and alkylate O^6-gaunine of DNA molecules. 3) DNA synthesis is disrupted as O^6-Gaunine of DNA is modified, which halts cancer cell division to stop tumor growth [39-41]. BCNU is widely used in the treatment of glioma, because BCNU is a small molecule, allowing for crossing of the blood brain barrier. BCNU became the standard chemotherapeutic drug of choice for the treatment of glioma since

1962, and later on for treatment of melanoma, lung, colon and some other cancers [42-44]. The efficacy and the characteristics of BCNU have been evaluated frequently since its use as an anti cancer drug. One study in 2004 by Brandes and colleagues concluded that the activity of BCNU for treatment of glioma was comparable with those used in the past, as well as with the newest therapies such as temozolomide [45]. Although a similar drug like temozolomide with less cytotoxicity invented in the middle of the 1990's, the popularity of BCNU is not reduced. BCNU has turned out to be more valuable for the treatment of glioma, due to the use of biodegradable polymer wafers impregnated with BCNU that can be located in the surgical cavity after resection of a malignant glioma [46-48].

1.3.2 The disadvantage of BCNU

Therapeutic function and application of the BCNU regimen are limited by two major issues: development of drug resistance, and production of acute and chronic cytotoxicity after a short period of treatment [41, 42]. Two studies suggested that drug resistance is derived from the ability of living cells to restore DNA integrity via DNA repair mechanisms [49, 50]. The most recognized DNA repair protein is O^6-methylguanine-DNA methyltransferase (MGMT). When cancer cells experience DNA impairment, a DNA repair mechanism is initiated and expression of MGMT increases. MGMT is capable of removing the added methyl group from the DNA and further reversing the alkylation of O^6-guanine-DNA. DNA replication is then resumed [49, 50] and cancer cells grow recurrently. The integrity of the original DNA is maintained by the action of MGMT, which is one of the leading causes of drug resistance and chemotherapeutic failure [51]. In other words, upregulation of MGMT for DNA repair is a major cause of drug resistance [52]. Besides the MGMT mechanism of DNA repair, other studies suggested that cancer stem-like cells that possess tumorogenic potential are a factor in drug resitance in glioma [51, 53]. However, in the present study, only the DNA repair pathway

for drug resistance was investigated. Usually, when patients develop drug resistance, the first step is to increase the dosage. However, with BCNU, this is not an option, since BCNU cytotoxicity is high and patient recovery is slow. This is because the drug generate side products such as chloroethynol and acetaldehyde after the decomposition of BCNU, which causes oxidative stress for normal cells [41]. Although the half life of BCNU is only 12 hours [54], carmustine chemotherapy in childhood was found to cause lung fibrosis that may remain asymptomatic for many years or become symptomatic at any time [55]. Treatment with BCNU for lung parenchyma has caused toxicity of pulmonary fibrosis [56]. Treatment of glioma involving BCNU also has been reported to cause lung fibrosis, and hematologic and long-lasting hepatic diseases in adult patients [45, 54, 57]. The challenge we face is developing a way to lower the cytotoxicity of anti cancer drugs for normal cells, while at the same time maintaining its efficacy in destroying cancer cells. It is an urgent and major goal for medical and pharmaceutical researchers to increase the sensitivity of cancer cells to anti cancer treatments. The present project is designed to use gene therapy in the downregulation of H-ferritin to reach the goal of increasing the sensitivity of cancer cells to toxins.

1.3.3 Increase the efficacy of BCNU

The objective of the present project is to enhance the efficacy of chemotherapeutic drugs by using gene therapy to down regulate H-ferritin. Based on the mechanism of drug resistance induced by the DNA repair protein MGMT in treated cancer cells [42], we expected that down regulating H-ferritin will increase the sensitivity of cancer cells and lower the dosage of BCNU required, while maintaining its efficacy. BCNU was selected for present study for the following reasons: a) BCNU is a small molecule that can cross blood brain barrier. b) Pure BCNU is commercially available in contrast to temozolomide. c) BCNU has been used since 1962 for treating multiple types of cancers, especially glioma [42] and BCNU

treatment appears to be a valuable therapeutic option for recurrent glioblastoma multiforme [58]. d) The drug resistance mechanism for BCNU is well studied and continually assessed [45]. e) The usage of BCNU has been modified and used in multidisciplinary approaches in recent years [48]. f) The combination of BCNU with surgery and radiation may provide an enhanced benefit compared with the use of either of these agents alone in select patients with high-grade glioma [46]. To achieve the goal of increasing the sensitivity of tumor cells for chemotherapy, H-ferritin small interferon RNA (siRNA) was used to down regulate H-ferritin expression.

1.4 Small interfering RNA (siRNA)

1.4.1 The mechanism of siRNA

Small interfering RNAs (siRNAs) are double-stranded RNA molecules 2-nucleotide 3' overhangs on each side of 20-25 nucleotides in length shown in **Figure 1.4**. Short interfering RNA and silencing RNA are the other two names of siRNA. It is likely that the major function of siRNA is to sequence-specifically and post-transcriptionally silence the targeted gene and cause a decrease of the messenger RNA (mRNA) and this should sequentially down regulated protein expression. SiRNAs were discovered in plants in late 1990's by Andrew Hamilton and David Baulcombe at the Sainsbury Laboratory in Norwich, England. Their work was published in *Science* in 1998 a paper titled "A species of small antisense RNA in posttranscriptional gene silencing in plants" [59]. These workers later were owned the Nobel Prize because of their siRNA discovery, which is one of the most dramatic events of the century in the field of molecular biology. The **mechanism** for specific gene silencing by siRNA in eukaryote and animals is a stepwise process related to activities of two enzymes: a member of the RNase-III family of ATP-dependent ribonuclease (Dicer), and RNA-induced silencing complex (RISK) that is shown in

Figure 1.5. In step one, when long double-stranded RNA (dsRNA ~200 nucleotides) molecules are introduced, Dicer binds dsRNAs with a high affinity and dsRNAs are processed into short fragments (20-25 nucleotides duplexes). In step two, RISK recruits these short fragments (20-25 nucleotides duplexes) forming a complex; the double stranded siRNA will then be unwound. In step three, the activated RISK will recognize and bind to complementary cognate mRNA. In step four, the target mRNA is cleaved and degraded. The actions of siRNA influence gene expression at the posttranscriptional or translational level [60, 61]. This mechanism has been elucidated in another two publications [62, 63], and has become an important tool for studying gene function in biomedical research and gene-specific therapies for treatment of different human diseases [59, 64-66]. Soon after its discovery, the revolutionary evolution of siRNA usage experienced a breakthrough in technology, which was developed by Webb K. Tuschl and colleagues in 2001. Their work was published in *Nature* in a paper entitled "Duplexes of 21-nucleotide RNAs mediate RNA interference in cultured mammalian cells" [64]. The important contribution by Webb K. Tuschl, is that they made synthetic siRNA possible as one of the most important milestones for molecular biology.

1.4.2 The applications of siRNA for human diseases

The success of synthetic siRNA further promoted the usage of siRNA and allowed siRNA to become a drugable molecule [64]. Custom designing of siRNA simplified and further promoted its applications. In 2004, there were more than six publications related to the selection of Web servers for siRNA design [67-73]. Chemically modified and cell type-specifically targeted [74, 75] siRNAs made this molecule more versatile for its application in different fields. Implicated in shaping chromatin structure of the genome, curing human diseases, and treating malignancies, the application of siRNAs shows a promising approach [76, 77]. For example, siRNA for anti-viral defense is related to prevention of transmission of HIV infection, inhibition

of HIV-1 replication, limitation of the production of Hepatitis B, and restriction of viral infections [77-80]. SiRNA has also been used to inhibit avian sarcoma-leukosis virus and HIV replication in cell culture [81-83]. In terms of treating neurodegenerative disease, one study revealed that siRNA down regulation of the mutant htt gene using siRNA diminished cell growth and provided potential for the treatment of Huntington's disease [84]. In addition to these examples, siRNA shows promise for the development of therapeutic strategies for the treatment of various cancers.

1.4.4 The applications of siRNA for treating malignant cancers

The use of siRNA for treating malignant cancer has become of great interest, and many promising siRNAs have been identified, synthesized, and characterized [66]. VEGF siRNA had been used with the treatment of glioma, the human epidermal growth factor receptor (EGFR) siRNA had been employed with management of GBM, and matrix metallopeptidase 9 (MMP-9) siRNA based therapeutics have also been administered for the treatment of malignant glioma [85-89]. One review article recently addressed the potential of silencing multiple messages at the same time, and suggested that siRNAs might become therapeutically relevant in a "one-hit multiple-target" context against brain tumor angiogenesis [89]. Some EGFR is overexpressed in all malignant tumor cells; an EGFR siRNA regimen prolongs survival in mice with intracranial human brain cancer [90]. Cathepsin B siRNA mediated inhibition both of cathepsin B and Urokinase-type plasminogen activator receptor (uPAR) leads to decreased cell invasion, angiogenesis and tumor growth in glioma [91]. One review summarized more than 28 target genes in different cancers that may be siRNA targets, including VEGF (vascular endothelial growth factor) siRNA for treating fibrosarcoma, Ewing’s sarcoma, and prostate cancer, HER-2 siRNA for the treatment of ovarian carcinoma and breast cancer, and EGFR and MMP-9^{+} siRNAs for the treatment of glioma [92]. Another sixteen siRNA genes including that for RAS, were identified that for treatment of GMB [93, 94]. SiRNA down regulation of telomerase activities

has also been proposed for the treatment of both carcinomas and sarcomas [95]. For the treatment of leukemia, siRNA for the fusion gene BCR-ABL induced apoptosis in K562 cells [96]. Furthermore, siRNA has been widely employed for treatment of lung cancer, prostate cancer and colon cancers [97-102]. In accordance with the promising potential of siRNA for the treatment of cancer, a major focus of our efforts has been to find a suitable siRNA target for **ferritin**, which is a key protein in maintaining cellular iron homeostasis [103]. The use of H-ferritin siRNA without a delivery vehicle, with reasonable transfection efficiency, has been employed in our laboratory since 2005 [1]. However, the mechanism as shown in **Figure 1.6**, we found that siRNA, delivered by cationic liposomes, not only down regulated H-ferritin, but also demonstrated increased transfection efficiency compared to H-ferritin siRNA without a delivery vehicle, the results will be revealed in later chapters.

1.5 Small hairpin RNA (shRNA)

More than a decade after its discovery, siRNA has demonstrated its enchanting ability to down regulate target genes as described in the preceding sections. However, the application (downregulation of target genes) is limited by its transient effect. In successful applications, long-term silencing of a cognate gene is required. A sequence of RNA that makes a tight hairpin turn, called a small/short hairpin RNA (shRNA) can provide long term silencing of a target gene via RNA interference. Its mechanism involves the initiation of transcription of shRNAs at a polymerase III (pol III) promoter and termination at position 2 of a 4-5-thymine transcription termination site. As shRNA's are expressed, a stem-loop structure with 3' UU-overhangs is folded. The ends are then processed and converted into about 21 nt siRNA-like molecules [104]. These siRNA-like molecules can, in turn, achieve long term gene-specific silencing in transfected mammalian cells [104].

For the treatment of glioma, shRNAs appeared to show promise of down regulating target genes as well as siRNAs, but with a characteristic that siRNA does possess: long-term silencing. Several studies revealed that shRNA successfully down regulates the surviving gene and inhibits angiogenesis in U251 cells and its xenograft, and targeted ASIca mRNA, EGFR, UPA and MMP-9 for the treatment of glioma [105-109]. ShRNA is not used in the present study; however, the use of H-ferritin shRNA is planned for the down regulation of H-ferritin in systemic treatment of glioma, and will be discussed in the future direction section.

1.5 Iron

1.5.1 The unique property of Iron

Iron has the symbol, **Fe**, and atomic number 26. It is a chemical element and metal in the first transition series and group 8 of the periodic table. The physical and chemical properties of iron stem from its atomic structure, which establishes its unique position among the other elements. Its atomic structure and the distribution of the electron-cloud on the outer-most shell can be viewed in **Figure 1.7**. Regarding the atomic structure of each element, the distribution of the electron-cloud on the outer-most shell is critical, as it drives the chemical properties. According to the atomic orbital theory, the energy state of electrons is stable when the orbital electron-cloud in the outside shell is half full or completely full. For instance, in the s orbital, two electrons in s^2 indicate that the s orbital is filled and one electron represents that the s orbital is half full filled. In the d orbital, ten electrons in d^{10} indicate that the d orbital is full filled and five electrons in d^5 indicate it is half full filled. The shell for the distribution of the electron-cloud of ^{26}Fe is: $1s^2 2s^2 2p^6 3s^2 3p^6 \mathbf{4s^2 3d^6}$. The outer most shell is $\mathbf{4s^2 3d^6}$, which is not a stable energy state for the electrons, because of the potential of two electrons to be lost from $\mathbf{4s^2}$ or $\mathbf{4s^2 3d^6}$. When two electrons at $\mathbf{4s^2}$ are lost, ^{o}Fe becomes Fe^{2+}, and the distribution of its electron-cloud is then at a

more stable energy state as: $1s^2 2s^2 2p^6 3s^2 3p^6 \mathbf{4s^1 3d^5}$. It is a stable energe state because of the half filled orbital of $\mathbf{s^1}$ and $\mathbf{d^5}$. When three electrons from $\mathbf{4s^2 3d^6}$ are lost, ^{o}Fe becomes Fe^{3+}, and the distribution of its electron-cloud is turned into an orbital state: $1s^2 2s^2 2p^6 3s^2 3p^6 \mathbf{3d^5}$. It is then in a most stable energy state, because $\mathbf{d^5}$ is a half filled orbital. Thus ferrous (Fe^{2+}) can be converted into ferric (Fe^{3+}) or vice-versa through donation of one electron or gain of one electron from the environment. The uniquely important role of iron in biological systems stems from its physical and chemical properties, which result from its special distribution of electrons in the outer shell.

1.5.2 Iron trafficking in human cells

In normal situations, humans receive both heme and nonheme iron from a variety of foods consumed daily. Upon absorption by intestine, nonheme iron is reduced to Fe^{2+} by brush border ferrireductase. Soon thereafter, transferrin, an abundant and high affinity iron-binding protein, recruits the iron and binds it. Transferrin, under normal conditions, takes up most of the iron in serum, solubilizes it, and controls its reactivity. Nearly 30% of the iron-binding sites on plasma transferrin, in a normal human subject, are occupied by iron [110]. Transferrin that is carrying iron forms a complex with the transferrin receptor-1 on the surface of cell membranes, and enters the endosome of the cell through receptor mediated endosytosis [111]. An acidified environment in the endosome assists in the release of iron upon its arrival. Divalent metal transport 1 (DMT1), iron exporters, also called SLC11A2, NRAMP2 and DCT1, recruit the iron and export it into the cytosol [112, 113]. After entering the cytosol, iron is used for four different purposes: 1) First, iron is used to generate heme or assembled with sulfur to generate Fe-S clusters in cytosol [114]. These Fe-S clusters facilitate the maturation of cytosolic and nucleic proteins, and participate in enzymatic activities including ribonucleotide reductase [115]. Fe-S biogenesis is critical for Iron regulatory proteins (IRPs) that regulate iron homeostasis and will be discussed in next section. Secondly, iron is transported into the mitochondria by a mitochondria

iron importer and produces the Fe-S cluster and heme inside the mitochondria [116, 117]. Thirdly, other irons, assisted by a chaperone protein named PCBP1, are sequestered by the iron storage protein ferritin [118]. And lastly, the rest of the iron in the cytosol is exported by ferroportin, also called SLC40A1, IREG1, and MTP1, which is a used to deliver the iron into the circulating system with the help of ferroxidase [119, 120].

1.5.3 Iron regulation and homeostasis

Being one of the most essential nutrients for cell growth and proliferation, iron is involved in many redox reactions at the cellular level [121]. Iron is actively involved with deoxyribonucleic acid and neurotransmitter synthesis, and is located in many active enzymatic centers and oxygen transporters [122, 123]. Mammalian cells need iron to maintain daily functions; however, excess iron can be fatal. To maintain iron homeostasis, cells created three protective mechanisms to systematically regulate iron content and iron related proteins in cytosol. Two cytosolic iron regulatory RNA binding proteins (IRPs) IRP1 and IRP2, serve as the first protective mechanism to maintain iron homeostasis. They recognize iron regulated elements (IREs) in a sequence and structure specific manner [124, 125]. IREs are the sequences of untranslated regions of mRNA that are related to iron transport and storage. Acting like an iron sensor, IRP1 senses the iron status via an Fe-S switch mechanism in the cytosol [126]. When iron content is limited, and Fe-S clusters is low, IRP1 is activated to be converted into IRE-binding proteins, which speed up the cellular iron uptake and slow down the rate of iron sequestration through the stabilization of transferrin 1 mRNA and the suppression of ferritin synthesis. When iron content is not limited, 4Fe-4S is completely developed and IRP1 cannot bind RNA rather as a cytoplasmic aconitase with the enzymatic functions [127]. The difference between IRP1 and IRP2 is that IRP2 does not have Fe-S clusters and is degraded and ubiquinated while iron is in excess. A second protective mechanism to maintain iron homeostasis is that cytosolic iron can be

sequestered by ferritin. Ferritin is a cage compound with 24-subunits of two types of chains (heavy and light chains), which store 4500 iron atoms and change iron into a bioavailable can form when iron is needed. As we know now, in the cytosol, iron regulation is maintained by IRPs and ferritin. However, outside the cells, another protein hepcidin, a circulating peptide hormone, regulates cellular iron homeostasis in the circulation. These regulations relate to the macrophage iron recycling, hepatocyte iron mobilization, erythroid iron need, hypoxia and iron deficiency or overload [128-130]. Hepcidin can be expressed by the liver, heart, and pancreas [131], and is elevated when iron is over-loaded in animals [130]. One study suggested that hepcidin mainly participates with cellular iron export and is functionally linked with the iron exporter ferroportin, by triggering its internalization and deprivation inside the lysosomes [132].

1.5.4 Iron and diseases

The process of iron trafficking and iron homeostasis demonstrates the importance of iron regulation at the cellular level. Iron dysregulation, caused by either iron deficiency or iron excess, can cause health problems. A consequence of disturbed iron homeostasis is neurodegenerative diseases. It is believed that the reactive oxygen species (ROS) generated by excess iron may cause brain cell death. For instance, several studies revealed that patients with Alzheimer's disease or Parkinson's disease have a dramatic increase in their brain iron content [133, 134]. On the other hand, imaging studies have indicated that iron levels in the substantia nigra of restless leg syndrome (RLS) patients are decreased [135]. Iron dysregulation not only contributes to multiple neurodegenerative diseases [136], but plays a critical role in the carcinogenesis of human malignant cancers [137]. It is known that excess iron causes oxidative damage through the generation of free radicals as the Fenton reaction described: $Fe^{2+} + H_2O_2 \rightarrow Fe^{3+} + OH\cdot + OH^-$, $Fe^{3+} + H_2O_2 \rightarrow Fe^{2+} + OOH\cdot + H^+$. Free radicals can further cause the generation of reactive oxygen species, which can modulate carcinogenesis involved with genetic mutations, by

activating carcinogens and by subsequent selective expansion of mutated cells [137, 138]. Iron can also help to maintain the growth of malignant cells as well as growth of pathogens [139, 140]. Glioma cells, like other malignant tumor cells, share a common characteristic of having a robust appetite for iron uptake to meet their increased energy requirements associated with their rapid growth [137]. Moderate elevation of body iron levels increases the risk of cancer for humans [141]. It is a challenge to maintain iron homeostasis. Three protective mechanisms, IRPs, ferritin and hepcidin are responsible for regulating iron homeostasis at the cellular level. In the present study, one of these protective mechanisms involving the iron storage protein ferritin will be addressed. Our intension is to lower the protective function by down regulating ferritin, while at the same time sensitizing cancer cells to have an increased susceptibility to anticancer drugs.

1.6 Ferritin

1.6.1 The properties of ferritin

Iron's importance makes the iron storage protein **ferritin** especially important. Ferritin has been intensively studied regarding its characteristics, structure, and functionalities [103, 142]. It is generally considered to be a cage compound, capable of storing 4500 ferric atoms, and consists of 24 subunits with two types of chains: heavy chain ferritin (H-ferritin) which is acidic (MW 21 kD), and light chain ferritin (L-ferritin) which is basic (MW 19 kD) as shown in **Figure 1.8**. The difference between H- and L-ferritin is that H-ferritin contains a ferroxidase site that is able to oxidize the ferrous Fe^{2+} to ferric Fe^{3+}. L-ferritin does not contain a ferroxidase site, but is able to adjust the microenvironment to take up more iron by iron nucleation [103]. The common characteristic of heavy and light chain ferritin is that both provide harbor for the storage of iron; however, H-ferritin stores iron temporarily, while L-ferritin may store iron for a longer period of time. Intracellular ferritin synthesis is regulated at both the transcriptional and translational level

in an iron-dependent/iron-independent manner [143]. At the translational level, iron tightly regulates ferritin synthesis through IRPs and IREs [124, 125, 144]. The ratio of H-and L-ferritin can be adjusted depending on the specificity of organs [145]. Ferritin tightly regulates the intracellular availability of iron in aerobic or anaerobic organisms and is thus essential to cell viability [146]. Importantly, homozygous lethal mutants for the H-ferritin gene *(Fth)* die in utero between 3.5 and 9.5 days of gestation [147], which suggests a cytoprotective role of ferritin that has further been recognized by several other studies described in a review by Orino [103]. Ferritin can be found located in the cytosol, mitochondria and nucleus, and plays a critical role in inflammatory, malignant and metabolic diseases in domestic and farm animals [103]. This is because of oxidative stress-mediated damage, which is regulated by iron status. The most detrimental are the free radicals generated by excess iron in the "Fenton reaction", as it was mentioned in the preceding sections.

1.6.2 H-ferritin as a target gene and the rationale

1.6.2.1 H-ferritin protect DNA

The rationale for consideration of ferritin as a potential target for gene therapy, is based on the discovery of over expression of one of the ferritin subunits, H-ferritin, in the nuclei of glioma cancer cells [2]. Furthermore, previous studies exposed that H-ferritin mRNA was elevated in cancer cells including metastatic lung carcinoma and cervical cancer Hela cells [148]. Overexpression of nuclear ferritin was also identified in leukaemia K562 cells [149] and ovarian cancer cells [150]. Ferritin expression in breast cancer tissue has been shown to be six-fold higher than normal or benign breast tissue [3, 4]. Ferritin is also over expressed in non-small-cell lung cancer tissue [151]. Expression of H-ferritin mRNA is additionally associated with clinical and histopathological prognostic indicators in breast cancer [152]; ferritin expression was enhanced in

breast carcinoma tissue and paralleled the degree of malignancy [153]. Ferritin, based on its functionality at both the genetic and cellular levels, was considered to play an important role in cancer development [154-156]. The most important evidence from our laboratory is that H-ferritin has been found to be over expressed in the nucleus of astrocytoma tumor cells, where it appears to interact with DNA and protect DNA from oxidative damage and promote transcription [1, 2, 5]. Nuclear ferritin has also been reported to protect DNA from UV damage in corneal epithelial cells [157-159]. Ferritin was also demonstrated to affect gene transcription, with activation of globin gene expression observed [6].

1.6.2.2 H-ferritin related with drug resistance

In addition to its cytoprotective functions, ferritin appears to also be involved with drug resistance. Drug resistant cell lines were observed to have an over expression of the ferritin gene. In hydroxyurea resistant cell lines, which were obtained through multiple exposures of Hela, Chinese hamster ovary, and rat L6 cells to hydroxyurea, ferritin mRNA expression was elevated compared to controls [20]. Furthermore, murine erythroleukemia cells transfected with H-ferritin commensurately acquired multidrug resistance properties [19].

1.6.2.3 H-ferritin related with the immune suppression

Antibodies to placental immunoregulatory ferritin (PLIF) with transfer of polyclonal lymphocytes arrested MCF-7 human breast cancer growth in a nude mouse model [15]. The biological function of ferritin goes far beyond its role as an iron storage protein, in that it has been shown to play a role in immune regulation [18]. First, iron as a cofactor, has been shown to be required for the proliferation and differentiation of cells for the immune system [12]. Secondly, overexpression of H-ferritin negatively regulated human and murine hematopoiesis *in vitro* [13,

160] and *in vivo* [160]. Thirdly, H-ferritin has been shown to inhibit the proliferation of T cells in response to mitogens and damage the maturation of B cells [17]. The immunosuppressive function of ferritin, suppressed function of lymphocytes, has also been demonstrated *in vitro* [16]. Melanoma cells were demonstrated to secrete H-ferritin the media, which has immunosuppressive effect during the progression of melanoma [14].

1.6.2.4 H-ferritin related with apoptosis

Besides serving as an immune regulator, H-ferritin is additionally involved with apoptosis. H-ferritin acts as an anti-apoptotic protein to protect the liver from ischemia-reperfusion injury [8]. In contrast, antisense ferritin oligonucleotides inhibits the growth and induced apoptosis of human breast carcinoma cells [11]. H-ferritin was also shown to be able to hinder the apoptotic pathway through inhibition of JNK activation, and then limited the signaling cascade pathway involving caspase-8 activation [9]. Upregulation of H-ferritin by NF-κB similarly inhibits TNF-α induced apoptosis in NF-κB/RelA null cells [10], while H-ferritin siRNA increased apoptosis in human mesothelial and mesothelioma cells [7].

1.6.2.5 H-ferritin is a target

Based on well documented evidence, we anticipate that down regulation of H-ferritin by siRNA in glioma cancer cells will likely offer a novel mechanism to increase the sensitivity of these cells to chemo/radiation. This mechanism involves removing the protective effects of H-ferritin on DNA; reversing drug resistant properties, activating apoptotic pathways, and possibly increasing immune abilities.

1.7 Cationic liposomes (C-liposomes)

1.7.1 The structure of liposomes

Liposomes are closed tiny vesicles of a lipid bi-layer that is self-formed in an aqueous environment, and were first discovered in 1961 by the British doctor Alec D. Bangham. Liposomes are composed of similar materials that make up cell membranes, phospholipids. Thus liposomes exhibit all of the characteristics demonstrated by a cell membrane. Liposomes are amphiphilic due to its structural building block of a polar (hydrophilic) head connected to an elongated nonpolar (hydrophobic) tail. The bi-layer is formed on the outside and inner surfaces. The heads of each building block line up to form the surface face, and are attracted to water. The tails of each building block line up to form the inner surface. The bi-layer inner surface are faced and attracted each other and away from water.

1.7.2 The characters of liposomes

The following six distinct features of liposomes make them safe and efficient gene/drug carriers of great potential. 1. They can be formulated by all kinds of single or mixed phospholipids, including phosphatidylethanolamine from nature [161], non phospholipids DC-cholesterol lipids from synthetic sources [162], or pure surfactant components like DOPE [163]. 2. Their size can be adjusted to be very small (on the nanometer scale) [164]. 3. Drugs/gene can be encapsulated into liposomes during their preparation [165, 166]. 4. Its surface can be modified to be positively or negatively charged according to what is needed. 5. The surface of liposomes can be conjugated with antibodies [167, 168] or ligands [165], which provide the possibility of specific targeting of liposomes for the treatment of cancer and other chronic diseases. 6. Since its composition is similar to biological cell membranes that are biodegradable, there is no cytotoxicity or anti-immunity associated with their use [169] in contrast to other gene delivery tools, including viral, polymer, dendrimers and quantum dots. The liposomes without positive or

negative charges are neutral liposomes that often used for drug delivery. The liposomes made by the lipids, carried the positive charges, are able to complex with negative charged gene siRNA/DNA through static electricity, and are cationic liposomes. Cationic liposomes as gene delivery vehicle are based on the fact that phosphorous backbones of DNA/siRNA are negatively charged. In present study we only used cationic liposomes.

1.7.3 The application of cationic liposomes

In 1987, Felgner and colleagues first used synthetic cationic liposomes as a DNA carrier composed of the lipid N-[1-(2,3-dioleyloxy) propyl]-N,N,N-trimethylammonium chloride (DOTMA) [170]. Although this was only a monocationic lipid, the liposomes were described as a simple, efficient and highly reproducible gene delivery tool in a simian kidney cell line. Two years later, the same group reported that cationic liposomes of DOTMA or lipofectin efficiently transfected DNA/RNA into rat, mouse, Xenopus, and Drosophila cells [171, 172]. Fabricated monocationic or bicationic lipids were used in the preparation of liposomes by Nejet and colleagues, who prepared five different types of liposomes: lipofectin, lipofectamine, cellfectin, DC-cholesterol and DMRIE-DOPE. The ability of these liposomes to deliver DNA was compared in subcutaneous human tumor xenografts in SCID mice. Among these five liposomes, DC-cholesterol was found to be superior for transfection *in vivo* [173]. The cationic liposome "Lipofectmine 2000" was a successful DNA/siRNA gene delivery tool with high transfection efficiency if the cell density, ratio of liposomes/DNA, the time of liposome/DNA complexing and the presence or absence of media components such as antibiotics and serum could be handled properly [174]. This paper also discussed that Lipofectamine 2000 can be applied for the transfection of primary neurons, which provides potential for the treatment of neurodegenerative diseases.

Cationic liposomes formulated by other monocationic lipids such as DOTAP (1,2 Dioleoyl-3-trimethylammonium-propane), could send siRNAs into various cell types efficiently. Through the comparison of freshly isolated human monocytes and mouse cells, siRNAs could activate non-specific pathways in freshly isolated human monocytes and increase TNF-alpha and IL-6(Interlukin-6) production. Their results indicated that certain siRNA sequences could activate innate immunity response genes that can be beneficial for the treatment of cancer [169].

One investigator suggested that "Liposome-mediated RNA transfection should be used with caution", and described that reporter mRNAs introduced into HeLa cells by cationic liposomes by the lipofection-protocol do not present the expected behavior [175]. Thus, we should be aware of this fact and use liposomes with caution. However, another study carried out by Grayson and colleagues demonstrated that the conditions, reagent selection, and experimental design, for a successful performance of siRNA are all critical in HeLa and NIH/3T3 cells [176].

Cationic liposomes of DC-cholesterol /DOPE prepared with other agents such as ethanol helped in the release of DNA [177], while combination with vitamin D 6 increased the yield of liposomes.

1.7.5 The cationic liposomes of DC-Cholesterol/DOPE

Bicationic lipids are an even more successful formulation for the composition of cationic liposomes as gene delivery tool. Back in 1991, Gao and colleagues were the first group use bicationic lipids, DC-Cholesterol/DOPE (ratio 1:3), its formulation as shown in **Figure 1.9,** to prepare cationic liposomes of, that were used in A549 human carcinoma cells. Cationic liposomes of DC-Cholesterol/DOPE were compared with lipofectin and were less toxic and more efficient than lipofectin [178]. Two human gene therapy clinical trials using cationic liposomes of DC-Cholesterol/DOPE as DNA delivery tool, were conducted four years later [179]. Liu and

colleagues composed cationic liposomes of DC-Cholesterol/DOPE lipids with Tween-80, which as a surfactant component which appeared to have more favorable physical and biological activities than traditional cationic liposomes as a carrier for DNA delivery [180]. The transfection efficiency of cationic liposomes of DOPE/DC-cholesterol lipids in tracheal epithelial cells strongly correlated with the charge ratio of liposomes/DNA, which was evaluated using transmission electron microscopy and confocal laser scanning microscopy [181]. As cationic liposomes of DOPE/DC-Cholesterol bicationic lipids have been widely used as DNA carrier, its properties have been further investigated. The thermodynamic properties of liposomes were studied in detail by Miller's group through various methods including the combination of isothermal titration calorimetry, circular dichroism, photon correlation spectroscopy, and a turbidity assay. Through the comparison of DC-Cholesterol/DOPE and CDAN/DOPE (ratio1:1), it was determined that DC-Cholesterol/DOPE (ratio 3:2) was optimal when experiments were performed in serum free media [163]. Fast digesting the complex of cationic liposomes/DNA by serum within short period of time promoted a goal to increase the circulate time of the complex in the blood. This goal was reached by one group, Choi and colleagues prepared cationic liposomes of DC-cholesterol/DOPE in Castor-Oil/Tween-80, which demonstrated prolonged circulating time in blood, and prolonged expression in various tissues, compared with cationic liposomes of DC-cholesterol/DOPE [182]. B717 siRNA delivered by cationic liposomes of LIC100 successfully down regulated bcL-*2* and increased the cytotoxicity of tumor cells *in vitro,* and inhibited the growth of prostate cancer in a mouse model [183]. Cationic liposomes of DC-Cholesterol/DOPE bicationic lipids demonstrated better characteristics for DNA transfection, compared with DOTAP based liposomes on parameters of electrons spin resonance spectroscopy and zeta potential [184]. The charge issue is an important parameter of transfection efficiency, as previously addressed [181]. We learned that cationic liposomes of DC-cholesterol/DOPE efficiently transfected DNA into the rat glioma C6 cell line [185], and the **ratio** of

liposomes/DNA [185] and **zeta potential** were again emphasized as important parameters [184] as first addressed by Dalby [174]. Cationic liposomes of DC-cholesterol/DOPE bicationic lipids provided a much better DNA transfection efficiency, than liposomes of DDAB/DOPE lipids in rat glioma C6 cell line [186], when energy dispersive diffraction techniques and the role of serum on the size of lipoplexes were studied by dynamic light scattering. Serum was found to affect the size of lipoplexes, and the structure of cationic liposomes offered static spaces, both of which are important factors affecting transfection efficiency. Cationic liposomes of DC-cholesterol /DOPE bicationic lipids were prepared with other agents like ethanol to help release DNA [177], or vitamin D6 to increase its yield. One investigator pointed out that the mechanism of transfection of siRNA and pDNA are different when cationic liposomes of DC-cholesterol/DOPE. DC-Cholesterol/DOPE/pDNA (1:2 molar ratio) or DC-Cholesterol/DOPE/pDNA (1:1 molar ratio) are utilized. The transfection efficiency of DC-Cholesterol/DOPE liposomes increased along with the increased weight ratio of DC-Cholesterol/siRNA. However, the transfection efficiency of DC-Cholesterol/DOPE liposomes decreased along with the increased weight ratio of DC-Cholesterol/pDNA [187]. The molar ratio of liposomes/siRNA or DNA affects the final characteristics of the complex, including size, zeta potential, stability and reproducibility, and thereby reflects the transfection efficiency [188].

1.7.6 The cationic liposomes of DC-cholesterol/DOPE served in present study

In summary, cationic liposomes of DC-cholesterol/DOPE were found to be an attractive gene siRNA/DNA delivery tool, with better transfection efficiency than the other liposome varieties reviewed above [163, 178, 186, 189]. Cationic liposomes of DC-Cholesterol/DOPE demonstrated superior performance in terms of zeta potential [184], less toxicity [189], a lack of a negative immune response [169] and reasonable static space shape [186].

Thus, cationic liposomes of DC-cholesterol/DOPE (molar ratio of 2:1), the structure as shown in **Figure 1.10**, were selected as a siRNA delivery tool for this project based on the previous studies mentioned in the former paragraph, as well as our nanotechnology platform that uses neutral liposomes conjugated with Interleukin-13 to effectively deliver doxorubicin to glioma cells [165]. The C-liposomes in the present study and the neutral liposomes we have used previously share some common physical properties. Both were simple to prepare in the nanometer scale with similar methods, non-toxic, and have high transfer efficiency. Both liposomes are internalized by glioma cells through endosomal pathways. However, the C-liposomes were synthesized with positively charged lipids so they were capable of forming a complex with siRNA by electrostatic interaction [178, 179]. Cytotoxicity and transfection efficiency of C-liposomes depend on the uniformity of their size. In the process of preparation, C-liposomes were extruded multiple times with various sized filters to result in a uniform size, which contributed to a transfection efficiency of up to 95%. The even size distribution of the C-liposomes diminished the chance of aggregation and toxicity, consistent with previous studies [179, 186].

1.8 Figures and legends

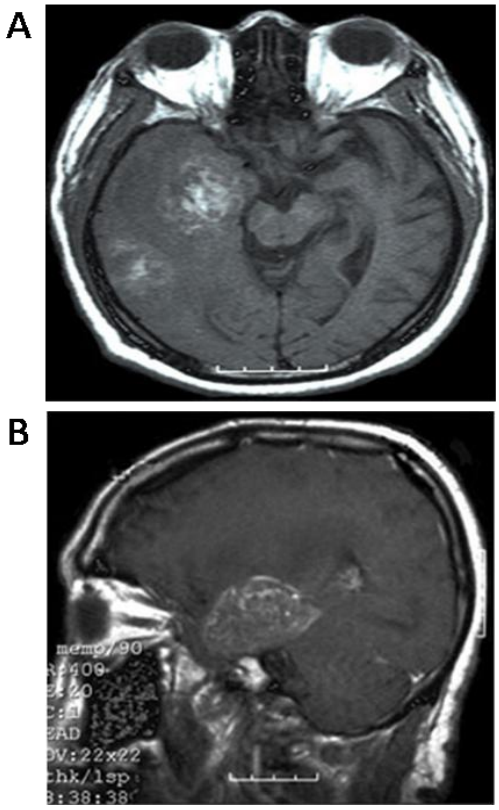

-Jeffrey N Bruce and Edgar M Housepian, Oct. 2009

Figure 1.1. Gliomas. Glioma presented by magnetic resonance imaging (MRI). **A,** T1-weighted axial MRI without intravenous contrast. This image demonstrates a hemorrhagic multicentric tumor (glioblastoma multiforme [GBM]) in the right temporal lobe. Effacement of the ventricular system is present on the right, and mild impingement of the right medial temporal lobe can be observed on the midbrain. **B**, T1-weighted sagittal MRI with intravenous contrast in a patient with GBM.

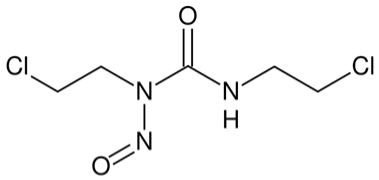

Systematic (IUPAC) name
N,*N*′-bis(2-chloroethyl)-*N*-nitroso-urea

Figure 1.2. **BCNU.**

Its formula: $C_5H_9Cl_2N_3O_2$, molecular mass: 214.049 g/mol.

Chemical Degradation of Nitrosoureas Leading to Alkylating Products
Source: Lemoine et al. (1991)

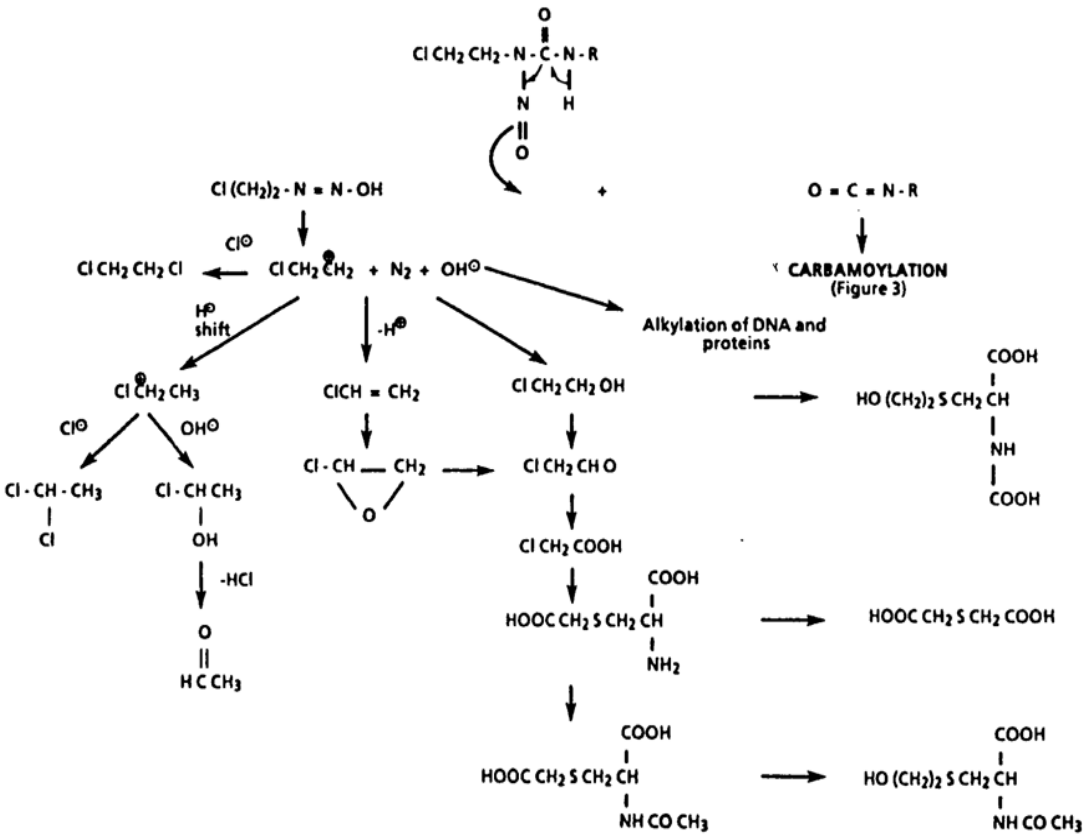

The chemical degradation of nitrosoureas leading to alkylating products, as described by Colvin *et al.* (1976), and some of the subsequent glutathione adducts.

Figure 1.3. The decomposition of BCNU. First, Chloroethyldiazohydroxide $Cl(CH_2)_2$.N=NOH is generated from BCNU. Second, Chloroethyl carbonioum iron $ClCH_2CH_2$• is produced from Chloroethyldiazohydroxide. Carbonioum iron alkylated DNA through adding alkyl adduct to the O^6-guanine.

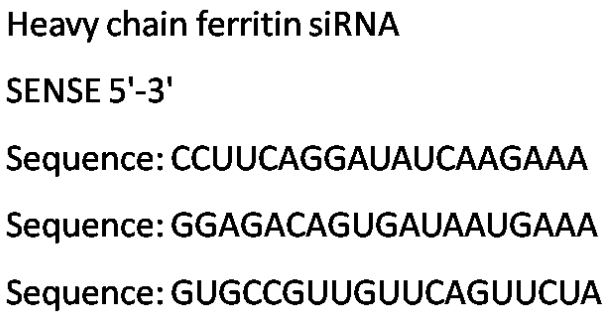

Figure 1.4. The sequences of heavy chain ferritin siRNA. The H-ferritin siRNA is a pool of 3 target specific 19 nu siRNAd designed to knock down H-ferritin gene expression. Generated by Santa Cruz Biotechnology Inc.,cat.no. sc-40575. Molecular weight: 13000 g/mole.

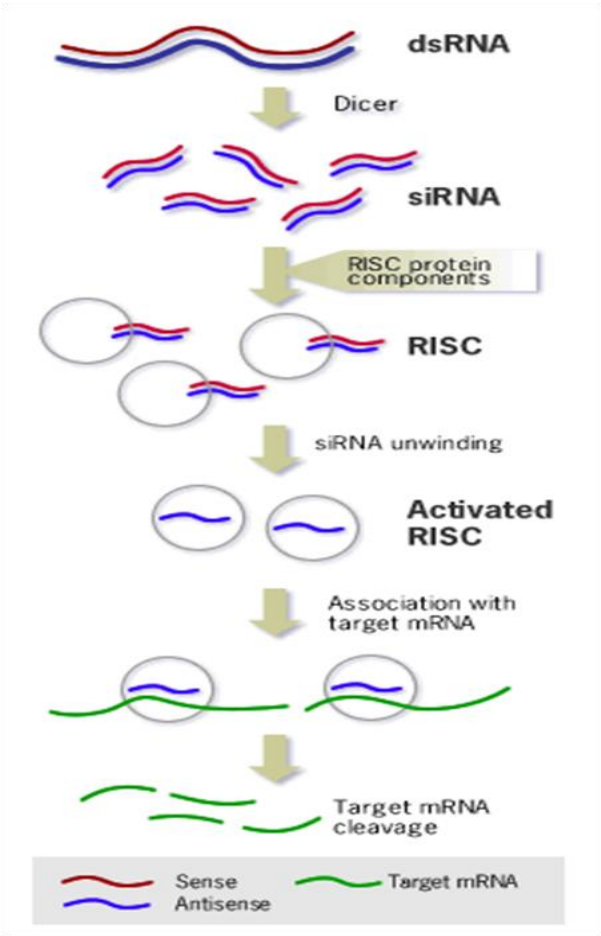

Figure 1.5. The mechanism of siRNA. An RNase III-like enzyme known as Dicer processes dsRNA into small interfering RNA (siRNA) 20-25 nucleotides in length. Then, endoribonuclease-containing complexes known as RNA-induced silencing complexes (RISCs) will assemble with the siRNA and unwind it. The unwound siRNA will guide the RISCs to complementary cognate messenger RNA molecules, and then cleave the cognate RNA.

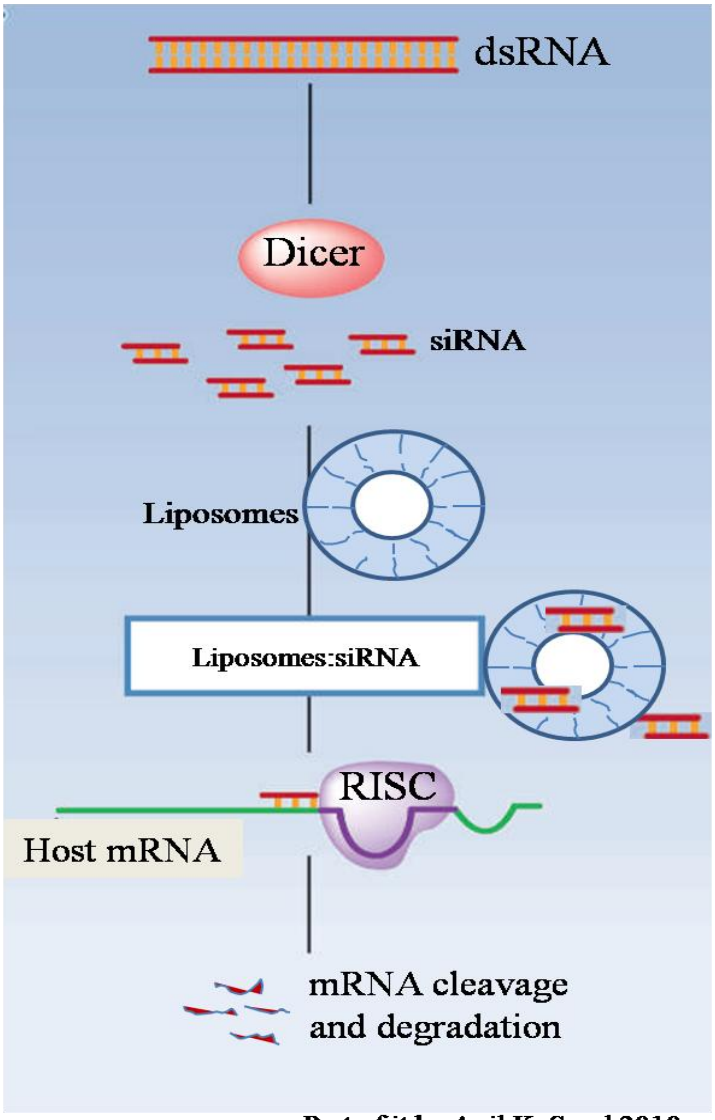

Figure 1.6. The mechanism of C-liposomes:siRNA. The siRNA is encapsulated into C-liposomes to generate the C-lipoosmes:siRNA complexes, which will enter cells. SiRNA will recruit the RISC and recognize the cognate mRNA that will be cleaved and destroyed sequentially.

Iron Fe, its atomic number is 26.

The atomic structure of iron is as following:

(The blue color indicates the outer most shell).

For Fe^{o}; **$1S^2\ 2S^2\ 2P^6\ 3S^2\ 3p6\ 4S^2\ 3d^6$** (outer most shell)

For Fe^{2+}; **$1S^2\ 2S^2\ 2P^6\ 3S^2\ 3p6\ 4S^1 3d^5$** (outer most shell) **-2e**

For Fe^{3+}; **$1S^2\ 2S^2\ 2P^6\ 3S^2\ 3p^6\ 3d^5$** (outer most shell) **-3e**

Fenton reactions;

$$Fe^{2+} + H_2O_2 \rightarrow Fe^{3+} + OH\cdot + OH^-$$

$$Fe^{3+} + H_2O_2 \rightarrow Fe^{2+} + OOH\cdot + H^+$$

Figure 1.7. Properties of iron and the Fenton reactions.

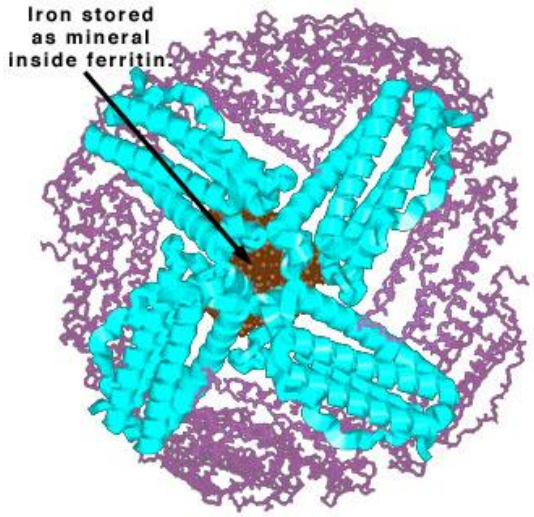

-Rachel Casiday and Regina Frey, Nov. 2000

Department of Chemistry, Washington University St. Louis, MO 63130

Figure 1.8. Ferritin is an iron storage protein. Ferritin is a 450 kDa iron storage protein consisting of 24 subunits with two types of chains, heavy chains (21 kD) and light chains (19 kD). Ferritin is a spheroid and able to store 4500 iron atoms. Ferritin stores iron and releases it in a controlled manner. For storing iron in ferritin, Fe (II) is oxidized to Fe (III) by ferroxidase on H-ferritin. This process is also described as nucleation in other literature. After nucleation, Fe (II) is incorporated in the mineral ferrihydrite, $[FeO(OH)]_8[FeO(H_2PO_4)]$, which is attached to the inner wall of the sphere. To release bioavailable iron, Fe (III) is reduced to Fe (II), which leaves through channels in the spherical structure. Thus, the most important property of ferritin is its structure, which is capable of storing and releasing iron in a controlled manner through channels in the spherical structure. An enchanting property of Ferritin is its cage compound like structure that makes the compound unique.

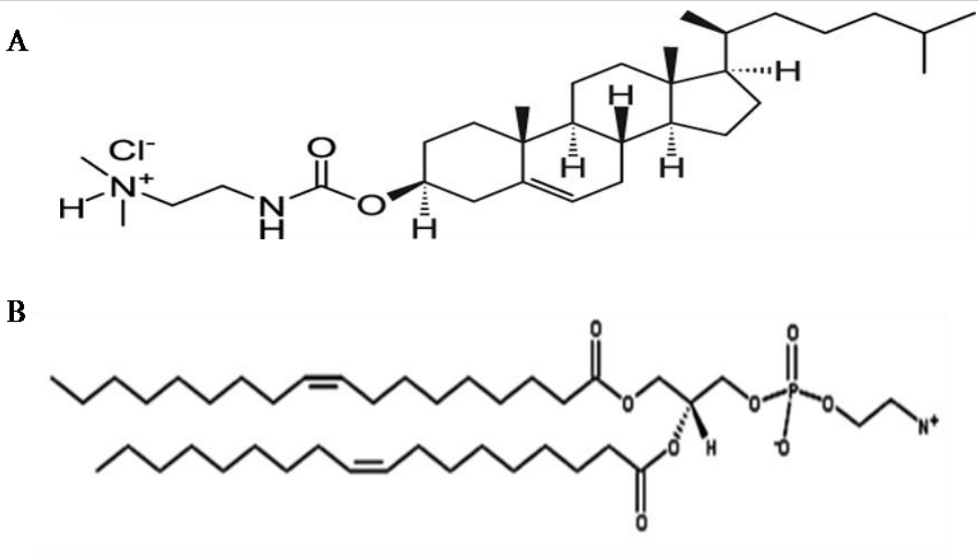

Figure 1.9. Lipids for the building blocks of the C-liposomes.

A, 3ß-[N-(N',N'-dimethylaminoethane)-carbamoyl]cholesterol hydrochloride (DC-Cholesterol•HCl). Formula: $C_{32}H_{57}N_2O_2Cl$. Molecular Weight: 537.2 g/mole.

B, 1,2-dioleoyl-sn-glycero-3-phosphoethanolamine (DOPE).

Molecular Formula: $C_{41}H_{78}NO_8P$. Molecular weight: 744.034 g/mole. The building blocks of C-liposomes in this project are a blend of DC-Cholesterol/DOPE (30:70 w/w). This blend possesses good properties from both components, which make it a potential gene delivery vehicle.

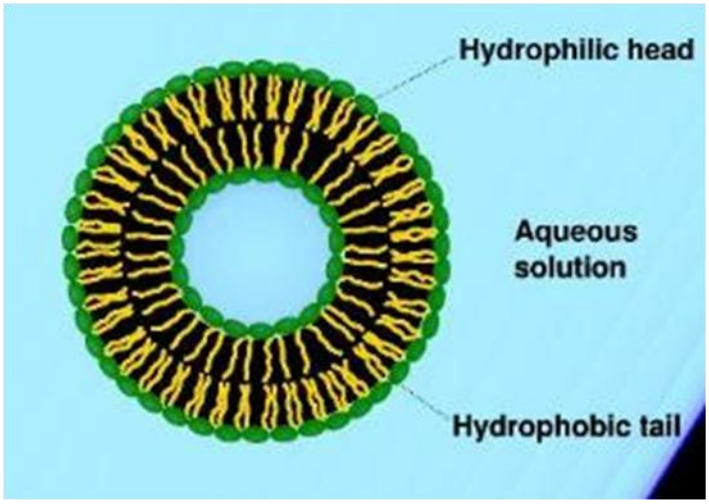

Figure 1.10. The structure of C-liposome. The green color is representative of hydrophilic heads. The yellow color is representative hydrophobic tails. Most of the siRNAs is encapsulated in the center of the C-liposome and in the double layer of two building blocks. The siRNA is protected inside the C-liposome.

Chapter 2

Development and Characterization of Cationic Liposomes

2.1 Introduction

In this chapter, the experimental procedures for the preparation and characterization of cationic liposomes (C-liposomes) will be described and illustrated in detail. Three major steps required for the use of C-liposomes will be discussed, including: first, the development and characterization of C-liposomes, secondly, the development and characterization of a complex containing C–liposomes with siRNA (C-liposome:siRNA) and lastly, the development of a specific targeting treatment of glioma using Interleukin-13 conjugated maleimide cationic liposomes with siRNA (IL-13-M-C-liposomes:siRNA).

To formulate C-liposomes as a siRNA delivery vehicle for this project, DC-Cholesterol/DOPE lipids with a ratio of 30:70 (w/w) were selected. Insight from the literature [1-4], regarding the desirable chemical compositions and physical properties of DC-Cholesterol/DOPE lipids, along with extensive prior experience of our laboratory in the use of liposomes as a drug delivery system [165, 166], made this an excellent choice for a delivery system. C-liposomes composed of DC-Cholesterol/DOPE lipids were first used by Gao et al for DNA delivery in 1991 [178], and are considered to be one of the most efficient gene delivery systems [186, 190]. After twenty years of research in this area, the biochemical and structural properties of these lipids are well understood. For the formation of C-liposomes [191], both DC-Cholesterol and DOPE provide sufficient positive electrical charges that can be measured macroscopically as zeta potential. The DOPE component is made of two seventeen-carbon-

hydrogen chains that form a hydrophobic tail, to provide a static space for holding gene cargo, such as DNA or siRNA, in an intact form inside the C-liposomes. The biodegradable DC-cholesterol, on the other hand, is composed of three six-carbon rings and one five-carbon ring that provide structural stability and high hydrophobicity to stabilize the C-liposome and increase its half life. One study demonstrates that the hexagonal conformation of C-liposomes comprised of DC-Cholesterol/DOPE lipids is considered a critical structural property for efficient endosomal escape of genetic cargo [186], which promotes transfection efficiency. Another study revealed a correlation between structure and transfection efficiency [185]. An additional study compared the transfection efficiency of five different cationic liposomes during *in vitro* gene transfer into human epithelial tracheal cell lines, and revealed a dramatic correlation between transfection efficiency and charge ratio, due to the morphological or structural changes of DC-Cholesterol/DOPE lipid [181]. DC-Cholesterol/DOPE is considered to be the most effective liposome formulation because of its composition [181]. For example, the structure affects the thermodynamic aspect and the index of biological properties [163, 181]. The molar ratio of DC-Cholesterol vs. DOPE is another key factor affecting the transfection efficiency. One group revealed that the most efficient molar ratio of DC-Cholesterol and DOPE in C-liposomes was 1:2 for pDNA delivery, and 1:1 for siRNA delivery, respectively [187]. Our laboratory has previously utilized neutral liposomes conjugated with Interleukin-13 to deliver doxorubicin to glioma cells specifically and effectively. This led to a successful suppression of intracranial tumor growth in an *in vivo* athymic nude mouse glioma model [165, 166]. With our experience in preparing the C-liposomes, we have concluded that the actual preparation processes plays a crucial role in the transfection efficiency. For example, the use of different sized filter membranes, as well as the number of times for which C-liposomes are passed through the extruder, plays an important role in transfection efficiency. In addition, the experimental conditions of the transfection itself,

including whether the transfection is processed with or without serum, is a critical factor that can affect the transfection efficiency of C-liposomes.

Overall, DC-Cholesterol/DOPE lipids exhibit suitable properties for the formulation of C-liposomes. The experimental results that are presented in the subsequent chapters demonstrate that the formulation of C-liposomes comprised of DC-Cholesterol/DOPE lipids provide stability and a high transfection efficiency, without any observable toxicity and inappropriate immune responses.

2.2 Materials and Methods

2.2.1 Chemicals and instruments

DC-Cholesterol/DOPE lipids (30:70 w/w) cat. no. 790625P, and Rhodamine labeled phospholipids [L-a-phosphatidylethanolamine-N-(lissamine Rhodeamine B sulfonyl) (ammonium salt)] were purchased from Avanti Polar Lipids (Alabaster, AL). BCNU (Carmustine) was purchased from Sigma Chemical (MO). H-ferritin siRNA (a combination of three different sequences), siRNA Fluorescence in Conjugate-A, and early endosomal antigen antibody (EEA1), were all purchased from Santa Cruz Biotechnology, CA. Non-specific (NS) siRNA was purchased from Qiagen Science, MD. The H-ferritin antibody was a gift from Paolo Arosio (Milan, Italy). Female adult athymic nude mice were acquired from Charles River Laboratories. Chamber slides were purchased from Nalge Nunc International, IL. Agarose 3:1HRB^{TM}CODE:E776-100G Amresco, Ohio. Criterion 4-20% gel, protein quantitation kit, protein loading buffer were all obtained from BIO-RAD, and PVDF was ordered from Westran S (cat. no. 10413096). Polycarbonate membranes, (50 nm cat. no. 110603 and 100 nm cat. no. 110605), were purchased from Whatman. A rotary evaporator (Rotavapor R210, HeatingBath B491) was acquired from Buchi, Switzerland, while a sonicator and extruder (Lipex extruder)

was from Northern Lipids, Inc., Vancouver, British Columbia, Canada. Ribonuclease A (RNase A) was purchased from Roche cat. no. 1010 9142 001. The mounting fluid purchased from Electron Microscopy Sciences cat. no. 17985-10.

2.2.2 Cell culture

The human glioma cell lines U251 and U87, human malignant peripheral nerve sheath tumor (MPNST) cell line NF96.2, and breast cancer cell line MCF-7, were acquired from ATCC (American Type Culture Collection, Rockville, MD). U251, U87 and MPNST cells were maintained in DMEM (Dulbecco's modified Eagle medium cat. no. 11885, GIBCO, CA) supplemented with 10% FBS (v/v), 0.1% (v/v), Gentamicin Reagent Solution (cat. no.18750-060 GIBCO, CA), and 1% (v/v) Non-Essential Amino Acid Solution, cat. no. M7145, Sigma. MCF-7 cells were maintained in MEM (cat. no. 11095, GIBCO) supplemented with 10% FBS (v/v), and 0.1% (w/v) insulin from bovine pancreas, (cat. no. 16634 GIBCO). All cells were maintained in a humidified atmosphere at 37°C with 5% CO_2.

2.2.3 Preparation of C-liposomes

To formulate C-liposomes, the DC-Cholesterol/DOPE lipids were dissolved in methanol/chloroform (1:1 v/v) and subsequently rotary evaporated to obtain a lipid film, which was dried over Nitrogen for 10 minutes at room temperature, and further dried at 4^{o} C in a desiccator overnight. The lipid film was hydrated with PBS (2.8 mg/mL w/v), and then sonicated in a bath-type sonicator for 10 minutes. In order to produce small unilamellar vesicles, different polycarbonate membranes with decreasing pore sizes were utilized. Vessicles were formed by extrusion through a 0.1µm polycarbonate membrane in conjuction with a 0.05 um polycarbonate membrane using a nitrogen pressure–operated extruder (Lipex extruder, Northern Lipids, Inc.,

Vancouver, British Columbia, Canada). All the extrusions were performed for a total of 10 times at an operating pressure of 800 p.s.i. (5,440 kPa). To study cellular uptake, the C-liposomes were labeled with rhodamine by adding rhodamine-labeled phospholipids [L-a-phosphatidylethanolamine- N-(lissamine Rhodamine B sulfonyl) (ammonium salt) to the DC-Cholesterol/DOPE lipids (30:70 w/w) in a 1% molar ratio.

2.2.4 Characterization of C-liposomes

2.2.4.1 The size and zeta potential of C-liposomes

The size distributions of C-liposomes and IL-13 conjugated maleimide cationic liposomes (IL-13-M-C-liposomes) were determined by light scattering analysis through an ALV/DLS/SLS-5022F compact gonimeter system (ALV, Germany). The zeta potential and poly dispersity index of C-liposomes were measured by PALS Zeta Potential Analyzer Ver. 3.16, Brookhaven Instruments Corp.

2.2.4.2 Complex formation of C-liposomes with siRNA

To determine the optimal ratio of components in the C-liposome-siRNA complex, a number of conditions were tested. C-lipospomes and siRNA's were mixed on ice in the following ratios: 0:1, 2:1, 3:1, 4:1, 5:1, 6:1 (C-liposomes:siRNA v/w µL/µg). Mixtures were equilibrated at room temperature for 5 minutes before 20 µL of DNA loading buffer was added. Samples were then loaded onto a 1% agarose gel and electrophoresed at 100 volts for 18 minutes in TAE buffer. Images were captured by an Image Reader (Fuji Film Las-3000).

2.2.4.3 Cytotoxicity of C-liposomes: Evaluation *in vitro* and *in vivo*

2.2.4.3.1 Cytotoxicity of C-liposomes: Evaluation *in vitro*

To evaluate the potential cytotoxic effects of the C-liposomes *in vitro*, U251 cells were seeded in 96-well plates at a concentration of 4,000cells/well and allowed to attach overnight at 37ºC. Cultures were transfected with 0, 2, 4 or 6 µL of the C-liposome stock solution (2.8 mg/mL) in DMEM serum free medium. After 3 hours culture medium was replaced with complete medium. An MTS assay was performed at 24, 48 and 72 hours post transfection.

2.2.4.3.2 Cytotoxicity of C-liposomes: Evaluation *in vivo*

Cytotoxicity of C-liposomes was also evaluated *in vivo*. Athymic nude mice were divided into three groups, with three mice/group. Control mice were injected intraperitoneally (IP) with 50 µL of PBS, while treatment group 1 received 6 µL of C-liposomes, and treatment group 2 received 6µL/1.5µg of C-liposomes:siRNA complex once/week for six weeks. After 6 weeks, blood was collected; liver and kidney toxicity, total bilirubin, blood urea nitrogen (BUN), creatine, aspartate amino transferase (AST, also called SGOT), alanine aminotransferase (ALT, also called SGPT) and alkaline phosphatase were determined using an automated chemistry analyzer and kits from Thermo Electron, Inc. following the manufacturers instruction.

2.2.4.4 Uptake of C-liposomes:siRNA

In order to visualize the uptake of the C-liposomes:siRNA complex, U251 and U87 cells were seeded at a concentration of 10,000cells/well in 8-well chamber slides and allowed to attach overnight at 37ºC. After 24 hours the cells were exposed to siRNA-FITC:DMEM (serum free media) 1µL/1mL or C-liposomes-rhodamine:siRNA-FITC:DMEM 0.5µL/1µL/1mL for 1 hour. The cells were then fixed at room temperature with 4% paraformaldehyde and washed in PBS. Cells were then stained with 1% (w/v) of DAPI (4, 6-diamidino-2-phenylindole) and mounted, dried overnight in the dark. Images were captured with confocal microscopy.

2.2.4.5 Internalization of C-liposomes by endosomal pathway

To determine whether C-liposomes are internalizing into cells by the endosomal pathway, immunocytochemistry was performed. U251 and U87 cells were seeded at a concentration of 10,000cells/well in 8-well chamber slides and allowed to attach overnight at 37ºC. After 24 hours the cells were exposed to C-liposomes-rhodamine: for 1 hour. The cells were then fixed at room temperature with 4% paraformaldehyde. Immunocytochemistry was performed using a primary antibody for an early endosomal marker EEA1 (1:15dilution) followed by a secondary FITC conjugated anti-goat IgG antibody (1:500). Cells were then stained with 1% (w/v) of DAPI and mounted, dried overnight in the dark. Images were captured through a confocal microscopy.

2.3 Characterization of complex of C-liposomes:siRNA

2.3.1 Complexation of C-liposomes with siRNA

To determine whether siRNA could be encapsulated by C-liposomes, freshly prepared C-liposomes and siRNA-FITC (v/v) were mixed on ice under the following eight conditions: (the ratio of C-liposomes:siRNA v/w µL/µg) 0:1, 1.2:1, 2.4:1, 3.6:1, 4.8:1, 6.0:1, 7.2:1 and 8.4:1. The mixtures were equilibrated at room temperature for 5 minutes and then 20 µL of DNA loading buffer was added. Samples were then loaded onto a 1% agarose gel and electrophoresed at 100 volts for 18 minutes in TAE buffer. The images were captured by an Image Reader (Fuji Film Las-3000).

2.3.2 Determination of the encapsulation by C-liposomes using RNaseA

To explore the location of the siRNA in the C-liposome:siRNA complex, the following components: C-liposomes, siRNA-FITC(v/v) and RNaseA were mixed on ice under the following

eight conditions: (the ratio of C-liposomes:siRNA: RNaseA, v/w/U µL/µg/U) 0:1:0, 4:1:0, 0:1:1.6, 0:1:3.2, 0:1:4.8, 4:1:1.6, 4:1:3.2 and 4:1:4.8. The mixtures were equilibrated at room temperature for 60 minutes and then 20 µL of DNA loading buffer was added. Samples were then loaded onto a 1% agarose gel and electrophoresed at 100 volts for 18 minutes in TAE buffer. The images were captured by an Image Reader (Fuji Film Las-3000).

2.3.3 Stability of C-liposomes:siRNA exposed in RNase A at 37^{o}C

To test the stability of the C-liposomes:siRNA related to temperature, the C-liposomes, siRNA-FITC(v/v) and RNaseA were mixed on ice under the following eight conditions: (the ratio of C-liposomes:siRNA:RNaseA, v/w/unit, µL/µg/unit. The first group of four samples (0:1:0, 0:1:1.6, 4:1:1.6, 4:1:3.2) were incubated at room temperature for 1 hour. The second group of samples (0:1:0, 0:1:1.6, 4:1:0, 4:1:1.6, 4:1:3.2 and 4:1:4.8) were incubated at 37^{o}C for 1 hour. The mixtures were equilibrated at room temperature for 5 minutes and then 20 µL of DNA loading buffer was added. The mixtures were then loaded onto a 1% agarose gel and electrophoresed at 100 volts for 18 minutes in TAE buffer. The images were captured by an Image Reader (Fuji Film Las-3000).

2.3.4 Stability of C-liposomes:siRNA exposed in human serum

To exam the stability of C-liposomes:siRNA in human serum, the C-liposomes, siRNA-FITC(v/v) and human serum were mixed on ice under the following eight conditions: (the ratio of C-liposomes:siRNA: v/w/%, µL/µg/%) 0:1:0, 4:1:0, 0:1:20, 0:1:40, 0:1:60, 4:1:20, 4:1:40 and 4:1:60. All the samples were incubated at 37^{o}C for 1 hour. The mixtures were equilibrated at room temperature for 5 minutes and then 20 µL of DNA loading buffer was added. The mixtures were then loaded onto a 1% agarose gel and electrophoresed at 100 volts for 18 minutes in TAE buffer. The images were captured by an Image Reader (Fuji Film Las-3000).

2.4 Development of Interleukin-13 conjugated C-liposomes:siRNA

In order to target C-liposome:siRNA specifically to glioma tumor cells, as well as increase the circulating time of the complex in the blood, Interleukin-13 (IL-13) was conjugated to the C-liposomes [165, 166]. This was achieved by the incorporation of maleimide and polyethylene glycol (PEG) into the C-liposomes, thereby generating maleimide C-liposomes (M-C-liposome) that can attach IL-13 covalently. Two alternative formulas were investigated for M-C-liposomes in this work and their preparation is described as followed.

2.4.1 No.1 formulation for the preparation of M-C-liposomes

All lipids were purchased from Avanti Polar Lipids (Alabaster, AL). In the No.1 formulation for the preparation of M-C-liposomes, 5.0 mg of 1,2-dipalmitoyl-sn-glycerol-3-phosphochlorine(DPPC) cat. no. 850355P, 0.5 mg of 1,2-Distearoyl-sn-Glycero-3-Phosphoethanolamine-N-maleimide Polyethylene Glycerol (DSPE-PEG-Mal) cat. no. 880126P, 0.8 mg of 1,2-Distearoyl-sn-Glycero-3-Phosphoethanolamine-N-Amino(PoluethyleneGlycecol) 2000 (Ammonium Salt, MW 279052 cat. no. 880128P (DSPE-PEG) and 8.0 mg of DC-cholesterol/DOPE were placed into a round bottom glass with a 250 mL volume. The mixture of lipids were dissolved in methanol/chloroform (1:1v/v) and subsequently rotary evaporated to obtain a lipid film, which was dried over N_2 for 10 min at room temperature and further dried at 4^o C in a desiccator overnight. The lipid film was hydrated in PBS (2.8 mg/mL w/v) and then sonicated in a bath-type sonicator at room temperature for 10 min. In order to produce small unilamellar vesicles, different polycarbonate membranes with decreasing pore sizes were utilized. Vessicles were formed by extrusion through a 0.1µm polycarbonate membrane in conjuction with a 0.05 um polycarbonate membrane using a nitrogen pressure–operated extruder (Lipex extruder, Northern Lipids, Inc., Vancouver, British Columbia, Canada). All the extrusions were performed

for a total of 10 times at an operating pressure of 800 p.s.i. (5,440 kPa). To study cellular uptake, the C-liposomes were labeled with rhodamine by adding rhodamine-labeled phospholipids [L-a-phosphatidylethanolamine- N-(lissamine Rhodamine B sulfonyl) (ammonium salt) to the DC-Cholesterol/DOPE lipids (30:70 w/w) in a 1% molar ratio.

2.4.2 No. 2 Formulation for preparation of M-C-liposomes

In the No.2 formulation for preparation of M-C-liposomes, 10 mg of 1,2-dipalmitoyl-sn-glycerol-3-phosphochlorine(DPPC) cat. no. 850355P, 1.0 mg of 1,2-Distearoyl-sn-Glycero-3-Phosphoethanolamine-N-maleimide Polyethylene Glycerol (DSPE-PEG-Mal) cat. no. 880126P, 1.6 mg of 1,2-Distearoyl-sn-Glycero-3-Phosphoethanolamine-N-Amino(PoluethyleneGlycecol) 2000 (Ammonium Salt, MW 279052 cat. no. 880128P (DSPE-PEG) and 8.0 mg of DC-cholesterol/DOPE were placed into a round glass with a 250 mL volume. The mixture of these four lipids was dissolved in methanol/chloroform (1:1v/v) and subsequently rotary evaporated to obtain a lipid film, which was dried over N_2 for 10 min at room temperature and further dried at 4^o C in a desiccator overnight. The lipids film was hydrated in PBS (2.8 mg/mL w/v) and then sonicated in a bath-type sonicator for 10 min. In order to produce small unilamellar vesicles, different polycarbonate membranes with decreasing pore sizes were utilized. Vessicles were formed by extrusion through a 0.1µm polycarbonate membrane in conjuction with a 0.05 um polycarbonate membrane using a nitrogen pressure–operated extruder (Lipex extruder, Northern Lipids, Inc., Vancouver, British Columbia, Canada). All the extrusions were performed 10 times at an operating pressure of 800 p.s.i. (5,440 kPa). To study cellular uptake, the C-liposomes were labeled with rhodamine by adding rhodamine-labeled phospholipids [L-a-phosphatidylethanolamine- N-(lissamine Rhodamine B sulfonyl) (ammonium salt) to the liposomes formulation in a 1% molar ratio.

2.4.3 Complex formation of the M-C-liposomes with siRNA

To ensure that the siRNA could be complexed with the M-C-liposomes, M-C-liposomes and siRNA-FITC (v/w) were mixed on ice under the following eight conditions: for the gel of the No.1 formulation, the ratio of M-C-liposomes:siRNA (v/w µL/µg) was 0:.1, 0.8:1, 1.6:1, 2.4:1, 3.2:1, 4.0:1, 4.8:1. 5.6:1; for the gel of the No.2 formulation, the ratio of M-C-liposomes:siRNA (v/w µL/µg) was 0:.1, 0.8:1, 1.6:1, 2.4:1, 3.2:1, 4.0:1, 4.8:1. The mixtures were equilibrated at room temperature for 5 minutes and then 20 µL of DNA loading buffer was added. The mixtures were then loaded onto a 1% agarose gel and electrophoresed at 100 volts for 18 minutes in 1X TAE buffer. Images were captured by an Image Reader (Fuji Film Las-3000).

2.4.4 Conjugation of IL-13 with M-C-liposomes

After ensuring that the M-C-liposomes were able to encapsulate siRNA, IL-13 was prepared and conjugated with the M-C-liposomes. First, IL-13 was thiolated with 2-Iminothiolane Hydrochloride. The lL-13 protein, at a concentration of 1.5 mg/ml, was added into 1 mL of PBS with 5 mM of EDTA. Second, 100 µL of a 2 mg/ml stock solution of 2-Iminothiolane Hydrochloride (Sigma, Cat.l6256-500MG FW137g/mol) was dissolved in 2 ml of d H_2O, and added to the IL-13 samples. Third, the samples were stirred at room temperature for 30 minutes, and then at 4^{o}C for additional 30 minutes. Fourth, the thiolated IL-13 was purified through the Sephadex^{TM} G-25 Fine column (Amersham Biosciences, cat. no.17-0032-01). Fifth, the M-C-liposomes were added to the thiolated IL-13 samples. Sixth, IL-13-M-C-liposomes were further purified through a centricon 30,000 KD and spun at 3000 RPM at 4^{o}C for 1 hour. (For additional information on the preparation of IL-13, please refer to [165])

2.4.5 The size and zeta potential of IL-13-M-C-liposomes

The size distribution of IL-13 conjugated maleimide cationic liposomes (IL-13-M-C-liposomes) was determined by light scattering analysis through an ALV/DLS/SLS-5022F compact gonimeter system (ALV, Germany). Zeta potential and poly dispersity index of C-liposomes was measured by a PALS Zeta Potential Analyzer Ver. 3.16, Brookhaven Instruments Corp.

2.4.6 Complex formulation of the IL-13-M-C-liposomes with siRNA

To ensure the siRNA could be complexed with the IL-13-M-C-liposomes, IL-13-M-C-liposomes and siRNA-FITC (v/w) were mixed on ice under the following eight conditions: (the ratio of IL-13-M-C-liposomes:siRNA v/w µL/µg) 0:.1, *4:1, 0.8:1, 1.6:1, 2.4:1, 3.2:1, 4.0:1, 5.2:1. (Note: *4:1 is presented as a positive control which was used for the the C-liposomes:siRNA). The mixtures were equilibrated at room temperature for 5 minutes and then 20 µL of DNA loading buffer was added. The mixtures were then loaded onto a 1% agarose gel and electrophoresed at 100 volts for 18 minutes in 1X TAE buffer. The images were captured by an Image Reader (Fuji Film Las-3000).

2.5 Results

2.5.1 C-liposomes were uniformly sized and reproducible

The size of the C-liposomes was determined following the procedures described in section **2.2.4.1**. The average means of PDI and zeta potentials are presented from 3 independent batches of C-liposomes. As indicated in **Figure 2.1A**, the size (radius) of the C-liposome generated with our procedures were consistent and produced an average radius of 95 nm which is within the 80-180 nm range standard suggested in the literature. The PDI of the C-liposomes fell within the range of 0.1 to 0.2. Before the complex formation, the mean zeta potential of the C-

liposomes for the 3 different batches equaled 35 mV (+/-0.25), which represents a high positive charge that should provide efficient affinity to the future siRNA cargo shown in **Figure 2.1B**. After the complex formation of the C-liposomes with siRNA, the mean zeta potentials of C-liposomes:siRNA for the 3 different batches equal 5 mV (+/-0.25) shown in **Figure 2.1B**, which represents all the positive charges were neutralized by siRNA. Our data demonstrates that the C-liposome prepared in our laboratory possess a good quality of Index as the evidence illustrated in **Figure 2.1**.

2.5.2 C-liposomes could encapsulate siRNA with an ratio of C-liposomes:siRNA (v/w) 4:1

The maximum ratio of C-liposomes to siRNA was determined following the procedures described in **2.2.4.2**. The free siRNA is shown at the bottom of the agarose gel image, while the complex C-liposomes:siRNA is shown on the top of the image. This information demonstrates the following: 1) siRNA could be encapsulated by C-liposomes, and the complex generated is shown at the top of the image in lanes 4-8 of **Figure 2.2**. 2). More than 90% of the siRNA could be encapsulated by C-liposomes, as illustrated in lane 6 of **Figure 2.2**. 3). The C-liposome complex was saturated with siRNA when the ratio of C-liposome:siRNA reached 4µL/1µg(8µL). In this case, the bottom band in the corresponding column was lightest, while the top band in the same lane was darkest (shown in **Figure 2.2)**. Beyond this ratio, increasing the concentration of C-liposomes did not result in a greater formation of the complex, as illustrated in lanes 7-8. Thus the optimal ratio of C-liposomes to siRNA was determined to be 4:1, as shown in **Figure 2.2**. These results further revealed that the C-liposomes are capable of encapsulating the siRNA.

2.5.3 Lack of cytotoxicity with the use of C-liposomes *in vitro* and *in vivo*.

The cyctotoxicity of C-liposomes was determined by following the procedures described in **2.2.4.3**. The cyctotoxicity of C-liposomes was first evaluated *in vitro* described in **2.2.4.3.1**

with increasing concentrations (2, 4 and 6 µL) of C-liposomes stock (2.8 mg/mL) per mL of the DMEM media utilized. No significant differences in cell proliferation, as determined by an MTS assay at 24, 48 and 72 hours, were detected relative to control cultures not receiving C-liposomes (**Figure 2.3)**. Thus C-liposomes were not toxic to U251 cells as shown in **Figure 2.3**. Potential toxicity *in vivo* was evaluated by injecting athymic nude mice with C-liposomes described in **2.2.4.3.2**, C-liposomes:non-specific-siRNA, or C-liposomes:H-ferritin-siRNA. PBS treated mice served as controls. As shown in **Figure 2.4A** and **Figure 2.4B**, there were no increases seen in serum kidney or liver toxicology between treatment and control groups when the following toxicity markers were evaluated: SGOT, SGPT, Alkaline Phosphatase, and total bilirubin. Therefore, the use of C-liposomes resulted in no cytotoxicity based on both *in vitro* and *in vivo* experimental results (**Figure 2.3-2.4**).

2.5.4 C-liposomes:siRNA were uptaken by U251 and U87 cells and internalized through the endosomal pathway.

The uptake of the C-liposomes:siRNA by U251 and U87 cells was determined following the procedures described in **2.2.4.4**. When cells were exposed to free siRNA-FITC without C-liposomes, no siRNA was uptaken as detected in image **c** (U251 cells) of Figure **2.5A** and image **k** (U87 cells) of **Figure 2.5B**. In contrast, cultures exposed to C-liposomes-rhodamine:siRNA-FITC uptaken the siRNA, as demonstrated in image **g** (U251 cells) and **o** (U87 cells) of **Figure 2.5**, siRNAs were internalized by the cells. The mechanism of C-liposomes:siRNA internalization was determined following the procedures described in **2.2.4.5**. U251 and U87 glioma cells were exposed to C-liposomes-rhodamine and subsequently immunostained for the early endosomal marker EEA1. Co-localization was observed between C-liposomes-rhodamine and the endosomal marker EEA1-FITC, as shown in images **T** (U251 cells) and **X** (U87 cells) of **Figure 2.5C**. The

overlap of C-liposomes and the endosomal marker EEA1 suggested that the uptake of the C-liposomes was through the endosomal pathway (images **T** and **X** of **Figure 2.5c**). This finding is consistent with our previous reports for the uptake of nanovesicles [165, 166]. These results suggest that siRNA can be sent to U251 and U87 cells, and involves internalization of liposomes through the endosomal pathway.

2.5.5 C-liposomes:siRNA complex is stable in RNase A but unstable in human serum.

The stability of C-liposomes:siRNA was investigated following the procedures described in **2.3.1, 2.3.2, 2.3.3** and **2.3.4**. Four experiments were carried out for the investigation. The first experiment is related to the encapsulation of siRNA by newly prepared C-liposomes. The bands on top of the image shown in **Figure 2.6** demonstrate that the newly prepared C-liposomes are capable of encapsulating 100% of the siRNA as shown in **Figure 2.6**. This complete encapsulation, where no residual free siRNA was observed at the bottom of the image, was achieved with a C-liposome concentration of 4.8 µL of a lipids stock of 2.8 mg/mL.(**Figure 2.6**). For the second experiment, both free siRNA (control group) and the C-liposme;siRNA complex (treatment group) were exposed to varying amounts of RNAseA. When the treatment group was exposed to RNAseA, only a small portion of free siRNA (10%) was seen at the bottom of the image and big portion of siRNA (90%) carried by C-liposome complex was seen on the top of the image in lanes 6-8. This evidence demonstrates that 90% of the siRNAs was encapsulated within the C-liposomes, while less than 10% of the siRNAs were outside C-liposomes. The siRNA (10%) located outside of the C-liposomes was released by RNaseA during the 1 hour incubation at room temperature shown at the bottom of the image in lanes 6-8 (**Figure 2.7**). For the third experiment, the C-liposomes:siRNA complex was incubated with RNaseA at 37^{o}C for 1 hour. Under these conditions, 90% of the siRNA was contained in the C-liposomes:siRNA complex (seen at the top of the image) with only 10% of the siRNA free (seen at the bottom of the image)

in lanes 6-8 of **Figure 2.8**. The result from this third experiment indicate that the C-liposome:siRNA complex is stable in 4.8 units of RNAseA at body temperature. In the fourth experiment, the C-liposome:siRNA complex was exosed to varying amounts of human serum and incubated at 37^{o}C for 1 hour. Under these conditions, less than 20% of the C-liposome:siRNA complex remained in 20% human serum, and less than 5% of the C-liposomes:siRNAs complex remained in 40% human serum (**Figure 2.9**). These four experiments demonstrate that the C-liposomes:siRNA complex is stable in the presence of 5 units of RNAseA, yet is unstable in human serum at 37^{o}C (**Figure 2.6-2.9**). These findings poses a challenge for the administration of the current formulation of C-liposome by a vascular route, because of the instability of the C-liposomes:siRNA complex in serum. However, siRNA was stably located inside the C-liposomes in RNaseA at 37^{o}C for 1 hour.

2.5.6 IL-13-M-C-liposomes were prepared and complexed with siRNA.

IL-13-M-C-liposomes were prepared, characterized and further complexed with siRNA following the procedures described in **2.4.1-2.4.6.** Our data reveals that the M-C-liposomes from the No.1 formulation were capable of encapsulating siRNA completely at a low concentration (1.6 µL) of the lipid stock, without leaving any residu siRNA, which would be shown at the bottom of the image in lanes 3-8 of **Figure 2.10**. The M-C-liposomes of the No.2 formulation were also capable of completely encapsulating siRNA at a low concentration (0.8 µL) of the lipid stock, without leaving any residual siRNA, which would be seen at the bottom of the image in lanes 2-8 of **Figure 2.11**. The average particle size of M-C-liposomes from the No.2 formulation was 110 nm which is within the standard acceptable range of 65-180 nm. The PDI of C-liposomes from this same formulation was 0.175, which also falls within the standard acceptable range. Thus, our M-C-liposomes have an even size distribution with 90% falling around 110 nm, as shown in **Figure 2.12**. The measured mean zeta potential was 64 mV (+/-5), which indicates

that the positive charge stayed high (**Figure 2.13**). When M-C-liposomes from the No.2 formulation were conjugated with IL-13, the IL-13-M-C-liposomes appeared to fully encapsulate the siRNA without leaving any residual siRNA, which would be shown at the bottom of the image of **Figure 2.14**. Although the procedure of conjugating the C-liposome with siRNA was a long process, the IL-13-M-C-liposomes were able to encapsulate siRNA, and appear to be functional, as shown in **Figure 2.14**.

2.6 Summary

1) Untargeted C-liposomes composed of DC-Cholesterol/DOPE lipids were developed and characterized. 2) The C-liposomes had good physical properties, including an even size distribution, a desired PDI value, an expected zeta potential value, were non toxic both *in vitro* and *in vivo,* and did not result an immune response. The low level of toxic markers for kidney and liver function, following the injection of C-liposomes into nude mice, provided evidence of a lack of immune response. 3) The desired chemical properties of C-liposomes were confirmed by the demonstration that the C-liposomes could encapsulate siRNA through their electrostatistic force. 4) The C-liposomes:siRNA complex was stable when placed under conditions of of RNaseA (5units) at 37^{o}C for one hour. 5) The C-liposomes:siRNA complex was able to enter U251 glioma cells, MCF-7 breast cancer cells, and malignant peripheral nerve sheeth tumor (MPNST) NF96.2 cells. The mechanism for entry of the complex appears to be through the endosomal pathway. 6) Targeted IL-13-M-C-liposomes were also developed and partially characterized. 7) IL-13 –M-C- liposomes had desired physical properties including, an even size distribution, a desired PDI value, and a high zeta potential value. 8) The desired chemical properties of IL-13 –M-C- liposomes were confirmed by the demonstration that the IL-13-M-C-liposomes could completely encapsulate siRNA through their electrostatistic force.

2.6 Figures and legends

A

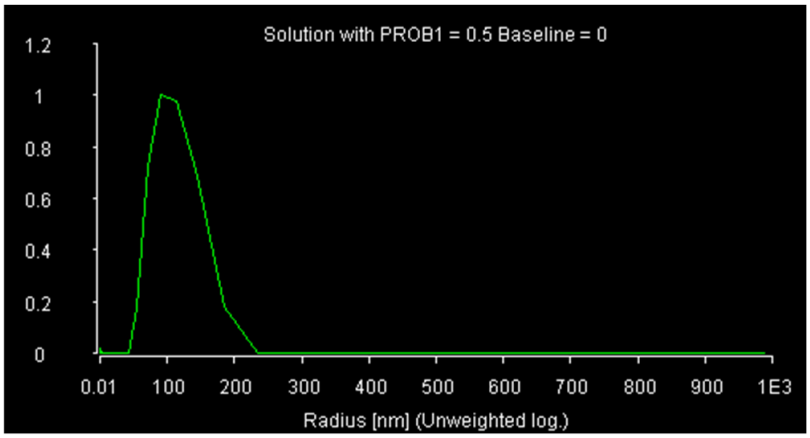

B

Category	PDI	Zeta Potential
C-liposomes	0.12 +/- 0.02	35 +/- 0.25
C-liposomes:siRNA	0.22 +/- 0.02	5 +/- 0.25

Figure 2.1. Characterization of C-liposomes. A: Size (radius) distribution of C-liposomes measured by dynamic light scattering. The average size of C-liposomes was 95 nm which is within the standard range of 80 to 180 nm. C-liposomes were evaluated from four independent batches. **B**: Corresponding PDI values are within a range of 0.1 to 0.2. The zeta potential was 35 (+/-) 0.25 for C-liposomes and 5 (+/-) 0.25 for C-liposome:siRNA complexes.

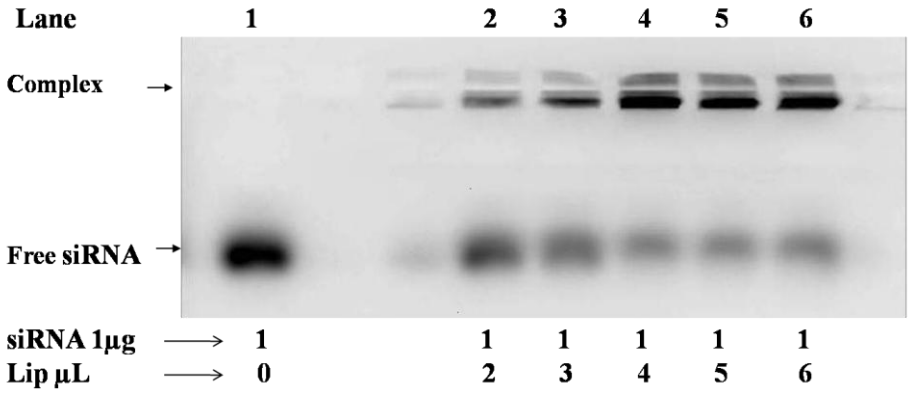

Figure 2.2. The optimal ratio of C-liposomes:siRNA, as determined by a 1% agarose gel. From left to right of the image, the ratio of C-liposomes:siRNA-FITC (v/w µL/µg) was 0:1, 2:1, 3:1, 4:1, 5:1 and 6:1. The top bands represent the C-liposomes:siRNA-FITC complex. The bottom bands represent free siRNA-FITC. The optimal ratio of C-liposomes to siRNA was 4:1 (µL/µg), where the band at the bottom is the lightest and the band on the top is the darkest.

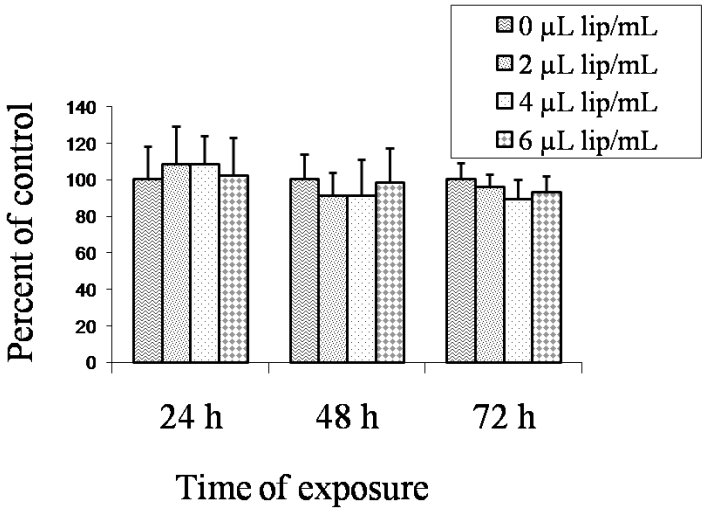

Figure 2.3. Lack of cytotoxicity of C-liposomes in U251 cells, as tested by an MTS assay. The graphs represent the optical density of treatment groups normalized to the control groups from three independent experiments. No significant differences in cell proliferation were observed with any concentration of C-liposome at 24, 48, or 72 hours post transfection, relative to control cultures receiving no C-liposome.

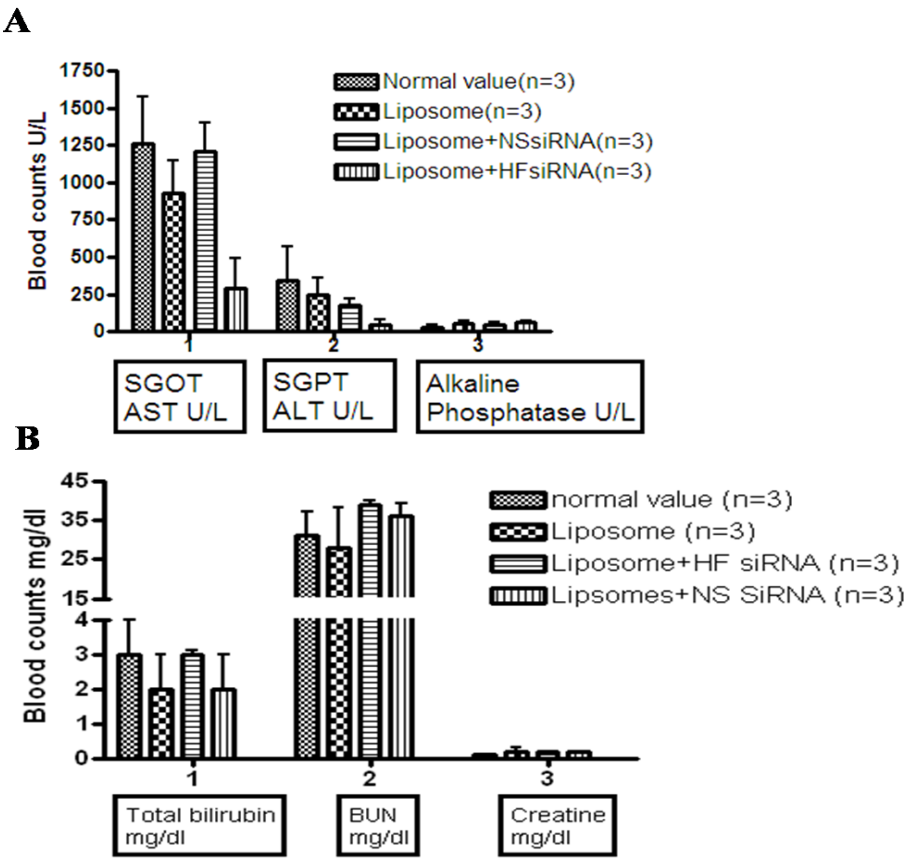

Figure 2.4. Lack of toxicity of C-liposomes *in vivo*, as evaluated by an automated chemistry analyzer and kits. Control animals were injected with PBS to represent normal conditions. Treatment groups included animals injected with C-liposomes, C-liposomes:H-ferritin siRNA, or C-liposomes:non-specific siRNA. No significant elevations were observed in the blood counts of any kidney or liver markers in any of the treatment groups, relative to the control group.

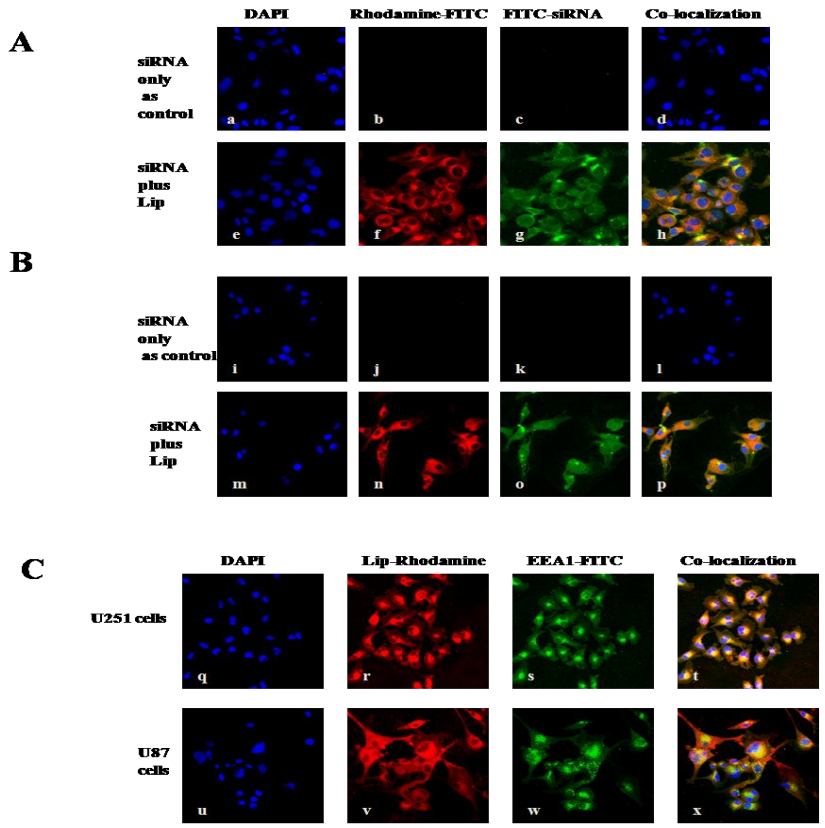

Figure 2.5. Internalization of C-liposomes:siRNAs in U251 and U87 cells and through the endosomal pathway in U251 cells. A, B, Panels a-d (U251 cells), i-l (U87 cells) are representative confocal images of the cells exposed to siRNA-FITC alone as control. FITC signal is not observed indicating lack of siRNA uptake. Panels e-h (U251 cells), m-p (U87 cells) are representative confocal images of the cells exposed to C-liposome-rhodamine:siRNA-FITC complexes. Rhodamine & FITC co-localization around DAPI-labeled nuclei indicative of cellular uptake of liposome:siRNA complexes is observed. Channels: blue, DAPI; red, C-liposomes-rhodamine; green, siRNA-FITC. **C,** co-localization of C-liposomes with endosomal marker EEA1. Panels q-t (U251 cells), u-x (U87 cells) representative confocal images of the cells exposed to C-liposome-rhodamine (red) and stained for EEA1 (with FITC secondary antibody, green); DAPI, blue. Rhodamine & FITC localization indicative of endosomal internalization pathway for C-liposomeslabeled C-liposomes (red) and the image in panel **k** shows the expression of the early endosomal marker EEA1 (green) after immunocytochemistry. Co-localization of C-liposomes (red) with EEA1 (green) demonstrates that the C-liposomes enter the cell via an endosomal pathway.

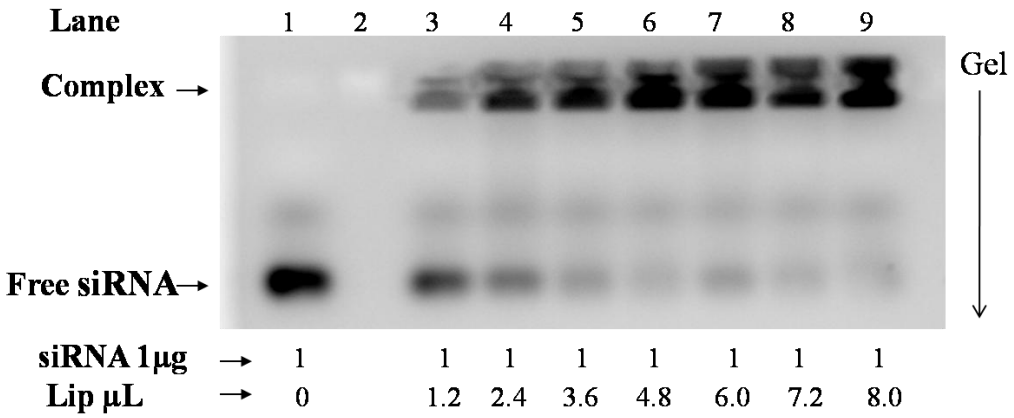

Figure 2.6. Encapsulation of siRNA by newly prepared C-liposomes under various concentrations of C-liposomes determined by 1% agarose gel. The top bands represent the complex of C-liposomes:siRNAs. The bottom bands represent free siRNA. Lane 1, siRNA without C-liposomes serves as a control. Lanes 3-9 contain the complex of C-liposomes:siRNAs as the treatment groups. C-liposomes can encapsulate siRNAs completely from a starting concentration of 3.6 µL/mL of the lipids stock without leaving any siRNA residues.

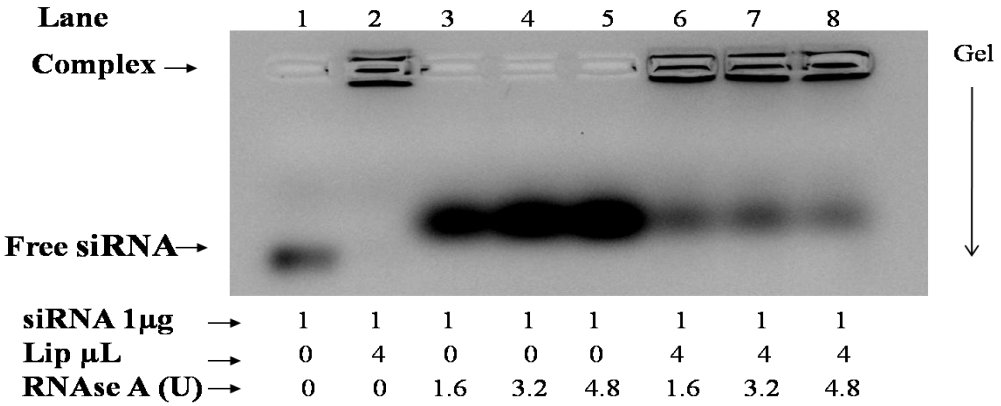

Figure 2.7. The complex of C-liposomes:siRNAs were stable in 4.8 unit of RNase A. Lane 1, siRNA without C-liposomes as control. Lane 2 contains the complex C-liposomes:siRNAs without RNase as another control. Lane 3-5 contains siRNAs with RNase A. Lane 6-8 contain the complex of C-liposomes:siRNA with RNase A. The complex of C-liposomes:siRNA were stable up to 4.8 unit of RNase A.

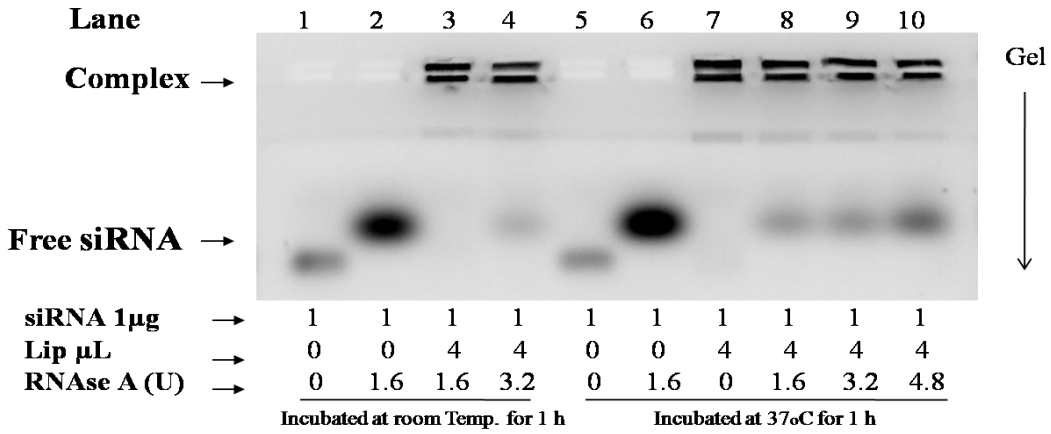

Figure 2.8. Stability of the C-liposomes:siRNAs complex in RNaseA at 37°C tested by a 1% of agarose gel. Lanes 1 and 5, conatin free siRNA and serve as the control group. Lanes 2 and 6, contain free siRNA with RNase, and serve as a positive control. Lanes 3 and 7, contain the C-liposomes:siRNAs complex with RNaseA and serve as another positive control group. Lanes 4, 8, 9 and 10 show the C-liposomes:siRNA complex with RNase. Lanes, 1, 2, 3, 4 and 5 represent the condition at room temperature, while lanes 6, 7, 8, 9 and 10 represent the condition at 37°C. The C-liposome complex is stable at 37°C.

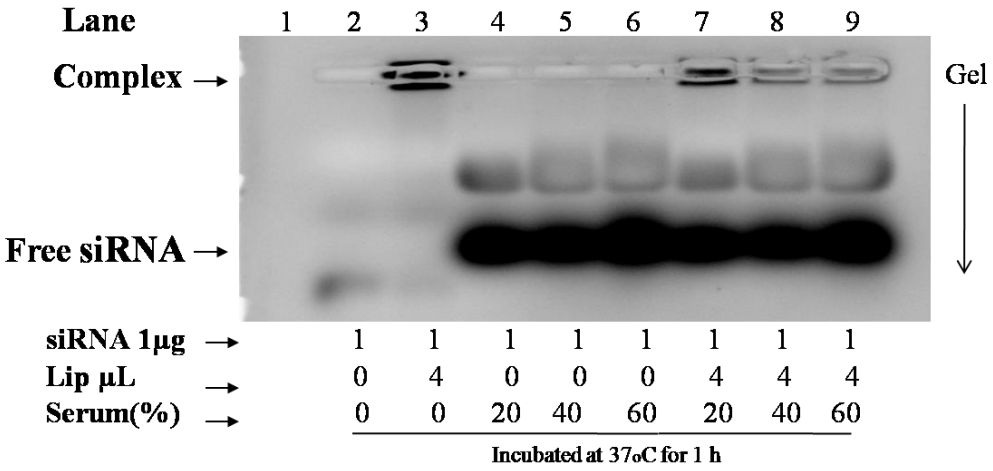

Figure 2.9. The stability of the C-liposomes:siRNAs complex in human serum tested using a 1 % agarose gel. Lane 2 contains free siRNA and serves as a control. Lane 3 shows the C-liposomes:siRNAs complex as a positive control. Lanes 4 -6, contain siRNAs with human serum. Lanes 7-9, contain the C-liposomes:siRNAs complex with human serum. The C-liposomes:siRNAs complexes were not stable in even 20% human serum.

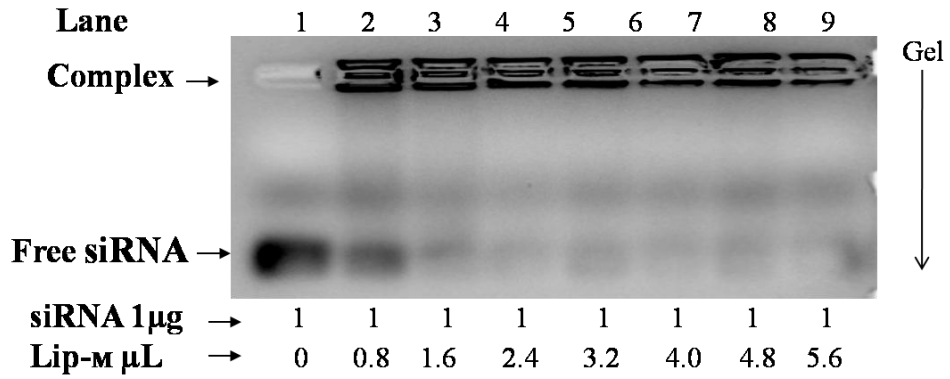

Figure 2.10. Encapsulation of siRNA using M-C-liposomes by No.1 formulation tested by 1 % agarose gel. Lane 1, contains free siRNA and serves as the control. Lanes 2-9 show the M-C-liposomes:siRNAs complex and serve as treatment groups. The top bands represent the M-C-liposomes:siRNAs complex. The bottom bands represent the free siRNA. M-C-liposomes encapsulated all available siRNAs completely starting with lipids stock concentration of 1.6 µL/mL. .

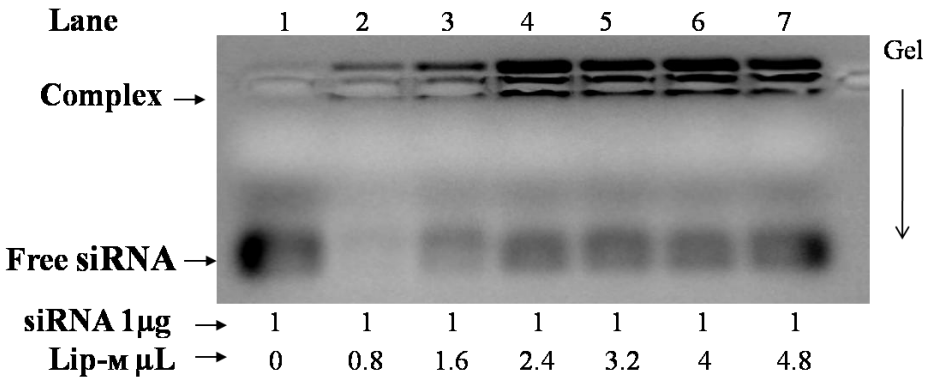

Figure 2.11. Encapsulation of siRNA by M-C-liposomes by No. 2 formulation, as tested with a 1 % agarose gel. Lane 1, shows free siRNA and serves as the control. Lanes 2-7, shows the M-C-liposomes:siRNAs complex, and serve as the treatment groups. The top bands represent the M-C-liposomes:siRNAs complex. The bottom bands represent free siRNA. M-C-liposomes encapsulated all available siRNAs completely starting from 0.8 µL/mL of the lipids stock.

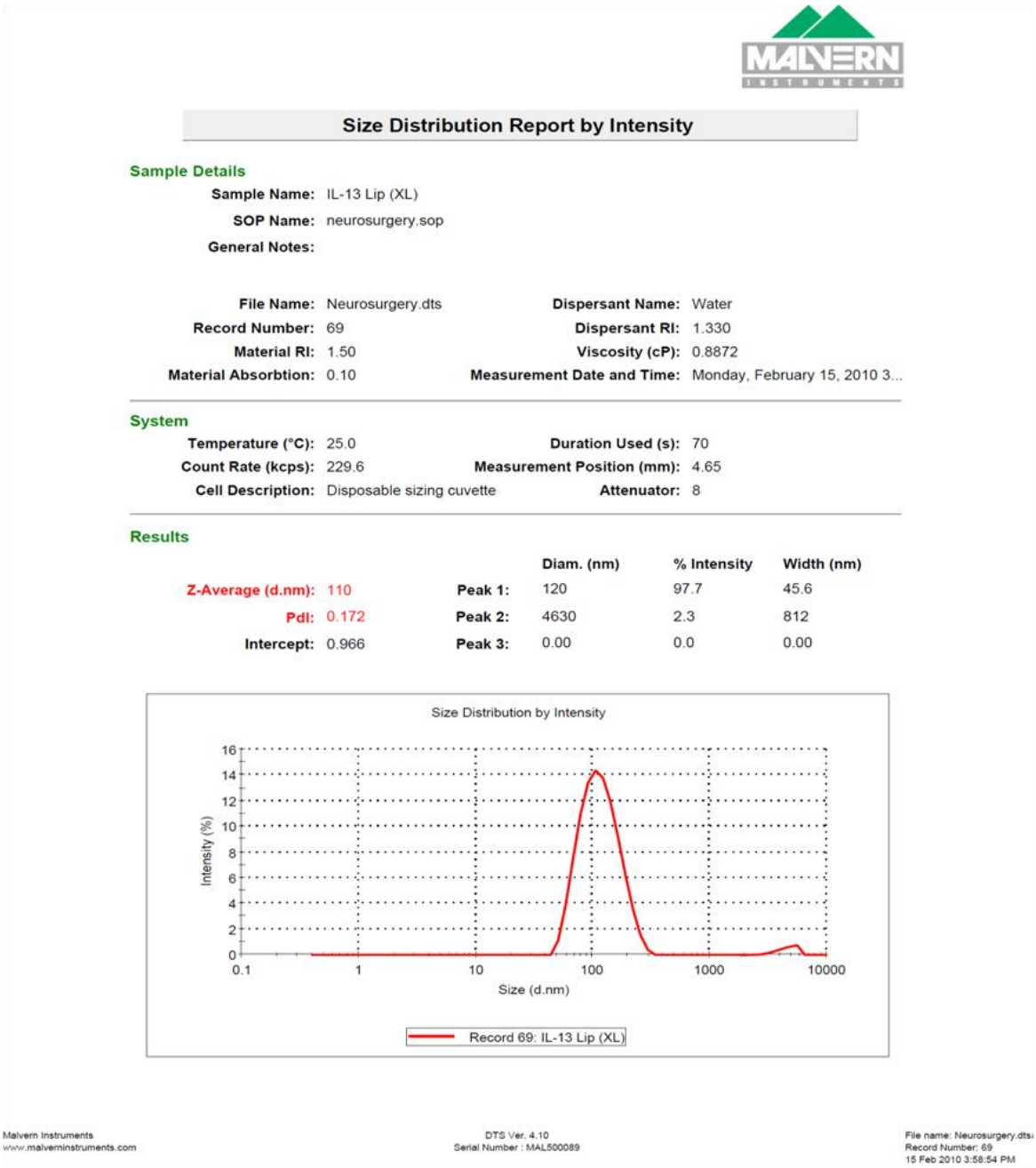

Size Distribution Report by Intensity

Sample Details

Sample Name:	IL-13 Lip (XL)		
SOP Name:	neurosurgery.sop		
General Notes:			
File Name:	Neurosurgery.dts	Dispersant Name:	Water
Record Number:	69	Dispersant RI:	1.330
Material RI:	1.50	Viscosity (cP):	0.8872
Material Absorbtion:	0.10	Measurement Date and Time:	Monday, February 15, 2010 3...

System

Temperature (°C):	25.0	Duration Used (s):	70
Count Rate (kcps):	229.6	Measurement Position (mm):	4.65
Cell Description:	Disposable sizing cuvette	Attenuator:	8

Results

			Diam. (nm)	% Intensity	Width (nm)
Z-Average (d.nm):	110	Peak 1:	120	97.7	45.6
PdI:	0.172	Peak 2:	4630	2.3	812
Intercept:	0.966	Peak 3:	0.00	0.0	0.00

Malvern Instruments
www.malverninstruments.com

DTS Ver. 4.10
Serial Number : MAL500089

File name: Neurosurgery.dts
Record Number: 69
15 Feb 2010 3:58:54 PM

Figure 2.12. The size distribution of IL-13-M-C-liposomes determined by dynamic light scattering. The average size of IL-13-M-C-liposomes measured was 110 nm which was within the standard range of 65 to 155 nm; 97.7% of the intensity lies on peak 1. Corresponding PDI values lie within the range of 0.172. This data represents only one batch of the IL-13-M-C-liposome preparations.

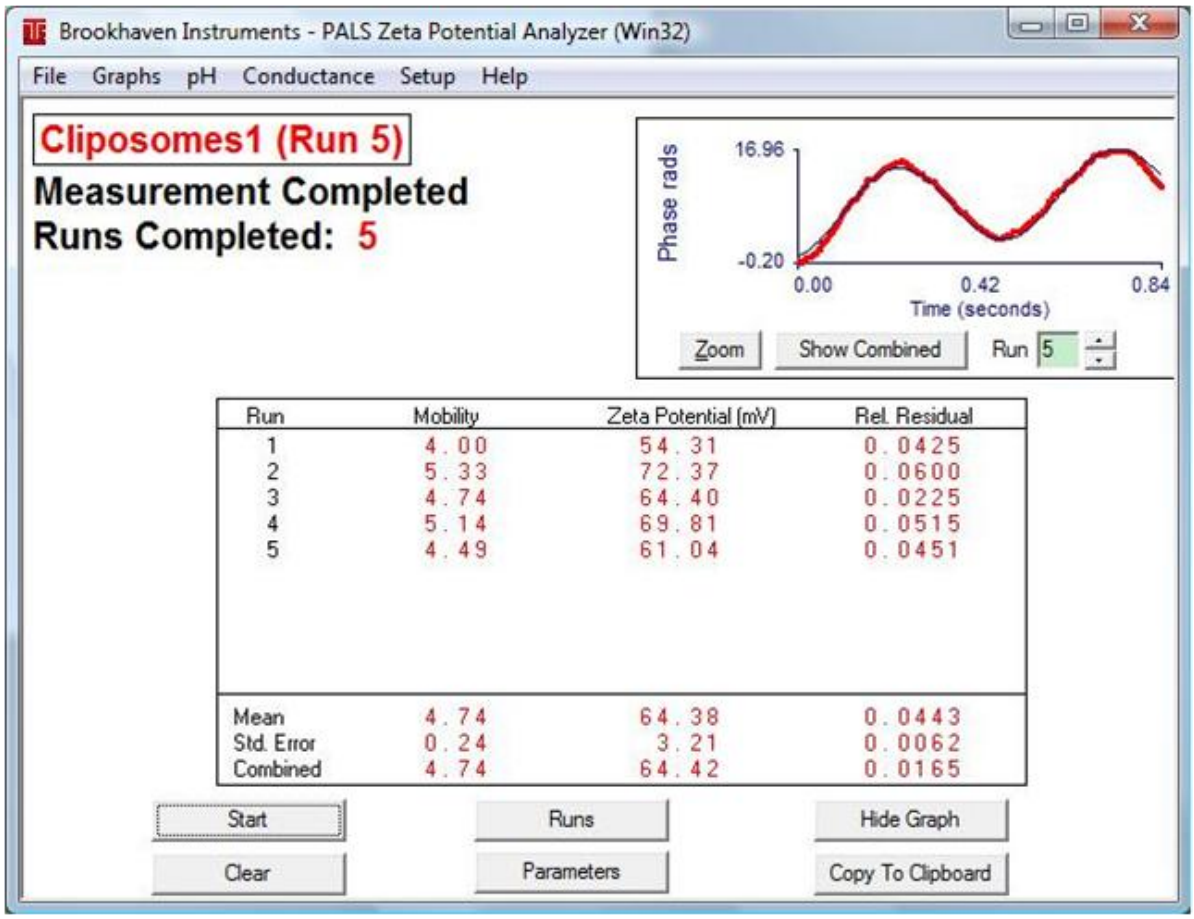

Figure 2.13. The zeta potential of IL-13-M-C-liposomes, as measured by PALS Zeta Potential Analyzer (Win36), Brookhaven Instruments Corp. The average zeta potential of IL-13-M-C-liposomes is 64 (+/-) 5 before it was complexed with siRNA. This data represents only one batch of M-C-liposome preparations.

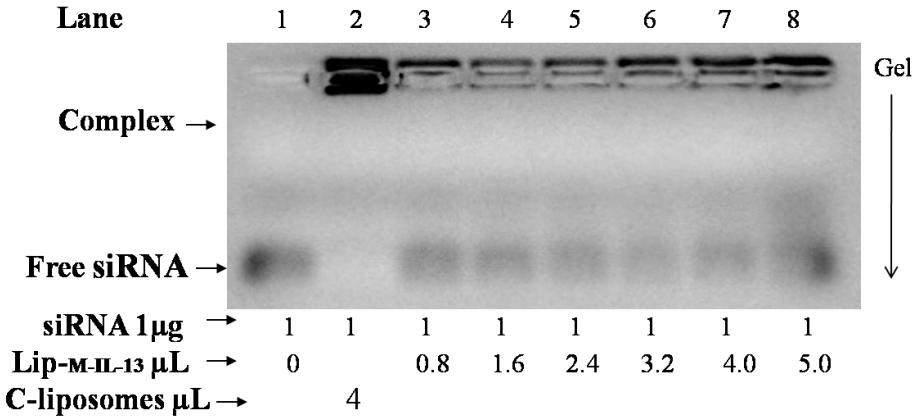

Figure 2.14. Encapsulation of siRNA by IL-13-M-C-liposomes prepared by No.2 formulation, as tested by a 1 % agarose gel. Lane 1 contains free siRNA and serves as the control. Lane 2 contains the C-liposomes:siRNA complex to serve as a positive control. Lanes, 3-8 show the M-C-liposomes:siRNAs complex, and serve as treatment groups. The top bands represent the IL-13-M-C-liposomes:siRNAs complex . The bottom bands represent free siRNA. IL-13-M-C-liposomes encapsulated all of the available siRNAs completely when starting with 0.8 µL/mL of lipids stock (No. 2 formulation).

Chapter 3

The Functional Role of H-ferritin in Cancer Development and Impact of Decreasing H-ferritin Expression on Radiation and Chemotherapeutic Efficacy in the Treatment of Glioma

Chapter 3 contains two sections. In section 1, H-Ferritin siRNA enhances radiation and chemotherapeutic efficacy for the treatment of glioma is described as part I. In section 2, the functional role of H-ferritin in cancer development is described as part II.

Part 1 H-ferritin siRNA enhances radiation and chemotherapeutic efficacy

3.I.1 Introduction

In part I of chapter 3, the experimental methods/procedures for testing the central hypothesis of the present project are described in detail. The central hypothesis of this thesis work is that down regulation of H-ferritin, using C-liposomes:siRNA, will increase the radiation and chemotherapeutic efficacy for the treatment of gliomas. The experimental basis for this hypothesis is that over-expressions of H-ferritin have been detected in malignant tumor cells. The following 6 kinds of experiments were carefully designed to test the central hypothesis:

1) Demonstration of over-expression of endogenous H-ferritin in malignant tumor cell lines. Three types of primary tumor cells were investigated, including glioma U251 and U87 cells, neurofibroma #215 and breast cancer MCF-7 cells.
2) Demonstration of H-ferritin expression that is co-localized with glioma stem cell marker CD133.

The results from these two studies provided the experimental evidence that H-Ferritin is over-expressed in a broad spectrum of malignant tumors.

3) Demonstration of down-regulation of H-Ferritin protein expression by C-liposome:H-ferritin-siRNA tested using Western blot analysis.

This study showed that down-regulation of H-ferritin was achieved with C-liposome:H-FerritinsiRNA in U251 and MCF-7 cells. Subsequently, the central hypothesis was tested in experiments 4-6 to investigate whether down-regulation of H-ferritin would facilitate tumor suppression.

4) Demonstration *in vitro* of enhanced chemotherapeutic sensitivity of malignant tumors by H-ferritin down-regulation tested by SRB assay.
5) Demonstration *in vitro* of enhancing radiation therapeutic sensitivity of glioma by H-ferritin down-regulation tested by an MTS assay.
6) Demonstration *in vivo* of enhancing radiation and chemotherapeutic sensitivity by down-regulation of H-ferritin.

The results from these three experiments provided *in vitro* and *in vivo* data and demonstrate that down-regulation of H-ferritin significantly improved the effectiveness of conventional radiation and chemotherapies. These results are highly significant, as they suggest a novel synergistic therapeutic approach with which drug resistance and side effect associated with conventional treatment may potentially be reduced.

3.I.2 Materials and Methods

3.I.2.1 H-ferritin expression in malignant tumor cells

In order to visualize the expression of H-ferritin expression in malignant cell cultures, human glioma U251 and U87 cells (at a density of 20,000cells/well), human malignant peripheral neuro sheath tumor (MPNST) NF#215 cells (at a density of 30,000cells/well) and breast cancer MCF-7 cells (at a density of 10,000cells/well) were seeded in 8-well chamber slides and allowed to attach overnight. The cells were fixed with 4% paraformaldehyde, and subsequently exposed to an H-ferritin polyclonal antibody (1:5000) at 4^{o}C overnight. Preparations were rinsed with PBS three times (15 minutes each), then exposed to secondary-FITC antibody (1:500) for 1 hour at room temperature and rinsed with PBS an additional three times (15 min each). Cultures were stained with 1% (w/v) of DAPI in DMEM (4, 6-diamidino-2-phenylindole) for 10 minutes to visualize nuclei, rinsed with PBS again, and mounted and dried overnight. Images were captured with fluorescence microscopy.

3.I.2.2 Co-localization of H-ferritin with the glioma stem cell marker CD133

With the intention of demonstrating the co-localization of the glioma stem cell marker CD133 with H-ferritin in human glioma, neurofibroma and breast cancer cells, immunohistochemistry was performed as follows: Human glioma U251 and U87 cells (at a density of 20,000cells/well), neurofibromatosis #215 cells (at a density of 30,000 cells/well) and human breast cancer MCF-7 cells (at a density of 20,000 cells/well) were seeded in 8 well chamber slides and allowed to attach overnight. Cultures were fixed with 4% paraformaldehyde, subsequently exposed to H-ferritin polyclonal antibody (1:5000) overnight at 4^{o}C, and then secondary-FITC antibody (1:500) for 1 hour at room temperature. Preparations were rinsed, and stained with 1% (w/v) of DAPI in DMEM (4, 6-diamidino-2-phenylindole) to visualize nuclei, and mounted and dried overnight. Images were captured with fluorescence microscopy.

3.I.2.3 Down-regulation of H-ferritin expression in U251 and MCF-7 cells tested by Western blott analysis.

To ensure that H-ferritin siRNA delivered by C-liposomes is able to down regulate H-ferritin expression, the levels of H-ferritin in glioma and breast cancer cells were determined quantitatively by Western blot analysis. Briefly, U251 cells (166,000 cells/well), and MCF-7 cells (200, 000 cells/well) were seeded into six-well plates and allowed to attach overnight. Cultures were transfected with C-liposomes:siRNA:DMEM (4uL/1µg/1mL) for 3 hours before media was changed to complete media. Cell lysate was harvested using RIPA buffer (Sigma, cat. no. R0278-50ML) at 24 h, 48 h, and 72 h post transfection. Lysate was centrifuged at 14,000 rpm for 10 minutes at 4^{o}C and supernatant containing total protein was collected. The total protein was quantified, and equal amounts of protein was loaded on a 4-20% Tris-HCL Criterion ^{TM} Precast Gel (Bio-Rad CA, Cat. no. C091007D1). Protein was later transferred to a PVDF membrane (Whatman UK, Cat. no. 10413096). Membranes were blocked for 1 hour with 5% (w/v) dry milk in TBS-T [Tris 25 mM (pH 7.6)]-buffered saline 0.9% (w/v)-Tween-20 0.1% (v/v)] at room temperature. Membranes were incubated overnight at 4^{o}C with a monoclonal H-ferritin antibody (1:50,000 dilutions). The secondary antibody (GE Healthcare UK, Cat. no. NA931V, 1:5000 dilutions) utilized was sheep anti-mouse IgG conjugated to horseradish peroxidase, and membrane were incubated in secondary antibody for 1.5 hours at room temperature. Subsequently, the blot was exposed to Western Lightning Chemiluminescence Reagent (Perkin Elmer Life Science, Cat. no. NEL 104) for 1 minute and exposed to X-ray film. H-ferritin bands migrated to an apparent molecular weight of 21 kDa. Bands were scanned by a Densitometer (GS-800 Calibrated, Bio-Rad) and quantified using Quantity One-4.5.0 software (Bio-Rad). Data are expressed as a percentage of the control value.

3.I.2.4 Enhancing chemotherapeutic sensitivity of malignant tumors by H-ferritin down-regulation tested *in vitro*

To test the central hypothesis that H-ferritin down-regulation by C-liposomes:H-ferritin-siRNA will increase chemotherapeutic sensitivity for treatment of malignant tumors, an SRB (sulforhodamine B) assay was performed in three cell lines. U251 and sNF96.2 cells were seeded into 96-well plates at a density of 2,000 cells/well and MCF-7 cells at a density of 4,000 cells/well, and allowed to attach overnight. Cultures were transfected with C-liposomes:H-ferritin-siRNA:DMEM (4μL/1μg/1mL) for 3 hours, before cell media was replaced with completed media. Preparations were exposed to BCNU at concentrations of 0, 20, 40, 60, 80 and 100 μM beginning 48 hours after transfection. SRB assays were performed 48 hours post BCNU exposure. Data are expressed as a percentage of the control with respect to untreated cells.

3.I.2.5 Enhanced sensitivity of glioma to radiation therapy by H-ferritin down-regulation tested by an MTS assay *in vitro*

In order to test the hypothesis that C-liposomes:H-ferritin-siRNA will increase radiation sensitivity for the treatment of glioma, an MTS assay was performed on glioma U251 cells. Cells were seeded into 96-well plates at a density of 2,000 cells/well and allowed to attach overnight. Preparations were transfected with C-liposomes:H-ferritin-siRNA:DMEM (4μL/1μg/1mL) for 3 hours. Following transfection, cell media was replaced with complete media. At 24 hours post transfection, cells were then exposed to γ-radiation with 20 Gy. An MTS assays was performed at 24, 48 and 72 hours post γ-radiation. Data are expressed as a percentage of the control with respect to untreated cells.

3.I.2.6 Enhanced radiation and chemotherapeutic sensitivity by ferritin down-regulation tested *in vivo*.

To further test the central hypothesis, an *in vivo* approach was taken. Subcutaneous tumors were prepared by implanting 15 x 10^6 human U251 glioma cells in the flank of adult female athymic nude mice. When tumor volume reached1.0 to 1.4 cm^3 in two weeks, the mice were assigned to the following three experimental regimes.

3.I.2.6.1 Down-regulation of H-ferritin expression in subcutaneous tumor xenograft tested by Western blotting analysis.

With the goal of testing whether C-liposomes:H-ferritin-siRNA is capable of decreasing H-ferritin expression in a tumor xenograft model, similar to the situation seen in cell culture models, a group of mice (n=9) with subcutaneous tumors were prepared. Animals were divided into three groups, with 3 mice in each group. Mice were intratumorally injected with (a) 0.1M PBS, (b) C-liposomes:non-specific-siRNA (6 µL/1.5 µg v/w) or (c) C-liposomes:H-ferritin-siRNA (6 µL/1.5 µg v/w). Tumors were excised 48 hours after the injection of C-liposomes:siRN, homogenized with RIPA buffer, and total protein isolated and quantified. Immunoblotting analysis was performed to determining expression levels of H-ferritin along with the house-keeping protein ß actin. Detailed procedures are described in the preceding section (**Section 3.2.3**).

3.I.2.6.2 Increased chemotherapeutic efficacy by C-liposomes:H-ferritin-siRNA tested *in vivo*.

With the purpose of testing whether C-liposomes:H-ferritin-siRNA is capable of increasing chemotherapeutic efficacy, mice were randomly assigned to receive either: (a) C-liposomes:non-specific siRNA or (b) C-liposomes:H-ferritin siRNA (6 µL/1.5 µg v/w). In both cases C-liposomes were intratumorally injected on a weekly basis. The following day after C-liposomes were injected, all mice received intraperitoneal injections of BCNU at a dosage of 12.5

mg/kg of body weight. This regimen was conducted for a total of 7 weeks. Tumor size was determined weekly by an individual blinded to treatment groups. A group receiving BCNU alone in this study was not included, as the effect of BCNU alone on tumors is well-established in the literature [192]. Furthermore, the goal of the study was to compare the effects of animals receiving BCNU and H-ferritin siRNA to animals receiving BCNU and non-specific siRNA to determine if there is a difference in efficacy between these two groups.

3.I.2.6.3 Increased radiation efficacy by C-liposomes:H-ferritin-siRNA tested *in vivo*.

To further assess whether C-liposomes:H-ferritin-siRNA increase radiation sensitivity, nine mice with subcutaneous tumors were randomly assigned to receive either: (a) 0.1M PBS, (b) C-liposomes: non-specific-siRNA or (c) C-liposomes:H-ferritin-siRNA (6 µL/1.5 µg v/w). Animals receiving C-liposomes (with either siRNA) were injected with the appropriate liposomes intratumorally on a weekly basis. Two days after the C-liposomes:siRNA injections, of all of the animals received systemic γ-radiation of 4Gy. This regimen was conducted for a total of 7 weeks. Tumor size was recorded weekly by an individual blinded to treatment groups. The goal of the study was to compare the effects of animals receiving radiation and H-ferritin siRNA to animals receiving radiation and non-specific siRNA to determine if there is a difference in efficacy between these two groups.

3.I.3 Results

3.I.3.1 Expression of H-ferritin in malignant tumor cells.

H-ferritin expression was monitored following the procedures described in Section **3.I.2.1.** Representative images from immunocytochemistry in **b, c, h** and **k** of **Figure 3.1** revealed that H-ferritin is expressed in human glioma cells (U251 in **b)**, (U87 in **e**), malignant peripheral

neuro sheeth tumor cells (#215 in **h**) and breast cancer cells (MCF-7 cells in **k**). It is also apparent that H-ferritin is expressed inside nucleus of all the tumor cells. It is likely that H-ferritin plays an important role in tumor cell proliferation. The results from this study provide evidence that H-ferritin is expressed in a broad spectrum of malignant tumors.

3.I.3.2 H-ferritin is co-localized with the glioma stem cell marker CD133 in malignant tumor cells

The co-localization of H-ferritin expression with glioma stem cell marker CD133 was monitored following the procedures described in Section **3.I.2.2.** The images obtained from immunocytochemistry revealed that CD133 expression (**b, h)** is co-localized with H-ferritin expression (**e, i**) as shown in **Figure 3.2-3.4;** co-localization of CD133 with H-ferritin is shown in image **j**. CD133 has been used, although not exclusively, as a marker for the identification of stem cells from normal and cancerous tissues. The co-localization of H-ferritin and CD133 in these cell lines established an experimental relationship between cancer stem cells marker and H-ferritin expression.

3.I.3.3 H-ferritin is down regulated in U251 and MCF-7 cells by C-liposomes:siRNA

H-ferritin expression was down-regulated following the procedures described in Section **3.I.2.3.** As shown in **Figure 3.5**, C-liposomes efficiently delivered H-ferritin siRNA into U251and MCF-7 cells, and released functional H-ferritin-siRNA that successfully down-regulated H-ferritin. In U251 cells, H-ferritin expression was reduced by 90% at 24 and 48 hours post transfection, and by 50% at 72 hours post transfection. Delivery of non-specific-siRNA by C-liposomes, as well as treatment with only C-liposomes, had no effects on H-ferritin expression. In MCF-7 cells, H-ferritin-siRNA was only slightly downreuglated at 24 hours, but was decreased by 60% at 48 hours, and 80% at 72 hours post transfectionin, as seen in **Figure 3.6**.

These results show that H-ferritin siRNA, delivered by C-liposomes, is able to silence H-ferritin gene and protein expression, which establishes the technical foundation for testing our hypothesis and proposed therapeutic strategies.

3.I.3.4 H-ferritin siRNA enhanced sensitivity of U251 cells to chemotherapy *in vitro* and *in vivo*.

H-ferritin siRNA enhanced chemotherapeutic efficacy *in vitro* following the procedures described in Section **3.I.2.4.** This set of experiments was pivotal for the entire research project i.e. that is it answered the question as to whether down-regulation of H-ferritin would facilitate conventional chemotherapy for cancer treatments. As demonstrated in **Figure 3.7**, the presence of H-ferritin siRNA decreased the LD50 for BCNU from > 100 µM to 40 µM in U251 cells. Similarly, for the cell lines MCF-7 and sNF96.2, knockdown of H-ferritin with siRNA decreased the LD50 for BCNU from > 100 µM to 20 µM as shown in **Figure 3.8** and **3.9.** These experiments provide *in vitro* evidence to support the hypothesis and demonstrate that C-liposome:H-ferritin-siRNA gene therapy can enhance the efficacy of chemotherapy for the treatment of malignant tumor cells.

H-ferritin siRNA delivered by C-liposomes down regulated H-ferritin locally and efficiently in subcutaneous xenograft (**Figure 3.11**) following the procedures described in Section **3.I.2.6.1.** Sequentially, H-ferritin siRNA was found to enhance chemotherapeutic sensitivity *in vivo* following the procedures described in Section **3.I.2.6.2.** The chemotherapeutic efficacy of BCNU was enhanced by the presence of C-liposomes:H-ferritin-siRNA. Tumor growth was effectively suppressed by 50% (*$p<0.01$) at week 5 and 100% (*$p<0.01$) at week 7, in animals receiving C-liposomes:H-ferritin-siRNA compared to the control group receiving C-liposomes:non-specific-siRNA (**Figure 3.12**). Throughout the course of the C-liposomes:siRNA

injections, both groups received 12.5mg/kg of BCNU weekly through IP injection route. This concentration of BCNU is less than 50% of the reported effective dose [192] and was chosen also based on the decreased LD50 observed in the cell culture study demonstrating proof of concept. The study was terminated at week 7 because the tumor growth was too large to continue in the control group. Our data revealed that silencing of H-ferritin by gene therapy enhanced chemotherapeutic efficacy for the treatment of glioma. These data provided *in vivo* evidence to support the hypothesis.

3.I.3.5 H-ferritin siRNA enhances sensitivity to radiation *in vitro* and *in vivo*

H-ferritin siRNA enhanced radiation efficacy in U251 cells following the procedures described in **3.I.2.5.** To determine whether H-ferritin siRNA could sensitize cells to radiation therapy, U251 cells were treated with C-liposomes:siRNA for 24 hours, and then subjected them to γ-radiation. The proliferation rate of U251 glioma tumor cells was suppressed by knockdown of H-ferritin with siRNA in the presence of 20 Gy by 35% at 24 hours, 50% at 48 hours and 60% at 72 hours post radiation exposure compared to cells treated with the NS siRNA (**Figure 3.10**). It was noted that C-liposome:non-specific-siRNA increased cells survival slightly at 48 and 72 hours post γ-radiation compared with controls; however, this increase in cell survival was not significant.

H-ferritin siRNA similarly enhanced radiation efficacy *in vivo* following the procedures described in **3.I.2.6.3**. The radiation efficacy was enhanced by the presence of C-liposomes:H-ferritin-siRNA. Tumor growth was effectively suppressed by 100 fold at week 5 and 1000 fold at week 7 in animals receiving C-liposomes:H-ferritin-siRNA compared to control animals receiving C-liposomes:non-specific-siRNA (**Figure 3.13**). Throughout the course of the C-liposome:siRNA injections, both groups received radiation (4 Gy) weekly by a systemic regimen.

The amount of radiation used in the literature ranges from 2 to25 Gy, most studies report using 5 Gy, and historic untreated controls are available [193-198]. We chose the lower range (4Gy) and showed a significant and dramatically increase of efficacy of this dose in the presence of siRNA for H-ferritin (**Figure 3.I.3)**. The study was terminated at week 7 because tumors were too large for the study to continue in the control group. This study demonstrated two things: that treatment effectiveness could be increased using a low dosage of radiation, such that side effects associated with treatment could be alleviated, and (in support of the hypothesis) that down regulation of H-ferritin expression could enhance radiation therapy for the treatment of glioma.

3.I.3.6 H-ferritin siRNA down regulated H-ferritin expression in a tumor xenograft model.

H-ferritin expression was down regulated following the procedures described in **3.I.2.6.1.** Direct intratumoral injection of C-liposomes:H-ferritin-siRNA in a subcutaneous xenograft model resulted in a greater than 60% decrease in H-ferritin expression at 48 hours post injection, compared with H-ferritin expression in animals injected with C-liposomes alone or C-liposomes:non-specific-siRNA (**Figure 3.11**). These results demonstrate that, although H-ferritin is downregulated *in vivo*, the extent of downreulation is not as much as *in vitro* (**Figure 3.5**).

3.I.4 Summary

The results presented in part I of chapter 3 provided concrete experimental data to positively test the central hypothesis. All data obtained support the central hypothesis that down-regulation of H-Ferritin enhanced the efficacy of chemo- and radiation treatments for cancer. In particular, the experimental results (Section **3.I.3.4**) showed that downregulation of H-ferritin reduced tumor volume by 60% when given in combination with only 40% of the standard BCNU dosage. Combining H-ferritin down regulation with radiation treatment showed a similar effect

(**Section 3.I.3.5**). These results suggest that combining H-ferritin down regulation with a lower dosage of conventional cancer treatments may bring great benefit to patients, as it would significantly reduce the side effects of chemo-/radiation therapies. The immunocytochemistry results (**Section 3.I.3.1**) suggest that a broad spectrum of malignant tumors may be treated with this synergetic approach, as H-ferritin expression was observed in all the cancer cell lines studied in this research (human glioma U251 and U87 cells, malignant peripheral neuro sheath tumor #215 cells, and breast cancer MCF-7 cells). Furthermore, the finding of co-localization of H-ferritin with the glioma stem cell marker CD133 (**Section 3.I.3.2**) suggested that this synergetic treatment strategy could be also effective in treating metastatic tumors.

3.I.5 Figures and Legends

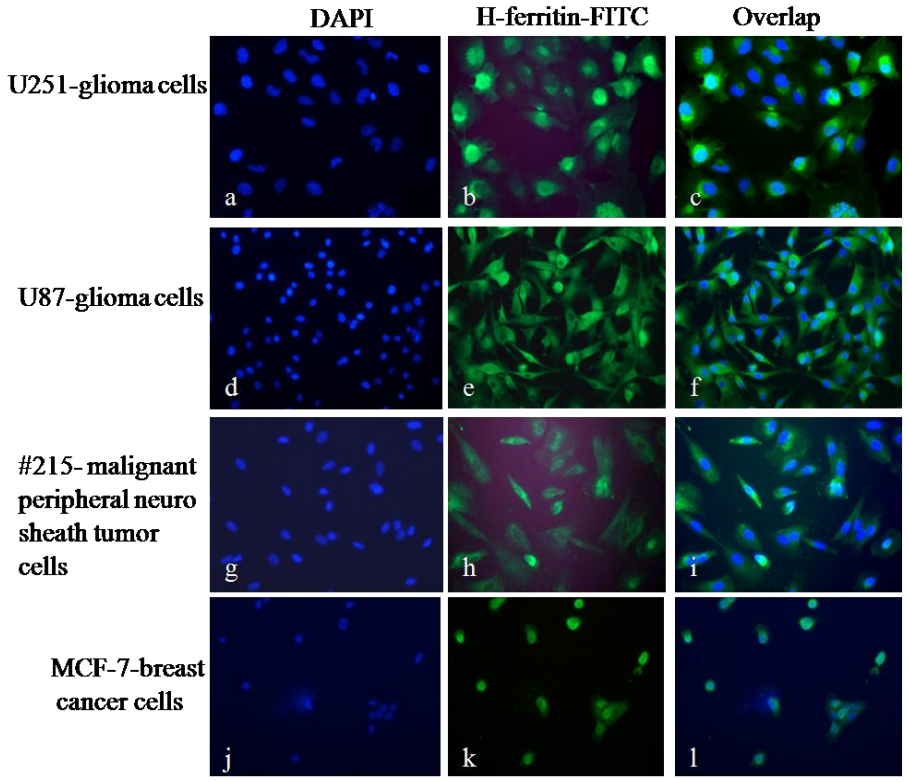

Figure 3.1. H-ferritin expression in malignant tumor cells detected by immunocytochemistry. The blue colors of three images **a, d, g** and **j,** represent DAPI. The green color of three images **b, c, h** and **k** represent H-ferritin expression and three images **c, f, I** and **l** represent the overlap. **A, b** and **c** represent U251, **d, e** and **f** represent U87 cells, **g, h** and **i** represent NF 215 and **j, k** and **l** represent MCF-7 cells.

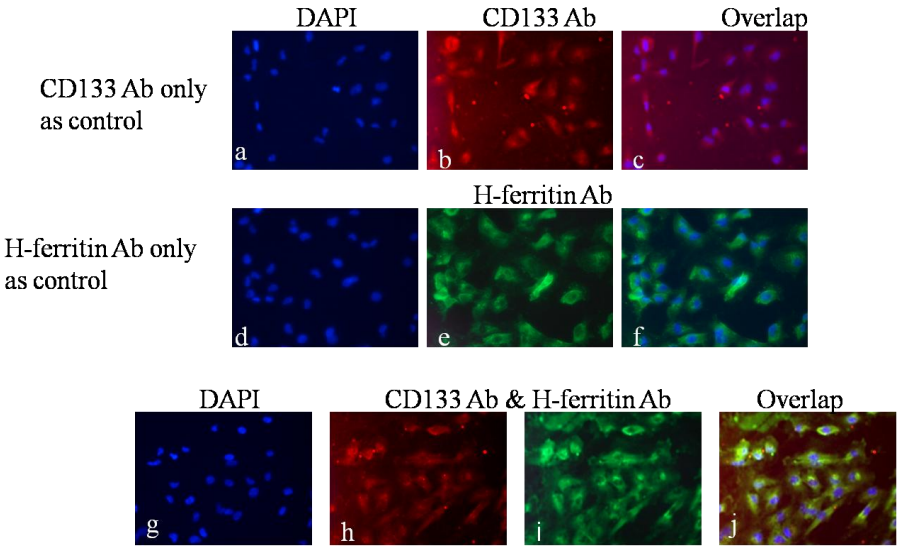

Figure 3.2. H-ferritin in U251 cells is associated with the glioma stem cell marker CD133, as tested by immunocytochemistry. The blue colors of three images **a, d** and **g** represent DAPI. The red color of the two images **b** and **h** represent CD133 expression. The green color of the two images **e** and **i** represent H-ferritin expression. The images **c, f** and **j** represent overlap. The co-localization of H-ferritin with CD133 demonstrated that glioma U251 cells share some stem cells properties.

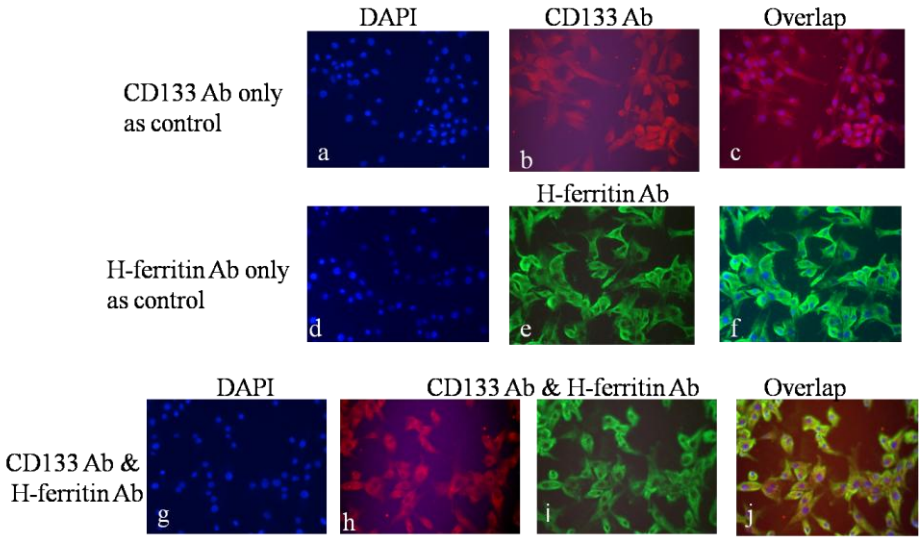

Figure 3.3. H-ferritin in U87 cells is associated with the glioma stem cell marker CD133, as tested by immunocytochemistry. The blue colors of three images **a, d** and **g** represents DAPI. The red color of the two images **b** and **h** represent CD133 expression. The green color of the two images **e** and **I** represent H-ferritin expression. The images **c, f** and **j** represent overlap. The co-localization of H-ferritin with CD133 demonstrated that glioma U87 cells share some stem cells properties.

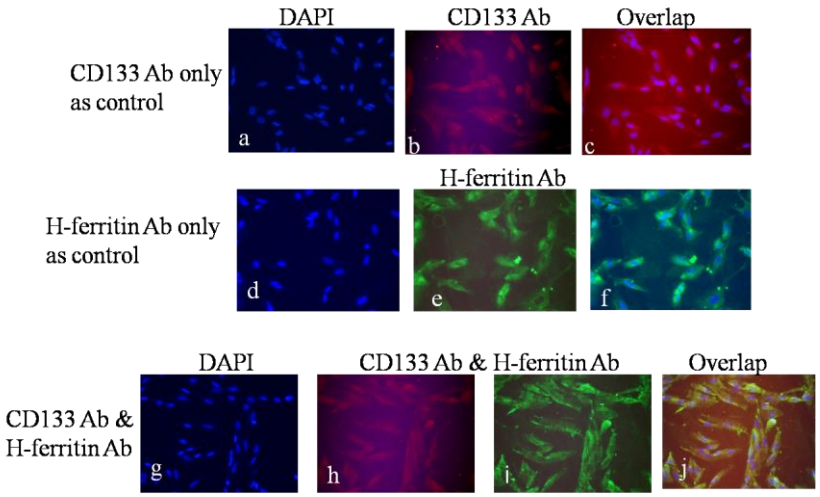

Figure 3.4. H-ferritin in NF #215 cells is associated with the glioma stem cell marker CD133, as tested by immunocytochemistry. The blue colors of three images **a, d** and **g** represents DAPI. The red color of the two images **b** and **h** represent CD133 expression. The green color of the two images **e** and **i** represent H-ferritin expression. The images **c, f** and **j** represent overlap. The co-localization of H-ferritin with CD133 demonstrated that malignant peripheral neuro sheath tumor #215 cells share some stem cells properties. Again this comment is uninformative.

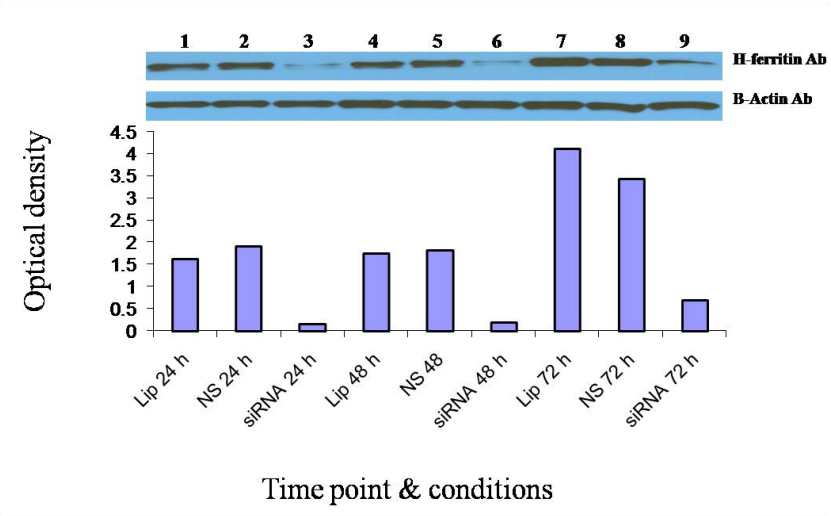

Figure 3.5. Down regulation of H-ferritin expression in U251 cells, as tested by Western blot. The image on the top of the graph shows downregulation of H-ferritin expression by H-ferritin siRNA in U251 cells tested by immunoblotting analysis. Lanes, 1, 4 and 7 were treated with C-liposomes alone as control group. Lanes 2, 5 and 8 were treated with C-liposomes containing non-specific-siRNA as additional control group. Lanes 3, 6 and 9 were treated wtih C-liposomes:H-ferritin-siRNA as a treatment group. H-ferritin siRNA down regulated H-ferritin at 24, 48 and 72 hours post transfection. The siRNA carried and released by C-liposomes is functional. ß-actin was used to demonstrate that equal amounts of protein were loaded in each lane. The graph represents the optical density of the scanned Western blots.

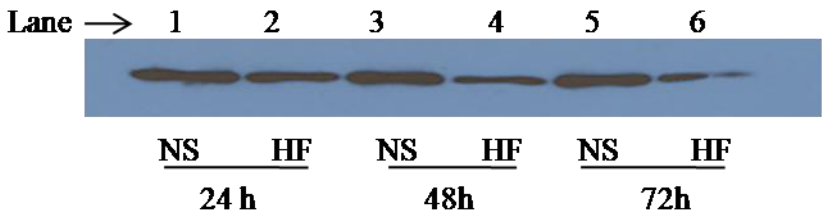

Figure 3.6. Down regulation of H-ferritin expression in MCF-7 cells, as tested by Western blot. The image represents the results of down regulating H-ferritin expression in MCF-7 cells by H-ferritin siRNA, as tested by immunoblotting analysis. Lanes, 1, 3 and 5 were treated with C-liposomes containing non-specific-siRNA as control group. Lanes 2, 4 and 6 were treated with C-liposomes containing H-ferritin-siRNA as treatment group. HH-ferritin was down-regulated by 10% at24 hours, 70% at 48 hours, and 90% at 72 hours post transfection. siRNA carried and released by C-liposomes was functional.

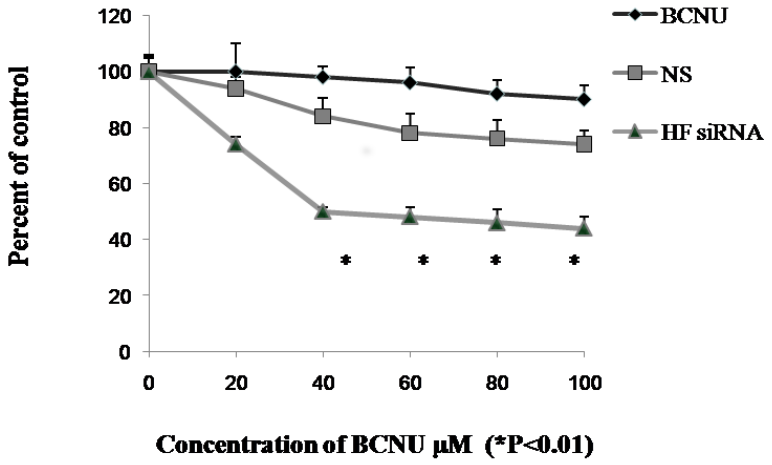

Figure 3.7. H-ferritin siRNA increases the chemotherapeutic sensitivity of glioma U251 cells, the cell survive was tested by SRB assay. The relative cytotoxicity of H-ferritin-siRNA vs. a non-specific siRNA in the presence of increasing concentrations of BCNU was determined by SRB assay. ♦, BCNU alone serves as a control group. ■, BCNU+ C-liposomes:non-specific-siRNA represents another control group. ▲, BCNU+ C-liposomes:H-ferritin-siRNA represent the treatment group. The data revealed that cells are more vulnerable to BCNU at each concentration examined in the presence of H-ferritin-siRNA, compared with non-specific siRNA. The data represent the mean and standard error of three experiments at each concentration (*p<0.01).

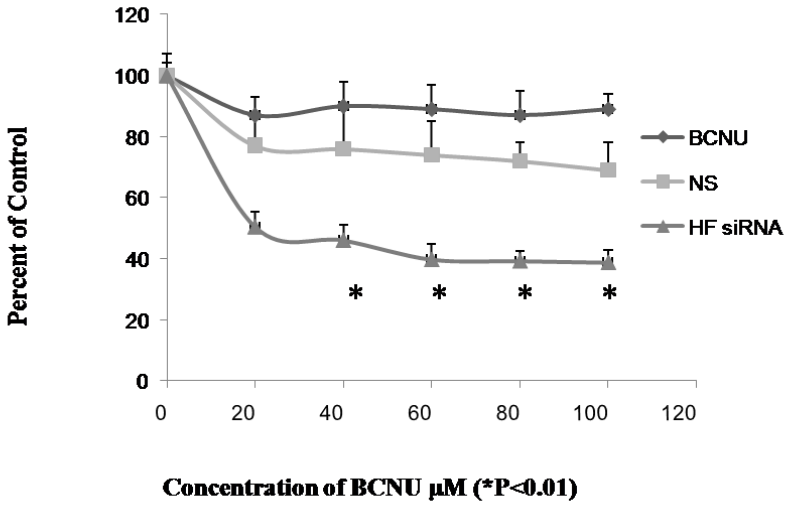

Figure 3.8. H-ferritin siRNA increases the chemotherapeutic sensitivity of breast cancer MCF-7 cells, as tested by an SRB assay. The relative cytotoxicity of H-ferritin-siRNA vs. a non-specific siRNA in the presence of increasing concentrations of BCNU was determined by an SRB assay. ♦, BCNU alone serves as a control group. ■, BCNU+ C-liposomes:non-specific-siRNA represents another control group. ▲, BCNU+ C-liposomes:H-ferritin-siRNA represents a treatment group. The data reveal that cells are more vulnerable to BCNU at each concentration examined in the presence of H-ferritin-siRNA compared with non-specific-siRNA. The data represent mean and standard error of three experiments at each concentration (*p<0.01).

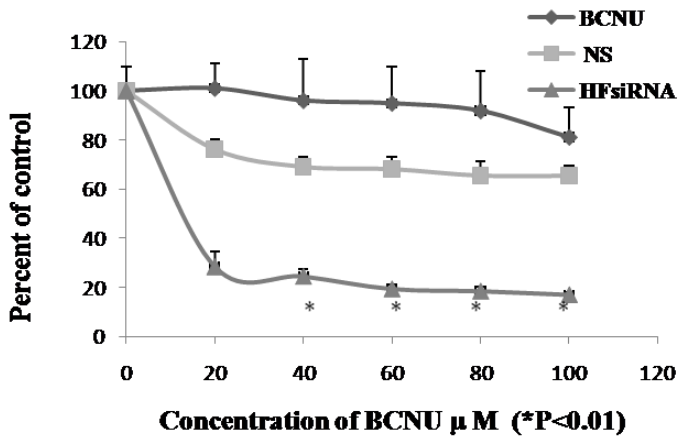

Figure 3.9. H-ferritin siRNA increases the chemotherapeutic sensitivity of malignant peripheral neuro sheeth tumor (MPNST) sNF96.2 cells, as tested by an SRB assay. The relative cytotoxicity of H-ferritin-siRNA vs. a non-specific siRNA in the presence of increasing concentrations of BCNU was determined by an SRB assay. ♦, BCNU alone serves as a control group. ■, BCNU+ C-liposomes:non-specific-siRNA represents another control group. ▲, BCNU+ C-liposomes:H-ferritin-siRNA represents a treatment group. The data revealed that cells are more vulnerable to BCNU at each concentration examined in the presence of H-ferritin siRNA, compared with the control group of non-specific siRNA. The data represent the mean and standard error of three experiments at each concentration (*p<0.01).

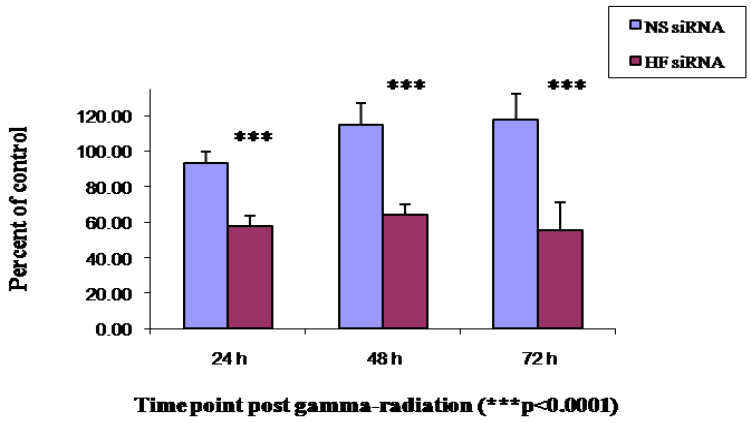

Figure 3.10. H-ferritin siRNA increases the sensitivity of glioma U251 cells to radiation, as tested by an MTS assay. The relative cytotoxicity of H-ferritin-siRNA vs. a non-specific siRNA in the presence of radiation (20 Gy) was determined by an MTS assay. The stripes represent C-liposomes:non-specific-siRNA and serve as a control group. The dots represents C-liposomes:H-ferritin-siRNA and are the treatment group. The data indicate that cells are more vulnerable to radiation at each time point examined in the presence of H-ferritin siRNA, compared with non-specific siRNA. The data represent the mean and standard error of three experiments at each concentration (***P<0.0001).

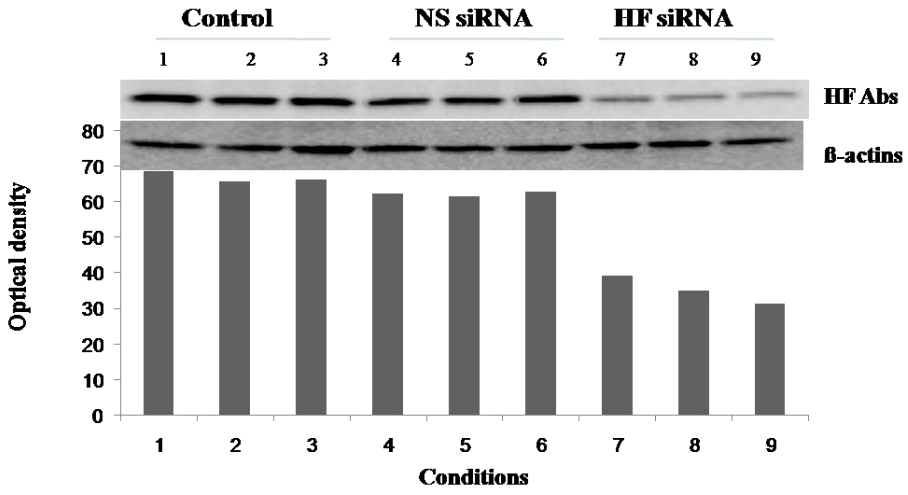

Figure 3.11. Down regulation of H-ferritin in a tumor xenograft model, as analyzed by Western blot. Images on the top of the graph represent the results of immunoblotting analysis. The bottom graph represents the optical density of the scanned images from the image on top. Lanes 1, 2 and 3 were treated with PBS as a control group. Lanes 4, 5 and 6 were treated with C-liposomes:non-specific-siRNA as another control group. Lanes 7, 8 and 9 were treated with C-liposomes:H-ferritin-siRNA and are the treatment group. H-ferritin expression was effectively decreased at 48 hours post injection of C-liposomes:H-ferritin-siRNA, as shown in lanes 7, 8 and 9. H-ferritin siRNA carried and released by C-liposomes is functional, even in a tumor xenograft.

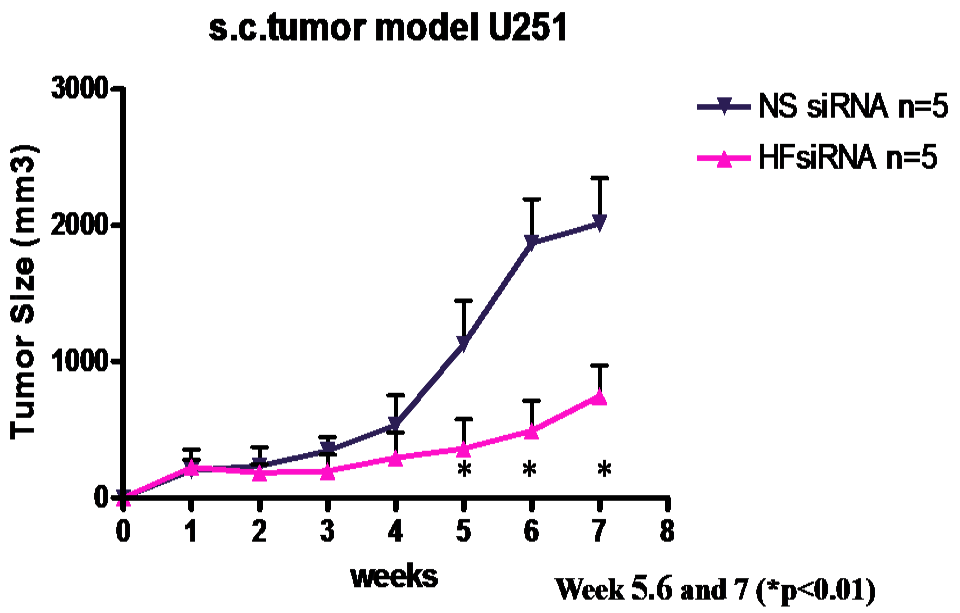

Figure 3.12. H-ferritin siRNA is an effective adjuvant for chemotherapy in a subcutaneous tumor mouse model. The data are plotted as average tumor size from measurements of 5 mice for each condition on a weekly basis.▼, C-liposomes:non-specific-siRNA.▲, C-liposomes:H-ferritin-siRNA. The differences between NS and H-ferritin siRNA were significant at week 5, 6 and 7 (*p<0.01).

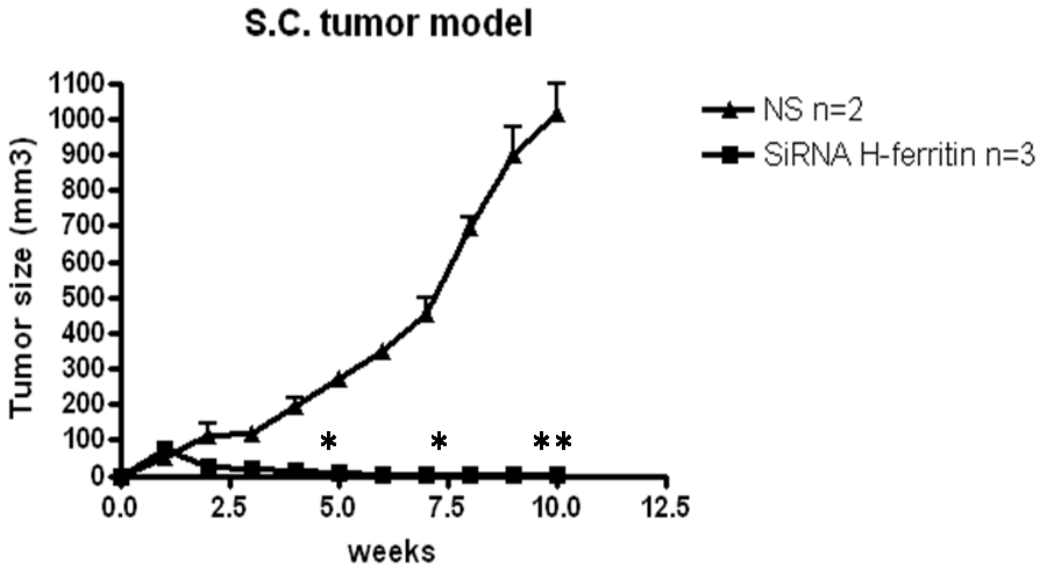

Figure 3.13. H-ferritin siRNA is an effective adjuvant for radiation therapy in a subcutaneous mouse tumor model. The data are plotted as an average tumor size from measurements of 2 or 3 mice for each condition on a weekly basis▼, C-liposomes:non-specific-siRNA.■, C-liposomes:H-ferritin-siRNA. The differences between NS and H-ferritin-siRNA were significant at week 5, 7.5 and 10 (*$p<0.01$, (**$p<0.001$).

Chapter 3

Part 2 The functional role of H-ferritin in cancer development

3.II.1 Introduction

In part II of chapter 3, **t**he experimental methods/procedures for investigating the functional role of H-ferritin in cancer development are described in detail. The experimental premise is based on the results of the part I of chapter 3; H-ferritin siRNA enhanced the radiation and chemotherapeutic efficacy for treatment of gliomas. The following 4 kinds of experiments were carefully designed to assess the functional role of H-ferritin in cancer development:

1) Investigation on the role of H-ferritin in DNA superhelical formation by supercoil relaxation assays.
2) Investigation of potential correlation between the DNA repair protein MGMT and H-ferritin.
3) Investigation of H-ferritin on apoptotic pathways.
4) Investigation of the role of H-ferritin role in DNA synthesis.

3.II.2. Materials and Methods

3.II.2.1 Supercoil relaxation assays

Following the successfully testing of the central hypothesis with in *vivo* and *in vitro* experiments described in part I of chapter 3, further experiments were performed to investigate the potential mechanisms by which H-ferritin may protect DNA during the rapid proliferation of tumor cells. A series of supercoil relaxation assays were performed to monitor the conversion of supercoiled circular DNA to relax and/or linear circular DNA. DNA back bone cleavage was

assessed in the presence or absence of H-ferritin/L-ferritin and the chemotherapeutic agent BCNU or radiation. Supercoiled DNA plasmid pUC19 (BioLabs) consists of covalently closed circular DNA, and was selected for use as an *in vitro* model system that has been applied to investigate DNA interactions previously in our laboratory [1]. The basic procedures for the supercoil relaxation assays are as follows. 1) 1 µg of supercoiled DNA plasmid pUC19 was dissolved in 10 mM Hepes (pH7.5), 50 mM NaCl, 2.5 mM $MgCl_2$ and 2.5 mM DTT (total volume 30 µL), which allows the resolution of topoisomers under standard electrophoresis without ethidium bromide. 2) The samples were loaded on a1.5% agarose gel and run at 40 mA for 6 hours at room temperature. Gels were then immersed in 100 ml of TAE buffer containing 5 µL of SYBR Safe DNA gel stain (Invitrogen) for 10 minutes. The conversion of DNA to relaxed (R), linear (L) and supercoiled forms (SC) was monitored using a LAS 3000 Fuji image reader. Three independent assays were performed as explained in the following section.

3.II.2.1.1 Heavy chain ferritin alters the effects of BCNU on DNA coiling.

To study how heavy chain ferritin affects the function of the chemotherapeutic agent BCNU, a supercoil relaxation assay was performed under conditions of BCNU and heavy chain ferritin. The supercoiled DNA plasmid pUC19 was treated with incremental concentrations of BCNU in the presence or absence of 2.5 µM H-ferritin for one hour at 37^{o}C. The reaction was terminated with 50% (v/v) glycerol, 50 mM EDTA and 0.1 % Bromophenol blue.

3.II.2.1.2 H-ferritin, but not L-ferritin alters the function of BCNU on DNA coiling.

To investigate whether the alterations on DNA by heavy chain ferritin are unique to H-ferritin, a supercoil relaxation assay was performed under the conditions of BCNU, heavy chain ferritin, or light chain ferritin. The supercoiled DNA plasmid pUC19 was treated with 5 µM of BCNU and incremental concentrations of heavy chain or light chain ferritin for one hour at 37^{o}C.

The reaction was terminated with 50% (v/v) glycerol, 50 mM EDTA and 0.1 % Bromophenol blue.

3.II.2.1.3 Protection of DNA by heavy chain ferritin even under radiation.

To investigate whether H-ferritin protects DNA in the face of radiation, a supercoil relaxation assay was performed under the conditions of H-ferritin, L-ferritin and 4 Gy of γ-radiation. The supercoiled DNA plasmid pUC19 was treated with 4 µM of heavy chain ferritin, 4 µM of L-ferritin, or not treated to serve as a control group for 1 hour at 37^{o}C. Subsequently all samples were treated with an incremental dosage of γ-radiation. The reaction was terminated with 50% (v/v) glycerol, 50 mM EDTA and 0.1 % Bromophenol blue.

3.II.2.2 Correlation between the expression of the DNA repair protein MGMT and H-ferritin.

To explore the role of H-ferritin in the process of DNA repair, the DNA repair proteinO^{6}-methylguanine-DNA methyltransferase (MGMT) expression was assessed by Western blot in U251 and MCF-7 cells. Briefly, U251 cells at a density of 166,000 cells/well and MCF-7 cells at a density of 333,000 cells/well were seeded into six-well plates and allowed to attach overnight. Cultures were transfected with either C-liposomes:non-specific-siRNA:DMEM or C-liposomes:H-ferritin-siRNA:DMEM (4uL/1µg/1mL) for 3 hours, before media was replaced with complete media. Cell lysate was harvested using RIPA buffer (Sigma, cat. no. R0278-50ML) at 24 h, 48 h, and 72 h post transfection. Total protein was quantified and Western blot analysis performed. Membranes were incubated overnight at 4^{o}C with a monoclonal MGMT antibody (Cell Signaling 1:1000 dilutions), followed by secondary anti-rabbit IgG conjugated to horseradish peroxidase (GE Healthcare UK, cat. no. NA934V, 1:5000 dilutions) for 1.5 hours at

room temperature. Blots were then exposed to the Western Lightning Chemiluminescence Reagent and examined using a LAS 3000 Fuji image reader.

3.II.2.3 H-Ferritin and the apoptotic pathway.

In order to test whether H-ferritin siRNA facilitates the apoptotic pathway or not, U251 cells (at a density of 166,000 cells/well) and MCF-7 cells (at a density of 333,000 cells/well) were seeded into six-well plates and allowed to attach overnight. Cultures were transfected with either C-liposomes:non-specific-siRNA:DMEM or C-liposomes:H-ferritin-siRNA:DMEM (4uL/1μg/1mL) for 3 hours, and then serum free media was changed to complete media. Cell lysate was collected using lysis buffer from the Caspase-3 Fluorometric kit (R&D cat. no. BF1100) at 48 hours post transfection; the assay was performed following the manufacturer's instruction. Data was analyzed using a fluorescence plate reader (Spectra A 340PC 384, Molecular Devices).

3.II.2.4. Heavy chain ferritin and DNA synthesis.

To investigate whether H-ferritin is involved in DNA synthesis, 5-Bromo-2´-deoxyuridine (BrdU) and ^{3}H-Thymidine incorporation into DNA in glioma cells was tested.

3.II.2.4.1. Heavy chain ferritin facilitates DNA synthesis, as measured by BrdU incorporation.

In order to test the effects of H-ferritin on DNA synthesis, immunocytochemistry was performed using a BrdU anti body. U251 and U87 cells (at a density of 20,000cells/well) were cultured in chamber slides overnight. Cultures were transfected with C-liposomes:siRNA:DMEM (4μL/1μg/1mL) for 3 hours and then serum free media was replaced with complete media. After

72 hours post transfection, 30 µM BrdU (Sigma, cat. no. B5002) was added to the cells for 3 hours. Cells were fixed by 4%PFA and then exposed to anti-BrdU-Alexa-Fluor 488 conjugate (Invitrogen, cat. no. 21303) Ab overnight at 4^{o}C. Preparations were rinsed, then stained with 1% (w/v) DAPI in DMEM (4, 6-diamidino-2-phenylindole for 10 minutes) to visualize nuclei, and mounted and dried overnight. Images were captured with fluorescence microscopy.

3.II.2.4.2 Heavy chain ferritin facilitates DNA synthesis, as measured by ^{3}H-thymidine incorporation.

To study the effects of H-ferritin on DNA synthesis, 3H-Thymidine incorporation was tested. U251 and U87 cells (at a density of 166,000/well) were cultured in six well plates and allowed to attach overnight. Cells were transfected with C-liposomes:siRNA:DMEM (4µL/1µg/1mL) for 3 hours and then serum free media was replaced with complete media. Cultures were then exposed to ^{3}H-Thymidine 72 hours post transfection. Cells were collected using 200 µL of 0.5 M of sodium hydroxide and 200 µL of 5% acidic acid following 2, 4 and 6 hours of ^{3}H-thymidine exposure. ^{3}H-Thymidine incorporation (counts per minute (CPM)) was detected with a scintillation counter.

3.II.3 Results

3.II.3.1 H-ferritin, but not L-ferritin, inhibited the action of BCNU on DNA coiling, affected DNA coiling under radiation.

Heavy chain ferritin altered the action of BCNU even when exposed to radiation, following the procedures described in **3.II.2.1.1.-3.II.2.1.3.** The results from the supercoil relaxation assay using pUC19 DNA plasmid revealed that BCNU exposure converted circular DNA to the supercoiled form, as seen in the right panel of the image in **Figure 3.14.** The effects

of BCNU were attenuated by H-ferritin, as shown in the left panel of the image in **Figure 3.14** and were concentration dependent **(**left panel of **Figure 3.15).** However, horse spleen ferritin (which is composed of 95% L-ferritin) was not able to attenuate the effect of BCNU on pUC19 DNA plasmid, as shown in the right panel of **Figure 3.15**. Furthermore, the presence of H-ferritin was associated with a 5-10% shift of total DNA into relaxation and linear form. in the presence of γ-radiation, as shown in **Figure 3.16**. The conformation of pUC19 DNA plasmid treated with L-ferritin (middle of the panel) looked similar to the control treated plasmid (left panel of the image) (**Figure 3.16),** while the H-ferritin treated plasmid showed a different pattern. H-ferritin administration shifted 5-10% DNA into a relaxed and linear form shown in the middle panel of **Figure 3.16**. These results demonstrate that H-ferritin is capable of maintaining pUC19 plasmid DNA in a relaxed and linear form under the anti-tumor agent BCNU and radiation (4Gy).

3.II.3.2 MGMT expression in malignant tumor cells.

MGMT expression levels were determined by immunoblotting analysis following the procedures described in **3.II.2.2.** MGMT expression was not observed in U251 cells, but was detected in MCF-7 cells. However, down regulation of H-ferritin did not alter MGMT expression in MCF-7 cells, as shown in **Figure 3.17**. These results demonstrate that H-ferritin is not involved with the MGMT related DNA repair pathway.

3.II.3.3 H-ferritin siRNA increased Caspase-3 activity in U251 and MCF-7 cells.

An anti-apoptotic effect by heavy chain ferritin was assessed following the procedures described in **3.II.2.3.** Caspase-3 activity, a protein involved in the apoptotic pathway, was tested 48 hours post transfection of C-liposoemes:siRNA. Compared to cells transfected with non-specific siRNA, Caspase-3 activity was increased by nearly 60% ***$p<0.0005$) in U251 cells

with silenced H-ferritin, as shown in **Figure 3.18**, and by 20% (*p<0.05) in MCF-7 cells, as shown in **Figure 3.19.** This data suggests that H-ferritin plays a role in anti-apoptotic functions during tumor development.

3.II.3.4 BrdU and ^{3}H-thymidine incorporation is decreased by H-ferritin downregulation.

The role of heavy chain ferritin in DNA synthesis was investigated following the procedures described in **3.II.2.4.** The images captured by fluorescence microscopy, demonstrated that BrdU incorporation in U251 and U87 cells was decreased by H-ferritin downregulation, as shown in image **b** and **h** of **Figure 3.20.** BrdU incorporation was higher in cultures treated with C-liposomes:non-specific siRNA as shown in image **e** and **k** of **Figure 3.20**. ^{3}H-thymidine incorporation in U251 and U87 cells, shown in **Figure 3.21-3.21,** corresponded with the results obtained from the study of BrdU incorporation **s**hown in **Figure 3.20.** The results of both the BrdU and 3H-thymidine incorporation implied that H-ferritin may promote DNA synthesis.

3. II.4 Summary

To understand the mechanism by which downregulation of H-ferritin sensitizes glioma cells to chemo- and radiation therapy. The functional role of H-ferritin in cancer development related with a number of biological pathways was investigated. The experimental results demonstrated that H-ferritin protects DNA from oxidative stress [1, 2] maintains DNA in a relaxed and linear form, which facilitates gene transcription [2, 149] and prevents apoptosis [7-10]. H-ferritin facilitated BrdU and ^{3}H-thymidine incorporation with DNA synthesis in U251 and U87 cells. However, down regulation of H-ferritin does not affect the MGMT DNA repair pathway. Further investigation is needed to completely determine the multifunctional role of H-ferritin in biological pathways of both normal and malignant cells.

3.II.5 Figures and legend

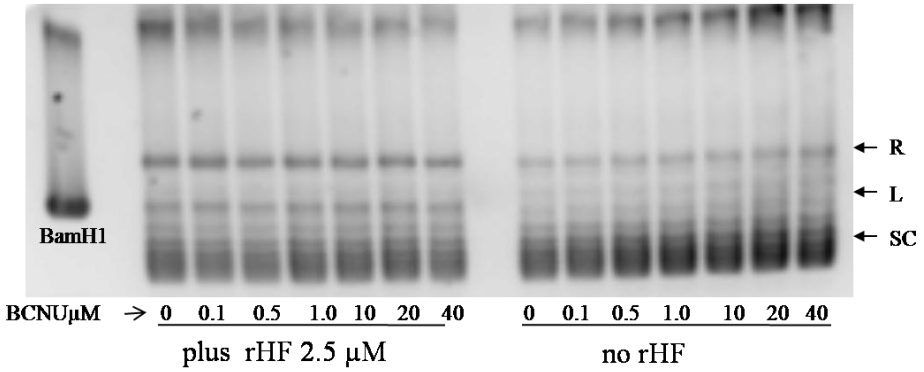

Figure 3.14. H-ferritin attenuated the effects of BCNU on DNA, as evidenced by a supercoil relaxation assay. The effect of BCNU with H-ferritin on DNA was tested by a supercoil relaxation assay on a 1% agarose gel. Supercoiled DNA plasmid pUC19 was treated with incremental concentrations of BCNU in the presence (left panel) or absence (right panel) of 2.5 μM H-ferritin. The conversion to the supercoiled form (SC) of DNA was induced by BCNU (right panel on the bottom). This effect was inhibited by H-ferritin (left panel on the bottom). (R; relaxation form, L; linear form, SC; Supercoiled form).

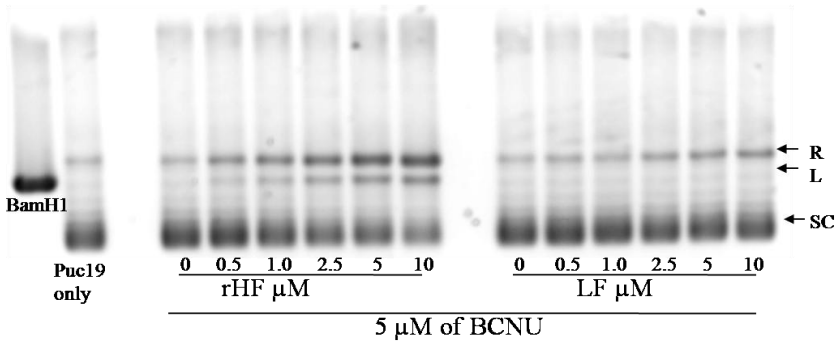

Figure 3.15. Influence of H-ferritin on DNA relaxation, as evidenced by a supercoil relaxation assay. A comparison of the effect of H-ferritin and L-ferritin on DNA was tested by a 1% agarose gel. Supercoiled DNA plasmid pUC19 was treated with 5µM of BCNU and then exposed to incremental concentrations of H-ferritin (left panel) or L-ferritin (right panel). The conversion to the relaxed (R) and linear (L) form was observed in the presence of H-ferritin (left panel) but not in the presence of L-ferritin (right panel). The presence of H-ferritin was associated with an increase in the relaxed and linear forms (left panel). L-ferritin had a minimal effect (right panel). (R: relaxation form, L: linear form, SC: Supercoiled form).

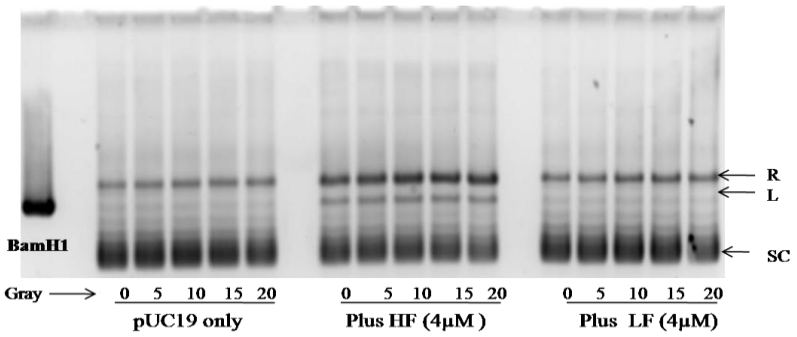

Figure 3.16. Influence of H-ferritin on DNA relaxation under radiation, as evidence by a supercoil relaxation assay. A comparison of the effect of H-ferritin and L-ferritin on DNA under radiation was tested by a supercoil relaxation assay. Supercoiled DNA plasmid pUC19 was treated with incremental dosages of γ-radiation; without ferritin (left panel), with H-ferritin (middle panel) or with L-ferritin (right panel). The conversion to the relaxed (R) and linear (L) forms was observed in the presence of H-ferritin (middle panel) but not in the presence of L-ferritin (right panel). H-ferritin kept DNA in a relaxed and linear form even under radiation (middle panel).

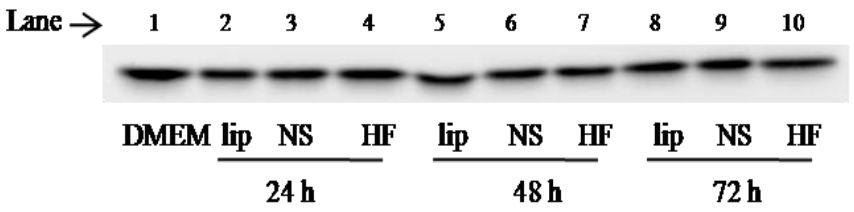

Figure 3.17. MGMT expression in MCF-7 cells, as tested by Western blot. Down regulating H-ferritin by siRNA did not alter MGMT expression in MCF-7 cells at 24 hours, 48 hour and 72 hours post transfection. The evidence demonstrates that H-ferritin is not associated with the MGMT related DNA repair pathway.

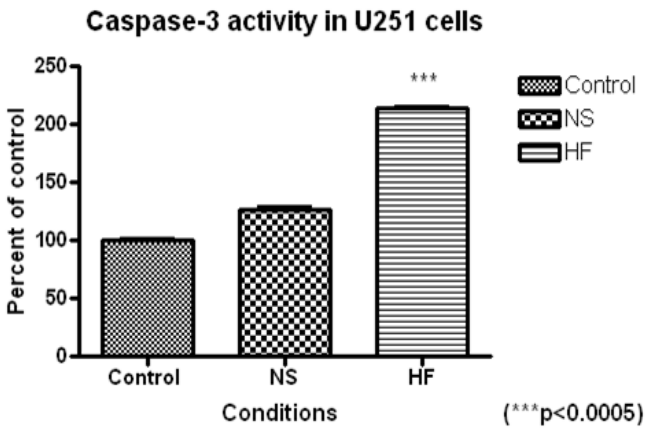

Figure 3.18. H-ferritin is associated with increased Caspase-3 activity in U251 cells. Caspase-3 activity in U251cells was examined. The exposure of U251 cells to C-liposomes:H-ferritin-siRNA (HF) is accompanied by an increase in Caspase-3 activity. There were no significant effects on Caspase 3 activity when cultures were exposed to C-liposomes:non-specific-siRNA (NS). The data suggest that H-ferritin plays a role in the apoptotic process in U251 glioma cells. Data are normalized to the control group. The differences between the NS and HF siRNA are significant (***p<0.0005).

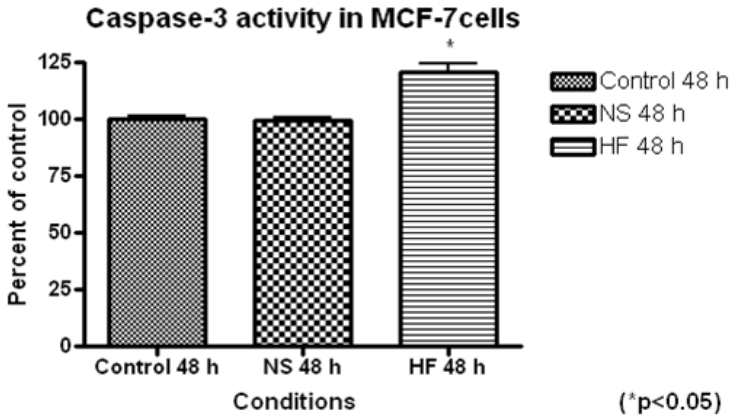

Figure 3.19. H-ferritin is associated with increased Caspase-3 activity in MCF-7 cells. Caspase-3 activity was measured in breast cancer cells MCF-7 cells. The exposure of MCF-7 cells to C-liposomes:H-ferritin:siRNA is accompanied by an increase in caspase-3 activity. No effects on Caspase-3 activity were seen when cultures were exposed to C-liposomes:non-specific-siRNAcompared to controls. . Thus, H-ferritin appears to prevent apoptosis in MCF-7 cells. Data are normalized to untreated controls. The differences between the NS and HF siRNA are significant (*p<0.05).

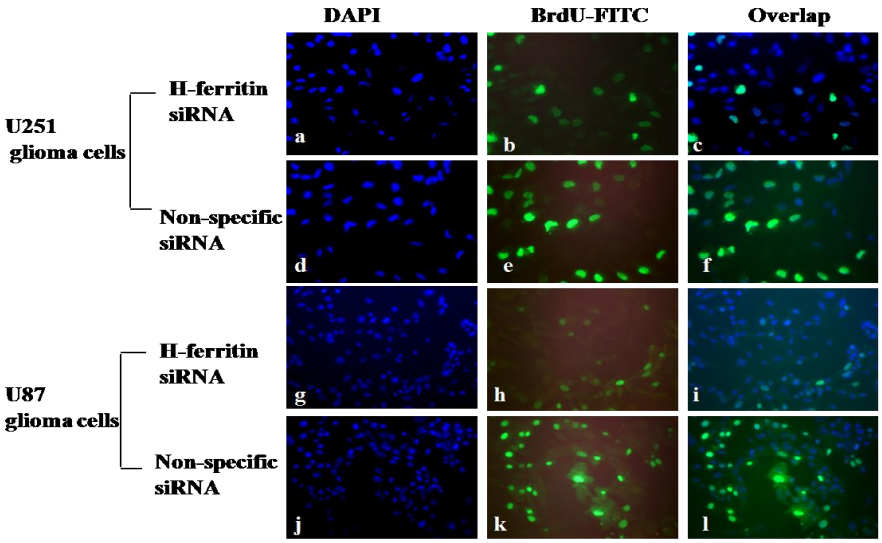

Figure 3.20. BrdU incorporation, as tested by immunocytochemistry. U251 cells: Panels a, b, and c represent H-ferritin-siRNA as treatment group, while panels d, e and f represent non-specific-siRNA as control group. U87cells: Panels g, h and i represent H-ferritin-siRNA as treatment group, while panels j, k and l represent non-specific-siRNA as control group. Blue color; DAPI. Green color; BrdU-FITC. Donwregulation of H-ferritin was associated with a decrease in BrdU incorporation (panels b and h).

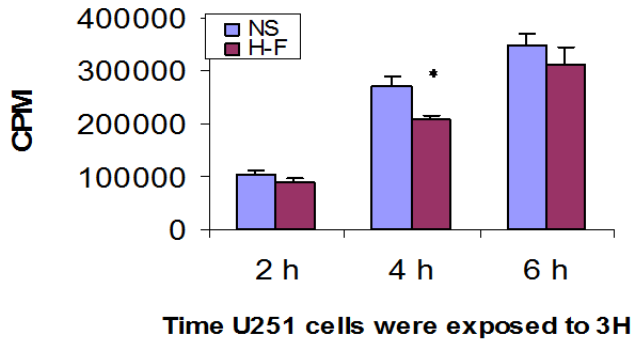

Figure 3.21. **^{3}H-Thymidine incorporation in U251 cells.** The blue color represents C-liposomes:non-specific-siRNA as control group. The red color represent C-liposomes:H-ferritin-siRNA as treatment group. Down regulation of H-ferritin decreased ^{3}H-Thymidine incorporation with DNA at 4 hours post exposure of ^{3}H-Thymidine(*$p<0.01$), but not at the 2 and 6 hour time point. These results indicate that H-ferritin may facilitate DNA synthesis in glioma U251cells.

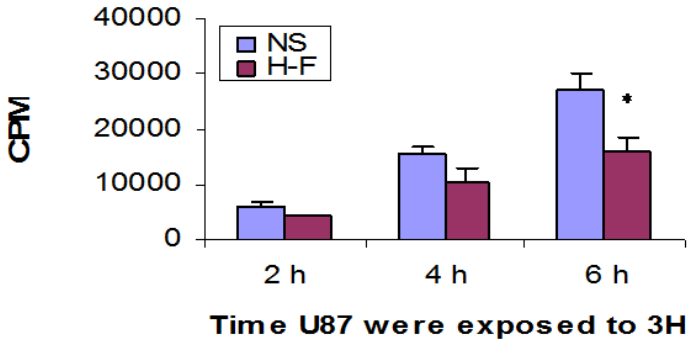

Figure 3.22. **^{3}H-Thymidine incorporation in U87 cells.** The blue color represents C-liposomes:non-specific-siRNA which serves as a control group. The red color represents C-liposomes:H-ferritin-siRNA which is the treatment group. Down regulation of H-ferritin decreased ^{3}H-Thymidine incorporation with DNA at 6 hours post exposure of ^{3}H-Thymidine (*$p<0.01$), but not at the 2 or 4 hour time point. These results indicate that H-ferritin may facilitate DNA synthesis in glioma U87cells.

Chapter 4

Discussion

4.1 Introduction

In this chapter, the scientific and clinical significance of the present work, including major issues in the development of C-liposomes, as well as the synergetic strategy for the treatment of glioma will be discussed. The mission of the present project is to demonstrate that knockdown of H-ferritin using gene therapy, is capable of enhancing radiation and chemotherapeutic efficacy for the treatment of glioma. However, the implication of this work has been extended for the potential treatment of malignant peripheral never sheath tumors (MPNST) and breast cancer. The discussion provided in this chapter may help to guide further studies initiated by this work.

4.2 Advantages and pitfalls of C-liposomes

C-liposomes were used as a gene delivery vehicle in the present study, and are an extension of the nanotechnology platform previously used in our laboratory [165, 166]. The C-liposomes in this study and the neutral liposomes used in previous studies in our laboratory, share some common physical properties. Both were prepared on a nanometer scale by similar methods, were non-toxic, and have high transfer efficiency. Both types of liposomes are internalized by glioma cells through the endosomal pathway. The C-liposomes were synthesized with positively charged lipids, so that they were capable of forming a complex with siRNA or DNA using electrostatic interactions, as demonstrated by the experimental results in **Figure 2.2** and **2.5**. The C-liposomes have been used as a gene (DNA/siRNA) delivery vehicle since they were first created in 1987 [170]. In addition to C-liposomes, various agents, including dendrimers,

polymers, cyclodextrins, lipofectamines, and C-liposomes from DOTAP/DOPE lipids, have been extensively investigated for their potential application as vehicles for gene delivery. Based on a careful literature study, C-liposomes of DC-Cholesterol/DOPE lipids appear to possess many competitive advantages over the other agents mentioned above. For instance, the transfection efficiency of dendrimers is significantly lower than for C-liposomes, mainly because it is difficult to the PDI to be reduced down to the level of our C-liposomes [199]. As for the polymers, the binding of polymer to siRNA or DNA is non-specific and difficult to control, because the the polymer:siRNA complex is heterogeneous. Thus, the release of the "payload" (decomplex) is generally not as simple as for lipoplexes (C-liposomes:siRNA) [200]. Cyclodextrins, another class of compounds that showed promises as a gene delivery agent, have inherent toxicity, as concentrated cyclodextrins easily aggregate to form micellar-type CD aggregates [201]. Lipofectamine has superior transfection efficiency; however, its potential application is limited by its high selectivity for cell types [202]. In other words, it is only effective for a limited number of cell lines. Further work is needed to overcome this obstacle. Lastly, in terms of the composition of C-liposomes, C-liposomes made from DOTAP/DOPE lipids, have a lack of stability when complexed with DNA/siRNA which leads to a lower the transfect efficiency [181]. With these considerations, C-liposomes composed of DC-Cholesterol/DOPE were selected for this thesis work. Our experimental results show that C-liposome-DC-Cholesterol/DOPE have several unique properties that make them a favorable compound to be further developed as a gene delivery agent.

It is important to understand the superior performance of C-liposomes, based on basic chemistry principles, as it may provide insights that can be utilized in the formulation of more effective molecular vehicles. DOPE has a long tail with 17 carbon hydrogen chains, which provides static space for the accommodation and protection of genes. As our results demonstrate, in **Figure 2.7-2.8**, 90% of the siRNA was encapsulated inside the C-liposome. DC-Cholesterol is

a biodegradable derivative of human cholesterol. This may be a factor contributing to its high transfection efficiency, as it is capable of releasing functional siRNA easily in a controlled manner. DC-Cholesterol is made of three six carbon member rings and one five carbon member ring, and is highly hydrophobic. Hydrophobicity and ratio of components in C-liposomes, are key parameters for optimizing a liposome's stability, cytotoxicity, and transfection efficiency. Other important physical parameters include the size distribution and the PDI of C-liposomes. Cytotoxicity and transfection efficiency of C-liposomes depend on the scale and uniformity of size. During the process of preparing C-liposomes, multiple extrusions with different sized membrane filters resulted in a uniform size of about 100 nm, which contributed to a transfection efficiency of over 90%. The homogeneous size distribution of the C-liposomes (90% of C-liposomes were 90 nm, with a range from 60 to 180 nm) reduced the chance of aggregation, thereby resulting in low toxicity. Transfection efficiency and toxicity were evaluated in an *in vivo* model, as shown in **Figure 2.4 A-B**. In the past, our laboratory has demonstrated that siRNA delivered through nuclear transfection without C-liposomes down regulated H-ferritin expression approximately for 5 fold in glioma cells compared with controls [5]. The same siRNA delivered with C-liposomes, down regulated H-ferritin expression by more than 9-fold in cell culture. Thus, the present study indicated that a nanoliposome delivery system can optimize the amount of siRNA delivered, and increase the siRNA efficacy. The effective down regulation of H-ferritin expression in the present study, using C-liposomes, resulted in effective suppression of glioma progression *in vivo* (**Figure 3.12-13**). The results of our study indicate that the size distribution and formulation of lipids play a key role in the ability of C-liposomes to serve as a gene delivery agent.

To prepare our C-liposomes for IV injection, the stability of the C-liposomes was tested using RNaseA and human serum. As the results indicate in **Figure 2.7-2.9**, 90% of the siRNA

was encapsulated inside of the C-liposomes, with only 10% of the siRNA released in 5 U of RNaseA at 37^{o}C, suggesting that C-liposomes are stable under these conditions at body temperature. However, the stability of C-liposomes:siRNA was greatly reduced in 40% human serum, and more than 50% of the siRNA was released in 20% human serum (**Figure 2.9**). This result limits the administration of C-liposome:siRNA via the vascular system, and further investigation is needed to address this issue. One potential solution involves modifying the composition of C-liposomes by adding a certain percentage of polyethylene glycol (PEG) and maleimide lipids. This could increase both the stability of C-liposomes and ability to conjugate with IL-13. Although IL-13 conjugated C-liposomes appeared to be able to encapsulate siRNA, as shown in **Figure 2.12**, their stability in serum is still unknown. Further characterization of IL-13-C-liposomes is required, and will be discussed in the future direction section.

4.3 Scientific significance of a synergetic strategy of H-ferritin down-regulation by gene therapy with conventional treatments

The use of siRNA for the treatment of cancer is an area of considerable interest and many promising siRNA targets have been identified. More than 28 target genes have been evaluated in different types of cancer. VEGF (vascular endothelial growth factor) siRNA has been implicated for the treatment of fibrosarcoma, Ewing's sarcoma, prostate cancer, and glioma. EGFR (epidermal growth factor receptor) siRNA is applied for the treatment of glioma [92]. The major focus of this thesis work is to demonstrate that H-ferritin is a suitable siRNA target for the treatment of cancer.

The targeting of a ferritin protein with siRNA may seem counterintuitive, as ferritin is typically considered to be a stable cytosolic iron storage protein with a slow turnover. It has been reported, however, that the half life of cytosolic ferritin in K562 cells [203], human fibroblast

cells [204] and in Hela cells [205] is approximately 12 hours. These reports are consistent with the dramatic down regulation of H-ferritin seen at 24 hours in the human astrocytoma cell line shown in **Figure 3.5**. Ferritin plays a key role in cellular iron homeostasis [206]. It tightly regulates the intracellular availability of iron in aerobic or anaerobic organisms [146], and is thus essential to cell viability. Ferritin functions as an iron storage and regulating protein that is located in the cytosol, mitochondria and nucleus [1]. Iron is an essential trace element for cell growth and proliferation, because it is involved in a variety of redox reactions [121] and is essential to maintaining cellular homeostasis [207]. Ferritin was chosen as a potential target for siRNA therapy after H-ferritin was found to be present in the nuclei of glioma cells [1, 2]. Nuclear ferritin, comprised mostly of H-ferritin, is non-randomly distributed, and is thought to be involved in facilitating DNA synthesis, as it has been found to associate with heterochromatin [2, 5]. Nuclear ferritin has been shown to have a protective function, as shown by its ability to protect the DNA of corneal epithelial cells from UV damage and oxidative stress [157-159]. Aside from protecting DNA, H-ferritin may also be involved in acquired drug resistance. Repeated exposure of cells to hydroxyurea results in resistance to this toxic agent, and is accompanied by an increase in ferritin mRNA [20]. Additionally, ferritin overexpression is associated in the development of various cancers [4, 149-151, 153]. Thus, our central hypothesis is that down regulation of H-ferritin by siRNA in cancer cells could provide a mechanism to increase chemotherapeutic sensitivity in the treatment of tumors, by removing the protective functions of H-ferritin, including anti-drug and anti-apoptotic effects. Successful testing of the hypothesis in the present work provides experimental evidence that H-ferritin is intimately involved in DNA synthesis of tumor cells. H-ferritin expression was found in human glioma U251, U87, neurofibroma #215 cells, and human breast cancer MCF-7 cells. Furthermore, H-ferritin expression was co-localized with the glioma stem cell marker CD133 in U251, U87 and NF#251 cell lines. H-ferritin's potential roles in DNA protection, DNA repair, apoptotic

pathways, and DNA synthesis, were investigated in the present project, and are described in the following section.

First, we postulated that the anti-tumor effects of H-ferritin siRNA may be associated with the ability of H-ferritin to alter the function of BCNU. BCNU is known to be a DNA alkaylating agent that is capable of converting DNA to a supercoiled form, as shown in **Figure 3.14**. H-ferritin is capable of reversing this function of BCNU, and maintains DNA in a relaxed and linear form, which may assist gene transcription. In contrast, L- ferritin was unable to reverse this function of BCNU, as shown in **Figure 3.15**. This finding is consistent with the presence of H-ferritin in the nuclei of cancer cells [1, 5] and the subsequent effects on gene transcription [149].

Second, H-ferritin may have an anti-apoptotic function in malignant tumor development. The data collected in the present work support this notion, as H-ferritin siRNA was associated with an increased activation of caspase-3, shown in **Figure 3.18-3.19**. These results correspond with the findings that overexpression of H-ferritin inhibited tumor necrosis factor (TNFα)–induced apoptosis [10], and down regulation of H-ferritin resulted in a 20% increase in apoptosis within malignant mesothelioma cells [7]. Up-regulation of H-ferritin is well known to prevent apoptotic activity [7, 8, 10]. In the radiation experiments of the present study, H-ferritin down-regulation greatly enhanced radiation therapy, with more than 90% tumor suppression, as shown in **Figure 3.13**. This may be because down regulation of H-ferritin by siRNA reduced the antiapoptotic function of H-ferritin and, thus, promoted apoptotic activity. The supercoil relaxation assays shown in **Figure 3.16** indicated that H-ferritin effectively protected DNA, by maintaining DNA in relaxed and linear forms even under radiation (4Gy). One potential mechanism, by which H-ferritin may prevent apoptosis, is by limiting the amount of iron available to participate in oxidative stress reactions.

Thirdly, H-ferritin may promote DNA synthesis and transcription. H-ferritin has been demonstrated to be concentrated in the nuclear heterochromatin containing fraction of SW1088 astrocytoma cells [5]. Additionally, H-ferritin has been shown to bind DNA in SW1088 glioma cells and promote DNA relaxation, and increase transcription [6]. In this study, knockdown of H-ferritin expression was shown to inhibit DNA synthesis, as demonstrated by decreased incorporation of BrdU and ^{3}H-thymidine, shown in **Figure 3.20-3.21**. The underlying mechanism appears to be the ability of H-ferritin to partially maintain DNA in relaxed and linear forms under radiation, which may be associated with the facilitating transcription The decreased BrdU and ^{3}H-thymidine incorporation seen with H-ferritin siRNA further implies that H-ferritin possess an ability to protect DNA (shown in **Figure 20-21**). Previous studies have demonstrated that ferritin releases iron in a controlled manner to promote DNA relaxation [2, 5]. These reports are consistent with the observations in this study, where H-ferritin maintained DNA in the relaxed form even in the presence of an akylating agent, or under radiation (4Gy). Thus the data presented herein provide a compelling argument for a protective and trophic role of H-ferritin in tumor growth, through direct protection of DNA, which may permit continued transcription and hence tumor growth. H-ferritin appears to not be involved in the MGMT related DNA repair pathway in glioma U251 cells and H-ferritin siRNA did not alter the expression of MGMT in MCF-7 cells, as shown in **Figure 3.17**.

4.4 Clinical significance of a synergetic strategy of H-ferritin down-regulation by gene therapy with conventional treatment

Successful testing the central hypothesis is of clinical significance. First, GBM is a deadly brain tumor and is difficult to treat because of its drug resistant characteristics. The difficulty for many chemotoxic agents is the need to traverse the blood-brain-barrier in effective amounts. Higher dosages of chemotherapeutic agents are generally not an option because they are

often accompanied by stronger adverse side effects [31]. Radiation toxicity is also a concern, as is surgical resection of tumor tissue in elegant brain regions [208]. One effective way to increase the efficacy of therapeutic agents is to increase the sensitivity of the cancer cells to these agents. As demonstrated *in vitro* and *in vivo* (**Figure 3.7-3.9, 3.12**,), the BCNU regimen, utilized with H-ferritin-siRNA, was only half of the concentration (12.5 mg/kg body weight) of the conventional dose (25 mg/kg body weight) used in previous studies [192]. This 50% reduction in dosage, when used it in combination with H-ferritin siRNA suppressed tumor growth by 80% at week 7 in a subcutaneous tumor model (**Figure 3.12**). A reduction in the dosage of either chemo- or radiation while maintaining treatment efficacy, would immediately benefit patients by alleviating the excruciating side-effect of conventional cancer treatments.

Second, the synergetic strategy demonstrated in present work may prove to be a potential solution for the problem of drug resistance in cancer. Drug resistance has been a major difficulty in the treatment of many cancers, particularly in glioma. No direct data was present presented in this study to demonstrate this; however, as discussed above in Section 4.2, H-ferritin is capable of reversing the effects of BCNU. Specifically, H-ferritin prevented the DNA supercoiling normally seen with BCNU, and instead maintained DNA in a relaxed and linear form. Therefore, down regulation of H-ferritin could attenuate these reversing effects, and subsequently defeat drug resistance.

4.5 Summary

In conclusion, our study demonstrated an increased vulnerability of cancer cells to radiation and chemotherapy, by reducing H-ferritin expression using gene therapy. The importance of ferritin in cancer cell biology suggests that efficient delivery of siRNA could be a viable therapeutic option for the treatment of cancer. The results from present project are a

promising initial step toward the development of siRNA gene therapy using H-ferritin as a target for the treatment of multiple tumor types. A key component of siRNA gene therapy is an effective delivery system.

4.6 Future directions

Project 1. Enhance radiation and chemotherapeutic efficacy through down regulating heavy chain ferritin gene by small hairpin RNA (shRNA) delivered by Interleukin-13 conjugated cationic liposomes for systematic treatment of glioma.

Reasoning: The present project has demonstrated that down regulation of H-ferritin enhances radiation and chemotherapeutic efficacy *in vitro*/*vivo*. However, the current regimen of present work cannot be applied for systematic treatment of glioma for two reasons. 1) C-liposomes as a gene delivery vehicle are not specific. 2) Cognate gene down regulation by siRNA is only a transient process. Thus, using IL-13-M-C-liposomes to target glioma cells would avoid non specificity, and gene downregulation using shRNA would be permanent.

Aim 1; Development and characterization of glioma targeted cationic liposomes such as Interneukin-13 conjugated M-C-liposomes.

1) Test the zeta potential, PDI and the size distribution of IL-13-M-C-liposomes formulated by different lipids.
2) Test the stability, toxicity of the IL-13-M-C-liposomes and its capability of encapsulating small hairpin RNA (shRNA). These C-liposomes should be stable in serums for several hours, and specifically target glioma cells.
3) Test the uptake of IL-13-M-C-liposomes:shRNA in glioma cells.
4) Study the mechanism by which IL-13-M-C-liposomes:shRNA are uptaken.

Aim 2; Enhance radiation and chemotherapeutic efficacy using IL-13-M-C-liposomes:shRNA-H-ferritin for the treatment of glioma.

1) Down regulation of H-ferritin in U251 cells by IL-13-M-C-liposomes:shRNA.
2) Testing enhancement of radiation and chemotherapeutic efficacy in vitro/vivo for the treatment of glioma.

Aim 3; Investigating the role of H-ferritin on DNA synthesis, apoptosis, and DNA repair pathways.

Significance: Lower side effects for the treatment of glioma during radiation/chemotherapy, while maintaining/increasing efficacy.

Project 2. The role of H-ferritin in drug resistance.

Reasoning: One study suggested that CD133 is related to drug resistance in cancer cells. The present study also demonstrated that H-ferritin attenuates the effect of the anti cancer drug BCNU on DNA supercoiling. H-ferritin is also co-localized with CD133.

Aim1: Down regulation of H-ferritin by siRNA/shRNA may decrease the CD133 expression in U251, U87 and MCF-7 cells.

1) Demonstrate H-ferritin expression.
2) Demonstrate CD 133 expression.
3) CD133 expression evaluated when H-ferritin is downregulated.

Aim 2: Drug resistance is decreased in H-ferritin negative cell lines.

1) Develop cell lines with or without H-ferritin. Isolate astrocytes from ferritin knockout mice. Transfect cell lines to stably express H-ferritin. Select cell lines with or without H-ferritin. Investigate drug resistance in cell lines expressing or not expressing H-ferritin.

Significance: This would further demonstrate the importance of H-ferritin in cancer treatment.

Project 3. Study the association of increased levels of H-Ferritin with immune responses using the primary cells from glioma patients.

Project 4. One study revealed "FHC is induced downstream of NF-kappaB and is required to prevent sustained JNK activation and, thereby, apoptosis triggered by TNFalpha. FHC-mediated inhibition of JNK signaling depends on suppressing ROS accumulation and is achieved through iron sequestration." Down regulation of H-ferritin by siRNA/shRNA may affect this signaling cascade pathway.

References

1. Surguladze, N., et al., *Characterization of nuclear ferritin and mechanism of translocation.* Biochem J, 2005. **388**(Pt 3): p. 731-40.
2. Thompson, K.J., et al., *Regulation, mechanisms and proposed function of ferritin translocation to cell nuclei.* J Cell Sci, 2002. **115**(Pt 10): p. 2165-77.
3. Elliott, R.L., et al., *Breast carcinoma and the role of iron metabolism. A cytochemical, tissue culture, and ultrastructural study.* Ann N Y Acad Sci, 1993. **698**: p. 159-66.
4. Weinstein, R.E., B.H. Bond, and B.K. Silberberg, *Tissue ferritin concentration in carcinoma of the breast.* Cancer, 1982. **50**(11): p. 2406-9.
5. Surguladze, N., et al., *Interactions and reactions of ferritin with DNA.* J Biol Chem, 2004. **279**(15): p. 14694-702.
6. Wu, Y.J. and C.T. Noguchi, *Activation of globin gene expression by cDNAs from induced K562 cells. Evidence for involvement of ferritin in globin gene expression.* J Biol Chem, 1991. **266**(26): p. 17566-72.
7. Aung, W., et al., *Potential role of ferritin heavy chain in oxidative stress and apoptosis in human mesothelial and mesothelioma cells: implications for asbestos-induced oncogenesis.* Carcinogenesis, 2007. **28**(9): p. 2047-52.
8. Berberat, P.O., et al., *Heavy chain ferritin acts as an antiapoptotic gene that protects livers from ischemia reperfusion injury.* FASEB J, 2003. **17**(12): p. 1724-6.
9. Bubici, C., et al., *NF-kappaB and JNK: an intricate affair.* Cell Cycle, 2004. **3**(12): p. 1524-9.
10. Pham, C.G., et al., *Ferritin heavy chain upregulation by NF-kappaB inhibits TNFalpha-induced apoptosis by suppressing reactive oxygen species.* Cell, 2004. **119**(4): p. 529-42.
11. Yang, D.C., et al., *Antisense ferritin oligonucleotides inhibit growth and induce apoptosis in human breast carcinoma cells.* Anticancer Res, 2002. **22**(3): p. 1513-24.
12. Bowlus, C.L., *The role of iron in T cell development and autoimmunity.* Autoimmun Rev, 2003. **2**(2): p. 73-8.
13. Broxmeyer, H.E., et al., *Identification of leukemia-associated inhibitory activity as acidic isoferritins. A regulatory role for acidic isoferritins in the production of granulocytes and macrophages.* J Exp Med, 1981. **153**(6): p. 1426-44.
14. Gray, C.P., et al., *Immunosuppressive effects of melanoma-derived heavy-chain ferritin are dependent on stimulation of IL-10 production.* Int J Cancer, 2001. **92**(6): p. 843-50.
15. Halpern, M., et al., *Antibodies to placental immunoregulatory ferritin with transfer of polyclonal lymphocytes arrest MCF-7 human breast cancer growth in a nude mouse model.* Neoplasia, 2007. **9**(6): p. 487-94.
16. Harada, T., et al., *Ferritin selectively suppresses delayed-type hypersensitivity responses at induction or effector phase.* Cell Immunol, 1987. **109**(1): p. 75-88.
17. Matzner, Y., et al., *Suppressive effect of ferritin on in vitro lymphocyte function.* Br J Haematol, 1979. **42**(3): p. 345-53.
18. Recalcati, S., et al., *New functions for an iron storage protein: the role of ferritin in immunity and autoimmunity.* J Autoimmun, 2008. **30**(1-2): p. 84-9.
19. Epsztejn, S., et al., *H-ferritin subunit overexpression in erythroid cells reduces the oxidative stress response and induces multidrug resistance properties.* Blood, 1999. **94**(10): p. 3593-603.

20. McClarty, G.A., et al., *Increased ferritin gene expression is associated with increased ribonucleotide reductase gene expression and the establishment of hydroxyurea resistance in mammalian cells.* J Biol Chem, 1990. **265**(13): p. 7539-47.
21. James Bobick, N.B., Sandra Bobick, and Laurel Bridges Roberts, *THE HANDY BIOLOGY ANSWER BOOK.* 2004: p. 71.
22. Zheng, T., et al., *Occupational risk factors for brain cancer: a population-based case-control study in Iowa.* J Occup Environ Med, 2001. **43**(4): p. 317-24.
23. Hambardzumyan, D., et al., *Glioma formation, cancer stem cells, and akt signaling.* Stem Cell Rev, 2008. **4**(3): p. 203-10.
24. Ohgaki, H. and P. Kleihues, *Population-based studies on incidence, survival rates, and genetic alterations in astrocytic and oligodendroglial gliomas.* J Neuropathol Exp Neurol, 2005. **64**(6): p. 479-89.
25. Ohgaki, H. and P. Kleihues, *Epidemiology and etiology of gliomas.* Acta Neuropathol, 2005. **109**(1): p. 93-108.
26. Hess, K.R., K.R. Broglio, and M.L. Bondy, *Adult glioma incidence trends in the United States, 1977-2000.* Cancer, 2004. **101**(10): p. 2293-9.
27. Kanu, O.O., et al., *Glioblastoma multiforme: a review of therapeutic targets.* Expert Opin Ther Targets, 2009. **13**(6): p. 701-18.
28. Kaatsch, P., et al., *Population-based epidemiologic data on brain tumors in German children.* Cancer, 2001. **92**(12): p. 3155-64.
29. *Stat bite: Childhood cancer deaths by site, 2004.* J Natl Cancer Inst, 2008. **100**(3): p. 165.
30. Yamanaka, R. and H. Saya, *Molecularly targeted therapies for glioma.* Ann Neurol, 2009. **66**(6): p. 717-29.
31. Skalski, V., et al., *The cytotoxicity of sarcosinamide chloroethylnitrosourea (SarCNU) and BCNU in primary gliomas and glioma cell lines: analysis of data in reference to theoretical peak plasma concentrations in man.* Cancer Chemother Pharmacol, 1988. **22**(2): p. 137-40.
32. Purow, B. and D. Schiff, *Advances in the genetics of glioblastoma: are we reaching critical mass?* Nat Rev Neurol, 2009. **5**(8): p. 419-26.
33. Barzon, L., et al., *HSV-TK/IL-2 gene therapy for glioblastoma multiforme.* Methods Mol Biol, 2009. **542**: p. 529-49.
34. Candolfi, M., et al., *Gene therapy for brain cancer: combination therapies provide enhanced efficacy and safety.* Curr Gene Ther, 2009. **9**(5): p. 409-21.
35. Shirakawa, T., *Clinical trial design for adenoviral gene therapy products.* Drug News Perspect, 2009. **22**(3): p. 140-5.
36. Chamberlain, M.C. and J. Raizer, *Antiangiogenic therapy for high-grade gliomas.* CNS Neurol Disord Drug Targets, 2009. **8**(3): p. 184-94.
37. Takahashi, H. and A. Teramoto, *Trial of targeting therapy against malignant glioma using monoclonal antibody.* J Nippon Med Sch, 2004. **71**(1): p. 2-3.
38. Adamson, C., et al., *Glioblastoma multiforme: a review of where we have been and where we are going.* Expert Opin Investig Drugs, 2009. **18**(8): p. 1061-83.
39. DeVita, V.T., et al., *The physiological disposition of the carcinostatic 1,3-bis(2-chloroethyl)-1-nitrosourea (BCNU) in man and animals.* Clin Pharmacol Ther, 1967. **8**(4): p. 566-77.
40. Parker, S., et al., *Reaction of 1,3-bis(2-chloroethyl)-1-nitrosourea (BCNU) with guanosine: evidence for a new mechanism of DNA modification.* Biochem Biophys Res Commun, 1986. **139**(1): p. 31-6.
41. Wiencke, J.K. and J. Wiemels, *Genotoxicity of 1,3-bis(2-chloroethyl)-1-nitrosourea (BCNU).* Mutat Res, 1995. **339**(2): p. 91-119.

42. Bacolod, M.D., et al., *Mechanisms of resistance to 1,3-bis(2-chloroethyl)-1-nitrosourea in human medulloblastoma and rhabdomyosarcoma.* Mol Cancer Ther, 2002. **1**(9): p. 727-36.
43. Russo, R., et al., *Differential pulse polarographic determination of BCNU pharmacokinetics in patients with lung cancer.* Cancer Treat Rep, 1981. **65**(7-8): p. 555-62.
44. Snyder, R.D., et al., *Combination therapy for advanced malignant melanoma with BCNU, pseudomonas vaccine, and heparin.* J Surg Oncol, 1981. **16**(1): p. 87-92.
45. Brandes, A.A., et al., *How effective is BCNU in recurrent glioblastoma in the modern era? A phase II trial.* Neurology, 2004. **63**(7): p. 1281-4.
46. La Rocca, R.V. and H.M. Mehdorn, *Localized BCNU chemotherapy and the multimodal management of malignant glioma.* Curr Med Res Opin, 2009. **25**(1): p. 149-60.
47. Aoki, T., N. Hashimoto, and M. Matsutani, *Management of glioblastoma.* Expert Opin Pharmacother, 2007. **8**(18): p. 3133-46.
48. Sabel, M. and A. Giese, *Safety profile of carmustine wafers in malignant glioma: a review of controlled trials and a decade of clinical experience.* Curr Med Res Opin, 2008.
49. Bandres, E., et al., *Gene expression profile induced by BCNU in human glioma cell lines with differential MGMT expression.* J Neurooncol, 2005. **73**(3): p. 189-98.
50. Bobola, M.S., et al., *O6-methylguanine-DNA methyltransferase, O6-benzylguanine, and resistance to clinical alkylators in pediatric primary brain tumor cell lines.* Clin Cancer Res, 2005. **11**(7): p. 2747-55.
51. Johannessen, T.C., R. Bjerkvig, and B.B. Tysnes, *DNA repair and cancer stem-like cells--potential partners in glioma drug resistance?* Cancer Treat Rev, 2008. **34**(6): p. 558-67.
52. Rabik, C.A., M.C. Njoku, and M.E. Dolan, *Inactivation of O6-alkylguanine DNA alkyltransferase as a means to enhance chemotherapy*. Cancer Treat Rev, 2006. **32**(4): p. 261-76.
53. Frosina, G., *DNA repair and resistance of gliomas to chemotherapy and radiotherapy.* Mol Cancer Res, 2009. **7**(7): p. 989-99.
54. Thompson, G.R. and R.E. Larson, *The hepatotoxicity of 1,3-bis (2-chloroethyl)-1-nitrosurea (BCNU) in rats.* J Pharmacol Exp Ther, 1969. **166**(1): p. 104-12.
55. O'Driscoll, B.R., et al., *Active lung fibrosis up to 17 years after chemotherapy with carmustine (BCNU) in childhood.* N Engl J Med, 1990. **323**(6): p. 378-82.
56. Hasleton, P.S., et al., *Late BCNU lung: a light and ultrastructural study on the delayed effect of BCNU on the lung parenchyma.* J Pathol, 1991. **164**(1): p. 31-6.
57. Taylor, P.M., et al., *Chronic lung fibrosis following carmustine (BCNU) chemotherapy: radiological features.* Clin Radiol, 1991. **44**(5): p. 299-301.
58. Reithmeier, T., et al., *BCNU for recurrent glioblastoma multiforme: efficacy, toxicity and prognostic factors.* BMC Cancer. **10**: p. 30.
59. Hamilton, A.J. and D.C. Baulcombe, *A species of small antisense RNA in posttranscriptional gene silencing in plants.* Science, 1999. **286**(5441): p. 950-2.
60. Filipowicz, W., et al., *Post-transcriptional gene silencing by siRNAs and miRNAs.* Curr Opin Struct Biol, 2005. **15**(3): p. 331-41.
61. Zhang, C., *Novel functions for small RNA molecules.* Curr Opin Mol Ther, 2009. **11**(6): p. 641-51.
62. Carmell, M.A. and G.J. Hannon, *RNase III enzymes and the initiation of gene silencing.* Nat Struct Mol Biol, 2004. **11**(3): p. 214-8.
63. Hutvagner, G. and P.D. Zamore, *RNAi: nature abhors a double-strand.* Curr Opin Genet Dev, 2002. **12**(2): p. 225-32.

64. Elbashir, S.M., et al., *Duplexes of 21-nucleotide RNAs mediate RNA interference in cultured mammalian cells.* Nature, 2001. **411**(6836): p. 494-8.
65. Elbashir, S.M., W. Lendeckel, and T. Tuschl, *RNA interference is mediated by 21- and 22-nucleotide RNAs.* Genes Dev, 2001. **15**(2): p. 188-200.
66. Elbashir, S.M., et al., *Functional anatomy of siRNAs for mediating efficient RNAi in Drosophila melanogaster embryo lysate.* EMBO J, 2001. **20**(23): p. 6877-88.
67. Cui, W., et al., *OptiRNAi, an RNAi design tool.* Comput Methods Programs Biomed, 2004. **75**(1): p. 67-73.
68. Dudek, P. and D. Picard, *TROD: T7 RNAi Oligo Designer.* Nucleic Acids Res, 2004. **32**(Web Server issue): p. W121-3.
69. Henschel, A., F. Buchholz, and B. Habermann, *DEQOR: a web-based tool for the design and quality control of siRNAs.* Nucleic Acids Res, 2004. **32**(Web Server issue): p. W113-20.
70. Levenkova, N., Q. Gu, and J.J. Rux, *Gene specific siRNA selector.* Bioinformatics, 2004. **20**(3): p. 430-2.
71. Naito, Y., et al., *siDirect: highly effective, target-specific siRNA design software for mammalian RNA interference.* Nucleic Acids Res, 2004. **32**(Web Server issue): p. W124-9.
72. Wang, L. and F.Y. Mu, *A Web-based design center for vector-based siRNA and siRNA cassette.* Bioinformatics, 2004. **20**(11): p. 1818-20.
73. Yuan, B., et al., *siRNA Selection Server: an automated siRNA oligonucleotide prediction server.* Nucleic Acids Res, 2004. **32**(Web Server issue): p. W130-4.
74. Chernolovskaya, E.L. and M.A. Zenkova, *Chemical modification of siRNA.* Curr Opin Mol Ther. **12**(2): p. 158-67.
75. Wu, Y., et al., *Durable protection from Herpes Simplex Virus-2 transmission following intravaginal application of siRNAs targeting both a viral and host gene.* Cell Host Microbe, 2009. **5**(1): p. 84-94.
76. Ito, M., et al., *Genome-wide application of RNAi to the discovery of potential drug targets.* FEBS Lett, 2005. **579**(26): p. 5988-95.
77. Tan, F.L. and J.Q. Yin, *RNAi, a new therapeutic strategy against viral infection.* Cell Res, 2004. **14**(6): p. 460-6.
78. McCaffrey, A.P., et al., *Inhibition of hepatitis B virus in mice by RNA interference.* Nat Biotechnol, 2003. **21**(6): p. 639-44.
79. Palliser, D., et al., *An siRNA-based microbicide protects mice from lethal herpes simplex virus 2 infection.* Nature, 2006. **439**(7072): p. 89-94.
80. Pomerantz, R.J., *RNA interference meets HIV-1: will silence be golden?* Nat Med, 2002. **8**(7): p. 659-60.
81. Hu, W.Y., F.D. Bushman, and A.C. Siva, *RNA interference against retroviruses.* Virus Res, 2004. **102**(1): p. 59-64.
82. Stevenson, M., *Dissecting HIV-1 through RNA interference.* Nat Rev Immunol, 2003. **3**(11): p. 851-8.
83. Jacque, J.M., K. Triques, and M. Stevenson, *Modulation of HIV-1 replication by RNA interference.* Nature, 2002. **418**(6896): p. 435-8.
84. Harper, S.Q., et al., *RNA interference improves motor and neuropathological abnormalities in a Huntington's disease mouse model.* Proc Natl Acad Sci U S A, 2005. **102**(16): p. 5820-5.
85. Lakka, S.S., C.S. Gondi, and J.S. Rao, *Proteases and glioma angiogenesis.* Brain Pathol, 2005. **15**(4): p. 327-41.

86. Lakka, S.S., et al., *Inhibition of cathepsin B and MMP-9 gene expression in glioblastoma cell line via RNA interference reduces tumor cell invasion, tumor growth and angiogenesis.* Oncogene, 2004. **23**(27): p. 4681-9.
87. Loew, S., et al., *The epidermal growth factor receptor as a therapeutic target in glioblastoma multiforme and other malignant neoplasms.* Anticancer Agents Med Chem, 2009. **9**(6): p. 703-15.
88. Mathupala, S.P., M. Guthikonda, and A.E. Sloan, *RNAi based approaches to the treatment of malignant glioma.* Technol Cancer Res Treat, 2006. **5**(3): p. 261-9.
89. Wurdinger, T. and B.A. Tannous, *Glioma angiogenesis: Towards novel RNA therapeutics.* Cell Adh Migr, 2009. **3**(2): p. 230-5.
90. Zhang, Y., et al., *Intravenous RNA interference gene therapy targeting the human epidermal growth factor receptor prolongs survival in intracranial brain cancer.* Clin Cancer Res, 2004. **10**(11): p. 3667-77.
91. Gondi, C.S., et al., *RNAi-mediated inhibition of cathepsin B and uPAR leads to decreased cell invasion, angiogenesis and tumor growth in gliomas.* Oncogene, 2004. **23**(52): p. 8486-96.
92. Takeshita, F. and T. Ochiya, *Therapeutic potential of RNA interference against cancer.* Cancer Sci, 2006. **97**(8): p. 689-96.
93. Thaker, N.G., et al., *Functional genomic analysis of glioblastoma multiforme through short interfering RNA screening: a paradigm for therapeutic development.* Neurosurg Focus. **28**(1): p. E4.
94. Thaker, N.G., et al., *Designing, optimizing, and implementing high-throughput siRNA genomic screening with glioma cells for the discovery of survival genes and novel drug targets.* J Neurosci Methods. **185**(2): p. 204-12.
95. Kosciolek, B.A., et al., *Inhibition of telomerase activity in human cancer cells by RNA interference.* Mol Cancer Ther, 2003. **2**(3): p. 209-16.
96. Wilda, M., et al., *Killing of leukemic cells with a BCR/ABL fusion gene by RNA interference (RNAi).* Oncogene, 2002. **21**(37): p. 5716-24.
97. Chien, P.Y., et al., *Novel cationic cardiolipin analogue-based liposome for efficient DNA and small interfering RNA delivery in vitro and in vivo.* Cancer Gene Ther, 2005. **12**(3): p. 321-8.
98. Choudhury, D., et al., *Dietary yeast RNA supplementation reduces mortality by Aeromonas hydrophila in rohu (Labeo rohita L.) juveniles.* Fish Shellfish Immunol, 2005. **19**(3): p. 281-91.
99. Guan, H., et al., *A small interfering RNA targeting vascular endothelial growth factor inhibits Ewing's sarcoma growth in a xenograft mouse model.* Clin Cancer Res, 2005. **11**(7): p. 2662-9.
100. Kim, W.J., et al., *Cholesteryl oligoarginine delivering vascular endothelial growth factor siRNA effectively inhibits tumor growth in colon adenocarcinoma.* Mol Ther, 2006. **14**(3): p. 343-50.
101. Takei, Y., et al., *A small interfering RNA targeting vascular endothelial growth factor as cancer therapeutics.* Cancer Res, 2004. **64**(10): p. 3365-70.
102. Xu, C.X., et al., *Poly(ester amine)-mediated, aerosol-delivered Akt1 small interfering RNA suppresses lung tumorigenesis.* Am J Respir Crit Care Med, 2008. **178**(1): p. 60-73.
103. Orino, K. and K. Watanabe, *Molecular, physiological and clinical aspects of the iron storage protein ferritin.* Vet J, 2008. **178**(2): p. 191-201.
104. Brummelkamp, T.R., R. Bernards, and R. Agami, *A system for stable expression of short interfering RNAs in mammalian cells.* Science, 2002. **296**(5567): p. 550-3.

105. Arwert, E., et al., *Visualizing the dynamics of EGFR activity and antiglioma therapies in vivo.* Cancer Res, 2007. **67**(15): p. 7335-42.
106. Gondi, C.S., et al., *Downregulation of uPA, uPAR and MMP-9 using small, interfering, hairpin RNA (siRNA) inhibits glioma cell invasion, angiogenesis and tumor growth.* Neuron Glia Biol, 2004. **1**(2): p. 165-176.
107. Weng, X.C., et al., *Inhibition of acid-induced apoptosis by targeting ASIC1a mRNA with short hairpin RNA.* Acta Pharmacol Sin, 2007. **28**(10): p. 1621-7.
108. Zhen, H.N., et al., *Short hairpin RNA targeting survivin inhibits growth and angiogenesis of glioma U251 cells.* Int J Oncol, 2007. **31**(5): p. 1111-7.
109. Zhen, H.N., et al., *[Inhibition of growth and angiogenesis of U251 cell xenograft in vivo by short hairpin RNA targeting survivin gene].* Zhonghua Wai Ke Za Zhi, 2006. **44**(18): p. 1270-4.
110. Uchida, T., et al., *Relationship among plasma iron, plasma iron turnover, and reticuloendothelial iron release.* Blood, 1983. **61**(4): p. 799-802.
111. Hentze, M.W., M.U. Muckenthaler, and N.C. Andrews, *Balancing acts: molecular control of mammalian iron metabolism.* Cell, 2004. **117**(3): p. 285-97.
112. Fleming, M.D., et al., *Microcytic anaemia mice have a mutation in Nramp2, a candidate iron transporter gene.* Nat Genet, 1997. **16**(4): p. 383-6.
113. Gunshin, H., et al., *Slc11a2 is required for intestinal iron absorption and erythropoiesis but dispensable in placenta and liver.* J Clin Invest, 2005. **115**(5): p. 1258-66.
114. Rouault, T.A. and W.H. Tong, *Iron-sulphur cluster biogenesis and mitochondrial iron homeostasis.* Nat Rev Mol Cell Biol, 2005. **6**(4): p. 345-51.
115. Liu, A. and A. Graslund, *Electron paramagnetic resonance evidence for a novel interconversion of [3Fe-4S](+) and [4Fe-4S](+) clusters with endogenous iron and sulfide in anaerobic ribonucleotide reductase activase in vitro.* J Biol Chem, 2000. **275**(17): p. 12367-73.
116. Lill, R. and U. Muhlenhoff, *Iron-sulfur protein biogenesis in eukaryotes: components and mechanisms.* Annu Rev Cell Dev Biol, 2006. **22**: p. 457-86.
117. Zorov, D.B., et al., *Mitochondria revisited. Alternative functions of mitochondria.* Biosci Rep, 1997. **17**(6): p. 507-20.
118. Shi, H., et al., *A cytosolic iron chaperone that delivers iron to ferritin.* Science, 2008. **320**(5880): p. 1207-10.
119. Cherukuri, S., et al., *Unexpected role of ceruloplasmin in intestinal iron absorption.* Cell Metab, 2005. **2**(5): p. 309-19.
120. Vulpe, C.D., et al., *Hephaestin, a ceruloplasmin homologue implicated in intestinal iron transport, is defective in the sla mouse.* Nat Genet, 1999. **21**(2): p. 195-9.
121. Outten, F.W. and E.C. Theil, *Iron-based redox switches in biology.* Antioxid Redox Signal, 2009. **11**(5): p. 1029-46.
122. Beard, J.L., J.R. Connor, and B.C. Jones, *Iron in the brain.* Nutr Rev, 1993. **51**(6): p. 157-70.
123. Kauppi, B., et al., *The three-dimensional structure of mammalian ribonucleotide reductase protein R2 reveals a more-accessible iron-radical site than Escherichia coli R2.* J Mol Biol, 1996. **262**(5): p. 706-20.
124. Leibold, E.A. and H.N. Munro, *Cytoplasmic protein binds in vitro to a highly conserved sequence in the 5' untranslated region of ferritin heavy- and light-subunit mRNAs.* Proc Natl Acad Sci U S A, 1988. **85**(7): p. 2171-5.
125. Rouault, T.A., et al., *Binding of a cytosolic protein to the iron-responsive element of human ferritin messenger RNA.* Science, 1988. **241**(4870): p. 1207-10.

126. Rouault, T.A., et al., *Structural relationship between an iron-regulated RNA-binding protein (IRE-BP) and aconitase: functional implications.* Cell, 1991. **64**(5): p. 881-3.
127. Kaptain, S., et al., *A regulated RNA binding protein also possesses aconitase activity.* Proc Natl Acad Sci U S A, 1991. **88**(22): p. 10109-13.
128. Nicolas, G., et al., *Lack of hepcidin gene expression and severe tissue iron overload in upstream stimulatory factor 2 (USF2) knockout mice.* Proc Natl Acad Sci U S A, 2001. **98**(15): p. 8780-5.
129. Park, C.H., et al., *Hepcidin, a urinary antimicrobial peptide synthesized in the liver.* J Biol Chem, 2001. **276**(11): p. 7806-10.
130. Pigeon, C., et al., *A new mouse liver-specific gene, encoding a protein homologous to human antimicrobial peptide hepcidin, is overexpressed during iron overload.* J Biol Chem, 2001. **276**(11): p. 7811-9.
131. Ilyin, G., et al., *Comparative analysis of mouse hepcidin 1 and 2 genes: evidence for different patterns of expression and co-inducibility during iron overload.* FEBS Lett, 2003. **542**(1-3): p. 22-6.
132. Nemeth, E., et al., *Hepcidin regulates cellular iron efflux by binding to ferroportin and inducing its internalization.* Science, 2004. **306**(5704): p. 2090-3.
133. Altamura, S. and M.U. Muckenthaler, *Iron toxicity in diseases of aging: Alzheimer's disease, Parkinson's disease and atherosclerosis.* J Alzheimers Dis, 2009. **16**(4): p. 879-95.
134. Lee, D.W. and J.K. Andersen, *Iron elevations in the aging Parkinsonian brain: a consequence of impaired iron homeostasis?* J Neurochem. **112**(2): p. 332-9.
135. Snyder, A.M. and J.R. Connor, *Iron, the substantia nigra and related neurological disorders.* Biochim Biophys Acta, 2009. **1790**(7): p. 606-14.
136. Perez, L.R. and K.J. Franz, *Minding metals: Tailoring multifunctional chelating agents for neurodegenerative disease.* Dalton Trans. **39**(9): p. 2177-87.
137. Kabat, G.C. and T.E. Rohan, *Does excess iron play a role in breast carcinogenesis? An unresolved hypothesis.* Cancer Causes Control, 2007. **18**(10): p. 1047-53.
138. Klaunig, J.E., L.M. Kamendulis, and B.A. Hocevar, *Oxidative stress and oxidative damage in carcinogenesis.* Toxicol Pathol. **38**(1): p. 96-109.
139. Reizenstein, P., *Iron, free radicals and cancer.* Med Oncol Tumor Pharmacother, 1991. **8**(4): p. 229-33.
140. Weinberg, E.D., *The role of iron in cancer.* Eur J Cancer Prev, 1996. **5**(1): p. 19-36.
141. Stevens, R.G., et al., *Moderate elevation of body iron level and increased risk of cancer occurrence and death.* Int J Cancer, 1994. **56**(3): p. 364-9.
142. Arosio, P., R. Ingrassia, and P. Cavadini, *Ferritins: a family of molecules for iron storage, antioxidation and more.* Biochim Biophys Acta, 2009. **1790**(7): p. 589-99.
143. Santamaria, R., et al., *Induction of H-ferritin synthesis by oxalomalate is regulated at both the transcriptional and post-transcriptional levels.* Biochim Biophys Acta, 2006. **1763**(8): p. 815-22.
144. Klausner, R.D. and J.B. Harford, *cis-trans models for post-transcriptional gene regulation.* Science, 1989. **246**(4932): p. 870-2.
145. Cairo, G., et al., *Expression of the genes for the ferritin H and L subunits in rat liver and heart. Evidence for tissue-specific regulations at pre- and post-translational levels.* Biochem J, 1991. **275 (Pt 3)**: p. 813-6.
146. Carrondo, M.A., *Ferritins, iron uptake and storage from the bacterioferritin viewpoint.* EMBO J, 2003. **22**(9): p. 1959-68.
147. Ferreira, C., et al., *H ferritin knockout mice: a model of hyperferritinemia in the absence of iron overload.* Blood, 2001. **98**(3): p. 525-32.

148. Arosio, P., M. Yokota, and J.W. Drysdale, *Structural and immunological relationships of isoferritins in normal and malignant cells.* Cancer Res, 1976. **36**(5): p. 1735-9.
149. Pountney, D., et al., *The identification of ferritin in the nucleus of K562 cells, and investigation of a possible role in the transcriptional regulation of adult beta-globin gene expression.* J Cell Sci, 1999. **112 (Pt 6)**: p. 825-31.
150. Tripathi, P.K. and S.K. Chatterjee, *Elevated expression of ferritin H-chain mRNA in metastatic ovarian tumor.* Cancer Invest, 1996. **14**(6): p. 518-26.
151. Kukulj, S., et al., *Altered iron metabolism, inflammation, transferrin receptors, and ferritin expression in non-small-cell lung cancer.* Med Oncol, 2009.
152. Yang, D.C., et al., *Expression of transferrin receptor and ferritin H-chain mRNA are associated with clinical and histopathological prognostic indicators in breast cancer.* Anticancer Res, 2001. **21**(1B): p. 541-9.
153. Guner, G., et al., *Cytosol and serum ferritin in breast carcinoma.* Cancer Lett, 1992. **67**(2-3): p. 103-12.
154. Cairo, G., et al., *Regulation of ferritin synthesis in malignant and non-malignant lymphoid cells.* Biochem Biophys Res Commun, 1986. **139**(2): p. 652-7.
155. Drysdale, J.W., et al., *Structural and immunologic relationships of human isoferritins in normal and disease states.* Birth Defects Orig Artic Ser, 1976. **12**(8): p. 105-22.
156. Theil, E.C., *Ferritin mRNA translation, structure, and gene transcription during development of animals and plants.* Enzyme, 1990. **44**(1-4): p. 68-82.
157. Cai, C.X., D.E. Birk, and T.F. Linsenmayer, *Nuclear ferritin protects DNA from UV damage in corneal epithelial cells.* Mol Biol Cell, 1998. **9**(5): p. 1037-51.
158. Linsenmayer, T.F., et al., *Nuclear ferritin in corneal epithelial cells: tissue-specific nuclear transport and protection from UV-damage.* Prog Retin Eye Res, 2005. **24**(2): p. 139-59.
159. Cai, C., et al., *Nuclear ferritin-mediated protection of corneal epithelial cells from oxidative damage to DNA.* Dev Dyn, 2008. **237**(10): p. 2676-83.
160. Broxmeyer, H.E., et al., *Suppressive effects in vivo of purified recombinant human H-subunit (acidic) ferritin on murine myelopoiesis.* Blood, 1989. **73**(1): p. 74-9.
161. Shangguan, T., et al., *A novel N-acyl phosphatidylethanolamine-containing delivery vehicle for spermine-condensed plasmid DNA.* Gene Ther, 2000. **7**(9): p. 769-83.
162. Frank L. Sorgi, L.H., *Large scale production of DC-Chol cationic liposoems by microfluidization.* International Journal of Pharmaceutics, 1996. **144**(1996): p. 131-139.
163. Keller, M., et al., *Thermodynamic aspects and biological profile of CDAN/DOPE and DC-Chol/DOPE lipoplexes.* Biochemistry, 2003. **42**(20): p. 6067-77.
164. Yokoyama, M. and T. Okano, *[Targeting of anti-cancer drugs with nano-sized carrier system]*. Nippon Rinsho, 1998. **56**(12): p. 3227-34.
165. Madhankumar, A.B., et al., *Interleukin-13 receptor-targeted nanovesicles are a potential therapy for glioblastoma multiforme.* Mol Cancer Ther, 2006. **5**(12): p. 3162-9.
166. Madhankumar, A.B., et al., *Efficacy of interleukin-13 receptor-targeted liposomal doxorubicin in the intracranial brain tumor model.* Mol Cancer Ther, 2009. **8**(3): p. 648-54.
167. Abu Lila, A.S., T. Ishida, and H. Kiwada, *Targeting Anticancer Drugs to Tumor Vasculature Using Cationic Liposomes.* Pharm Res.
168. Kuesters, G.M. and R.B. Campbell, *Conjugation of bevacizumab to cationic liposomes enhances their tumor-targeting potential.* Nanomedicine (Lond). **5**(2): p. 181-92.
169. Sioud, M. and D.R. Sorensen, *Cationic liposome-mediated delivery of siRNAs in adult mice.* Biochem Biophys Res Commun, 2003. **312**(4): p. 1220-5.

170. Felgner, P.L., et al., *Lipofection: a highly efficient, lipid-mediated DNA-transfection procedure.* Proc Natl Acad Sci U S A, 1987. **84**(21): p. 7413-7.
171. Malone, R.W., P.L. Felgner, and I.M. Verma, *Cationic liposome-mediated RNA transfection.* Proc Natl Acad Sci U S A, 1989. **86**(16): p. 6077-81.
172. Felgner, P.L. and G.M. Ringold, *Cationic liposome-mediated transfection.* Nature, 1989. **337**(6205): p. 387-8.
173. Egilmez, N.K., Y. Iwanuma, and R.B. Bankert, *Evaluation and optimization of different cationic liposome formulations for in vivo gene transfer.* Biochem Biophys Res Commun, 1996. **221**(1): p. 169-73.
174. Dalby, B., et al., *Advanced transfection with Lipofectamine 2000 reagent: primary neurons, siRNA, and high-throughput applications.* Methods, 2004. **33**(2): p. 95-103.
175. Barreau, C., et al., *Liposome-mediated RNA transfection should be used with caution.* RNA, 2006. **12**(10): p. 1790-3.
176. Grayson, A.C., J. Ma, and D. Putnam, *Kinetic and efficacy analysis of RNA interference in stably and transiently expressing cell lines.* Mol Pharm, 2006. **3**(5): p. 601-13.
177. Maitani, Y., et al., *Cationic liposome (DC-Chol/DOPE=1:2) and a modified ethanol injection method to prepare liposomes, increased gene expression.* Int J Pharm, 2007. **342**(1-2): p. 33-9.
178. Gao, X. and L. Huang, *A novel cationic liposome reagent for efficient transfection of mammalian cells.* Biochem Biophys Res Commun, 1991. **179**(1): p. 280-5.
179. Gao, X. and L. Huang, *Cationic liposome-mediated gene transfer.* Gene Ther, 1995. **2**(10): p. 710-22.
180. Liu, F., et al., *New cationic lipid formulations for gene transfer.* Pharm Res, 1996. **13**(12): p. 1856-60.
181. Colosimo, A., et al., *Gene transfection efficiency of tracheal epithelial cells by DC-chol-DOPE/DNA complexes.* Biochim Biophys Acta, 1999. **1419**(2): p. 186-94.
182. Choi, W.J., et al., *Low toxicity of cationic lipid-based emulsion for gene transfer.* Biomaterials, 2004. **25**(27): p. 5893-903.
183. Yano, J., et al., *Antitumor activity of small interfering RNA/cationic liposome complex in mouse models of cancer.* Clin Cancer Res, 2004. **10**(22): p. 7721-6.
184. Ciani, L., et al., *DOTAP/DOPE and DC-Chol/DOPE lipoplexes for gene delivery: zeta potential measurements and electron spin resonance spectra.* Biochim Biophys Acta, 2004. **1664**(1): p. 70-9.
185. Congiu, A., et al., *Correlation between structure and transfection efficiency: a study of DC-Chol--DOPE/DNA complexes.* Colloids Surf B Biointerfaces, 2004. **36**(1): p. 43-8.
186. Esposito, C., et al., *The analysis of serum effects on structure, size and toxicity of DDAB-DOPE and DC-Chol-DOPE lipoplexes contributes to explain their different transfection efficiency.* Colloids Surf B Biointerfaces, 2006. **53**(2): p. 187-92.
187. Zhang, Y., et al., *DC-Chol/DOPE cationic liposomes: A comparative study of the influence factors on plasmid pDNA and siRNA gene delivery.* Int J Pharm.
188. Barichello, J.M., T. Ishida, and H. Kiwada, *Complexation of siRNA and pDNA with cationic liposomes: the important aspects in lipoplex preparation.* Methods Mol Biol. **605**: p. 461-72.
189. Sato, A., et al., *Small interfering RNA delivery to the liver by intravenous administration of galactosylated cationic liposomes in mice.* Biomaterials, 2007. **28**(7): p. 1434-42.
190. Zhang, Y., et al., *DC-Chol/DOPE cationic liposomes: A comparative study of the influence factors on plasmid pDNA and siRNA gene delivery.* Int J Pharm, 2010. **390**(2): p. 198-207.

191. Armandodoriano Bianco, et al., *A Simple Approach to DC-Cholesterol, Its Analogues and Vitamin D-Based Cationic Lipids for Gene Therapy. Letters of Organic Chemistry*, 2005. **2**: p. 79-82.
192. Bowles, A.P., Jr., C.G. Pantazis, and W. Wansley, *Use of verapamil to enhance the antiproliferative activity of BCNU in human glioma cells: an in vitro and in vivo study.* J Neurosurg, 1990. **73**(2): p. 248-53.
193. de la Pena, L., et al., *Inhibition of Akt by the alkylphospholipid perifosine does not enhance the radiosensitivity of human glioma cells.* Mol Cancer Ther, 2006. **5**(6): p. 1504-10.
194. Geoerger, B., et al., *Potentiation of radiation therapy by the oncolytic adenovirus dl1520 (ONYX-015) in human malignant glioma xenografts.* Br J Cancer, 2003. **89**(3): p. 577-84.
195. Oertel, S., et al., *Human glioblastoma and carcinoma xenograft tumors treated by combined radiation and imatinib (Gleevec).* Strahlenther Onkol, 2006. **182**(7): p. 400-7.
196. Rogulski, K.R., et al., *Pronounced antitumor effects and tumor radiosensitization of double suicide gene therapy.* Clin Cancer Res, 1997. **3**(11): p. 2081-8.
197. Staba, M.J., et al., *Adenoviral TNF-alpha gene therapy and radiation damage tumor vasculature in a human malignant glioma xenograft.* Gene Ther, 1998. **5**(3): p. 293-300.
198. Verhoeff, J.J., et al., *Tumour control by whole brain irradiation of anti-VEGF-treated mice bearing intracerebral glioma.* Eur J Cancer, 2009. **45**(17): p. 3074-80.
199. Juliano, R.L., *Intracellular delivery of oligonucleotide conjugates and dendrimer complexes.* Ann N Y Acad Sci, 2006. **1082**: p. 18-26.
200. Yadava, P., D. Roura, and J.A. Hughes, *Evaluation of two cationic delivery systems for siRNA.* Oligonucleotides, 2007. **17**(2): p. 213-22.
201. Messner, M., et al., *Self-assembled cyclodextrin aggregates and nanoparticles.* Int J Pharm. **387**(1-2): p. 199-208.
202. Zhi, D.F., et al., *[Comparison of two kinds of cationic vectors-mediated gene delivery]*. Yao Xue Xue Bao, 2009. **44**(5): p. 553-7.
203. Roberts, S. and A. Bomford, *Ferritin iron kinetics and protein turnover in K562 cells.* J Biol Chem, 1988. **263**(35): p. 19181-7.
204. Radisky, D.C. and J. Kaplan, *Iron in cytosolic ferritin can be recycled through lysosomal degradation in human fibroblasts.* Biochem J, 1998. **336 (Pt 1)**: p. 201-5.
205. Hernandez-Yago, J., et al., *Autophagy of ferritin incorporated into the cytosol of Hela cells by liposomes.* Cell Tissue Res, 1980. **205**(2): p. 303-9.
206. Harrison, P.M., A. Treffry, and T.H. Lilley, *Ferritin as an iron-storage protein: mechanisms of iron uptake.* J Inorg Biochem, 1986. **27**(4): p. 287-93.
207. Pilon, M., et al., *Essential transition metal homeostasis in plants.* Curr Opin Plant Biol, 2009. **12**(3): p. 347-57.
208. Gwak, H.S., et al., *Radiosurgery for recurrent brain metastases after whole-brain radiotherapy : factors affecting radiation-induced neurological dysfunction.* J Korean Neurosurg Soc, 2009. **45**(5): p. 275-83.

CURRICULUM VITAE

Xiaoli Liu
Jill Drive, Hummelstown, PA 17036
xliu@hmc.psu.edu

Education/Experience

8/2002-present: PhD student in Integrative Biosciences Graduate Program of the Huck Institutes, Penn State University, College of Medicine, Hershey, PA 17033.

7/1992-7/2002: Junior/Senior Research Technician in Dept. of Physiology, College of Medicine, Penn State University, Hershey, PA 17033.

9/1988-12/1991: Master of Science, Dept. of Chemistry, Clerk Atlanta University, Atlanta, Georgia 30314.

Manuscripts

1. Morris Pasternack Jr., **Xiaoli Liu**, Robert A Goodman and D. Eugene Rannels,"Regulated Stimulation of Epithelial Cell DNA Synthesis by Fibroblast-Derived Mediators", *Am. J. Physiol*. 272 (Lung Cell. Mol. Physiol. 16): L619-L630, 1997.

2. Charles H. Lang, **Xiaoli Liu**, Gerald Nystrom, Duanqing Wu, Robert N. Cooney and Robert A. Frost. "Acute Effect of Growth Hormone in Alcohol-Fed Rats ". *Alcohol & Alcoholism* Vol. 35, No. 2, pp. 148-158, 2000.

3. Charles H. Lang, **Xiaoli Liu**, Gerald Nystrom Robert and Robert A. Frost. "Acute Response of IGF-I and IGF Binding Protein Induced by Thermal Injury." *Am J Physiol Endicrinol Metab* 278: E1087-E1096, 2000.

4. Lang, Charles H.; Kumar, Vinayshree; **Liu**, **Xiaoli;** Frost, Robert A.; Vary, Thomas C. "IGF-I Induced Phosphorylation of S6K1 and 4E-BP1 in Heart is Impaired by Acute Alcohol Intoxication." *Alcoholism: Clinical & Experimental Research*. 27(3):485-494, March 2003.

5. Jerron Lee Fisher, Kavi Devraj, Justin Ingram, Becky Slagle-Webb, Achuthamangalam Madhankumar, **Xiaoli Liu**, Marianne Klinger, Ian A. Simpson and James Connor. "Ferritin – A Novel Mechanism for Delivery of IRON to the Brain and other Organs." ." *Am J Physiol Cell Physiol. 2007 Apr 25*.

6. **Xiaoli Liu**, A.B. Madhankumar, Jonas Sheehan, Becky Slagle-Webb and James R. Connor. "H-ferritin siRNA Delivered by Cationic Liposomes Increases Chemotherapeutic Sensitivity for Treating Glioma." 2010 Submitted to Cancer research.